Estimation of thermal properties of randomly packed bed of silicagel particles using IHTP method

A Thesis Submitted to the College of

Graduate Studies and Research

In Partial Fulfillment of the Requirements

For the Degree of Master of Science

In the Department of Mechanical Engineering

University of Saskatchewan

Saskatoon

By

Mohammadreza (Mamzi) Naghash

PERMISSION TO USE

I agree that the Libraries of the University of Saskatchewan may make this thesis freely available for inspection. I further agree that permission for copying of this thesis in any manner, in whole or in part, for scholarly purposes may be granted by my supervisors (Professor R. W. Besant and Professor R.W. Evitts) or, in their absence, by the Head of the Department of Mechanical Engineering, or the Dean of the College of Engineering. It is understood that any copying or publication or use of this thesis or parts thereof for financial gain shall not be allowed without my written permission. It is also understood that due recognition shall be given to me and to the University of Saskatchewan in any scholarly use which may be made of any material in my thesis.

Requests for permission to copy or to make other use of material in this thesis in whole or part should be addressed to:

Head of the Department of Mechanical Engineering

University of Saskatchewan

Saskatoon, Saskatchewan S7N 5A9

ACKNOWLEDGEMENT

My special thanks and appreciations go to my supervisors Professor emeritus Robert Besant and Professor Richard Evitts who helped me from the beginning to the end of this research study.

I appreciate the guidance and suggestions of the committee members – Professor Carey Simonson and Professor David Torvi for this thesis.

I am also thankful to Mr. Dave Deutscher for his suggestions and comments during the experimental work.

I am grateful to Professor J. Podder, Dr. Xiaodong Nie, and Mr. Farhad Fathieh for their help during my research study.

Financial support from University of Saskatchewan, Potash Corporation of Saskatchewan (PCS), and Natural Sciences and Engineering Research Council (NSERC) are appreciated.

DEDICATION

I dedicate this thesis to my mother-Sedigheh Silanizadeh, and my father-Majid Naghash whose love and supports were the shoulders for me to stand up.

I also dedicate this work to my sisters- Parvaneh Naghash, Azadeh Naghash, and Nazanin Naghash, who were the first ones heard when I needed help.

ABSTRACT

Accurate values of thermophysical transport properties of particle beds are necessary to accurately model heat and mass transfer processes in particle beds that under-go preferred processes and changes. The objective of this study is to use a proven analytical/numerical methodology to estimate the unknown transport properties within test cells filled with silicagel particles and compare the results with the previously published data.

An experimental test cell was designed and constructed to carry out transient heat transfer tests for both step change conduction and convection heat transfer within a packed bed of silicagel particles.

For a known step change in the test cell temperature boundary condition, the temporal temperature distribution within the bed during heat conduction depends only on the effective heat conduction coefficient and the thermal capacity of the particle bed. The central problem is to, using only the boundary conditions and a few time-varying temperature sensors in the test cell of particles, determine the effective thermal conductivity of the test bed and specify the resulting measurement uncertainty. A similar problem occurs when the heat convection coefficient is sought after a step change in the airflow inlet temperature for the test cell. These types of problems are known as inverse heat transfer problems (IHTP).

In this thesis, IHTP method was used to estimate the convective heat transfer coefficient. Good agreement was seen in experimental and numerical temperature profiles, which were modeled by using the estimated convective heat transfer coefficient.

The same methodology was used to estimate the effective thermal conductivity of the particle bed. Comparison between the experimental temperature distribution and

numerical temperature distribution, which was modeled by using the estimated effective conductivity, illustrated good agreement. On the other side, applying the effective thermal conductivity, obtained from a direct steady state measurement, in the numerical simulation could not present agreement between the numerical and experimental results.

It was concluded that the IHTP methodology was a successful approach to find the thermophysical properties of the particle beds, which were hard to measure directly.

TABLE OF CONTENTS

LIST OF FIGURES

LIST OF TABLES

NOMENCLATURE

ACRONYMS

ASHRAE	American Society of Heating, Refrigerating and Air-Conditioning Engineers
HFM	Heat Flow Meter
HVAC	Heating, Ventilation, and Air Conditioning
IHTP	Inverse Heat Transfer Problem
RH	Relative Humidity

ROMAN SYMBOLS

A_c	Contact area between the aluminum plate and the particle bed, m^2
$A_{sf,v}$	Specific volumetric surface area, m^2/m^3
a	Upstream face of the control volume
B	Bias error
Bi	Biot number
b	Downstream face of the control volume

$COEF_k$	Unknown coefficient of effective thermal conductivity
C_p	Specific heat capacity, J/(kg.K)
D	Diameter, m
d	Diameter, mm
d_h	Hydraulic diameter, mm
d_h	Particle diameter, mm
g	Gravitational acceleration, m^2/s
h_t	Convective heat transfer coefficient, $W/(m^2.K)$
I	Grid point in the control volume
I+1	grid point in the downstream control volume
I-1	grid point in the upstream control volume
K	Permeability of the porous bed, m^2
k	Thermal conductivity, W/(m.K)
k_{eff}	Effective thermal conductivity of the porous bed, W/(m.K)
k_k	Kozeny constant

L	Length of the particle bed, m
l	Length of REV, m
M	Mass, kg or g
m	Mass, kg
N	Number of measurement readings
Nu	Nusselt number
P	Pressure, Pa; precision error
Pr	Prandtl number
Q	Volumetric flowrate, m^3/s
q	Heat flow, W
R	Gas constant, J/(kg.K)
Ra	Rayleigh number
R_{factor}	Relaxation factor
r	Residual, K
S	Objective function, K^2; standard deviation, K

SEE	Standard error of estimation
T	Temperature, K
t	Time, s; student t
t_n	Vector of time, s
U	Uncertainty
U_d	Interfacial velocity, m/s
U_p	Pore velocity, m/s
V	Output voltage, V; volume, m^3
X	Sensitivity coefficient
$\bar{X}$	Reduced Sensitivity coefficient, K
$\hat{X}$	Sensitivity coefficient matrix
x	Position, m
x_i	Vector of position, m
Y	Measured temperature vector, K

GREEK SYMBOLS

α	Vector of known parameters; thermal diffusivity, m^2/s
β	Unknown parameter; thermal volume expansion factor, 1/K
δ	Differential change
ε	Porosity
μ	Damping parameter; dynamic viscosity of the air, Pa.s
ν	Kinematic viscosity, m^2/s
ρ	Density, kg/m^3
Ω	Diagonal matrix
ΔP	Pressure difference, Pa
ΔT	Temperature difference, K
Δt	Time difference, s
ΔX	Length of control volume, m or mm

SUPERSCRIPT

k	Current iteration
$k+1$	Next iteration

SUBSCRIPT

Al	Aluminum plate
ave	Average
c	Contact
cal	Calibration
e	External
fit	Fitting
g	Gaseous phase
I	Present control volume
i	Internal; time node
k	Current iteration
$k+1$	Next iteration

$meas$	Measured
N	Outlet boundary
p	Particle
s	Solid; Solid phase (pure solid silicagel (SiO_2)+internal gaseous phase)
$silica$	Pure solid silicagel (SiO_2)
0	Initial time; inlet boundary

CHAPTER 1 INTRODUCTION

In this chapter an introduction to the applications of porous media in the energy industry is given. Convective and conductive heat transfer coefficients are introduced as the thermal transport properties that are necessary in the study of the transient heat transfer in the particle beds, and a review of the research related to the investigation of these parameters is presented. An introduction is given about the silicagel particles that were used in the porous test cell during the transient tests. Furthermore, an introduction is given to the IHTP method that is used to find the unknown properties of a system during transient tests. Finally, the objective of this research and the general method and procedure are stated.

1.1 Porous Media

Porous media, such as particle beds, have attracted researchers for the analysis, prediction and control of energy and mass transfer processes because of their importance in industries such as: food processing, HVAC, mining, nuclear reactors, and oil sands. Porous media, such as the desiccant silicagel coatings or beds, are widely used in energy transport applications such as air-to-air energy recovery from exhaust air to supply air because they are capable of transferring both heat and water vapor. Furthermore, many natural substances (soil, rock, seeds, wood, sand) are porous, and their physical and thermal properties can only be accurately modelled for diffusion processes using the theories of mass and energy transport in porous media.

Some particles (potash, urea) may undergo chemical reactions when exposed to moist environments such as humid air, and the energy and mass transfer phenomena that happen during reactions will change the properties of these particles in a way that makes them unsuitable for the needed applications.

Study of the energy transfer between the porous media and the surrounding flow stream, needs the determination of the energy transport properties. A porous bed is a volume composed of the solid matrix and the void spaces between the solid elements (particles), and it is commonly used to study the energy (heat) transfer in the porous media.

Effective thermal conductivity (k_{eff}) is the thermal conductivity of the porous bed that is a function of thermal conductivity of the phases, and the geometrical characteristics of the porous bed. Interfacial convective heat transfer coefficient (h_t) is a characteristic that, along with the temperature difference, is required to predict the heat flux at the interface of the fluid and solid phases in the porous bed. Effective thermal conductivity and convective heat transfer coefficients are the essential parameters in the study of energy transfer in the porous bed.

1.2 Convective Heat Transfer Coefficient

Attention to the convective heat transfer coefficient in porous media has increased in recent years because of the wide usage of porous materials in the cooling of electrical systems, combustors, fixed-bed reactors, and compact porous heat exchangers (Jiang et al. 2006). The particle to fluid heat transfer coefficient describes the rate of the convective heat transfer between the particle bed and the gas phase. The experimental and numerical models of the heat transfer between the solid matrix of the porous bed and the gaseous phase in it have used both thermal equilibrium and non-thermal equilibrium methods. In the thermal equilibrium assumption, it is considered that the solid matrix and the gaseous phase have the same temperature, but this consideration cannot lead to accurate results to solve most of the heat transfer problems. Therefore, in recent years, more consideration has been given to the non-thermal equilibrium method, used to analyze the convective heat transfer between the solid and gaseous phase in the porous bed (Lee & Vafai, 1999).

Whitaker (1972) found correlations for the Nusselt number versus Reynolds number when the gas flow passes through the particle beds of spherical particles and cylindrical particles in steady state conditions. His correlation introduced Nusselt number (dimensionless convective heat transfer coefficient) as a function of the Reynolds and Prandtl numbers for Reynolds numbers greater than 20.

Shah and London (1978) showed that the Nusselt number is a function of the Reynolds number, Prandtl number, and the geometry of the flow passage. In a narrow range of temperature change in porous media, the Prandtl number can be considered constant, which means the Nusselt number is only a function of the Reynolds number for a fully developed flow and not related to the properties of the solid matrix.

Kar & Dybbs (1982) investigated the internal heat transfer coefficient of porous metals experimentally and delivered a correlation for Nusselt number versus Reynolds number for porosity up to 0.65 in the Darcian regime of the airflow (Reynolds smaller than 10).

Peng et al. (2000) developed a correlation to find the convective heat and mass transfer coefficients in order to simulate the heat and mass transfer in a packed bed of potash particles that were exposed to humid airflow in the range of Reynolds numbers from 20 to 100. Their correlation for the lower Reynolds number was not successful because they expected to see the same Nusselt number for the Reynolds numbers that are smaller than 5, but they could not extract their expectation.

Jiang et al. (2006) studied the convective heat transfer coefficient between a sintered microporous media (particle diameter of 0.2 *mm*) and airflow by using both numerical and experimental methods. They considered that the temperature gradient in the solid phase is negligible in comparison with the temperature gradient in the gaseous phase. They produced an experimental graph for the variation of Nusselt number and Reynolds number for low Reynolds numbers (less than 10) and verified it by a one-dimensional numerical model.

Nie et al. (2008), studied temperature and moisture content distribution in a packed bed of urea particles that was subjected to a humid airflow. Urea particles have internal porosity which makes them more complex in terms of surface area exposed to the airflow. They concluded that urea particles and silicagel particles are similar to each other. They found a correlation for the Nusselt number as a function of the Reynolds number and Prandtl number for Reynolds numbers smaller than 10. Their model had a 20% uncertainty for the values of convective heat transfer coefficients.

Nie et al. (2011) investigated the convective heat transfer coefficient by using a numerical model and concentrating on the transient temperature change in the packed bed of spherical particles (glass, stainless steel, and lead). Employing a hot airflow passing through the particle bed, they used a new technique to apply a single step temperature change at the inlet of the packed bed. The linear transient temperature change in each position in the packed bed was applied for the temperature terms in the numerical simulation. They developed a correlation for the Nusselt number versus the Reynolds number for the range of

Reynolds numbers from 5 to 280. They mention that their correlation has a high uncertainty when the Reynolds number is less than 10.

Yang et al. (2012) developed an experiment to find the temperature distribution in structured packed beds that had been heated up to 70℃ and then were exposed to the cold airflow at room temperature. Four different structures of the spherical particles were tested and transient temperature changes in the inlet and outlet of the packed bed were recorded. A numerical model was developed to simulate the transient experiment and an inverse analysis was applied based on the minimizing experimental and numerical outcomes in order to estimate the convective heat transfer coefficient. The effects of the packing structure and size uniformity on the relation between Nusselt and Reynolds numbers were investigated. They found that both the packing form and particle shape had significant effects on the heat transfer characteristics of the packed beds.

Most of the available research studies on the relation between Nusselt number and Reynolds number are based on the steady state experiments, or measuring the transient temperature changes at the inlet and outlet of the packed bed. In this study, transient temperature change is measured inside the packed bed which can help to eliminate the entrance effect and provide more accurate information about the heat transfer in the packed bed.

1.3 Effective Thermal Conductivity

Existence of more than one phase in the porous medium makes the analysis of its thermal conductivity more complex than the solid materials. The ratio of the thermal conductivity of the solid phase to the gaseous phase, void fraction in the porous bed, and the particle size of the packed bed are parameters that influence the thermal conductivity of the porous material. Knowledge of thermal conductivity is becoming important in many applications because of the increasing usage of porous substances in high temperature furnaces, insulating envelopes in solar ponds, the ceramic industry, and nuclear reactors (Singh, 2004).

Prat (1990) developed a steady state numerical model for the conductive heat transfer between a porous volume and an external fluid that were in contact at the boundary. He found

a formulation to estimate the effective thermal conductivity of the porous volume at the boundary. He mentions that when the ratio of the thermal conductivities of the solid phase to the fluid phase in the porous medium is small the microscopic effects at the interface are negligible, but this effect grows with an increase in the difference between the thermal conductivity of the two mentioned phases.

Tavman (1996) reviewed the available models to predict the thermal conductivity of the porous medium and the range of the applicability of the models. He used a modified hot wire method based on the steady state temperature measurements of the porous material while it was held in a rectangular chamber attached to another rectangular material with a known thermal conductivity. A hot wire was mounted between these two rectangles and works as a heat source. Tavman could predict the thermal conductivity with an accuracy of ±5%. He compares his predictions with the previous correlations and claims that the new modified hot wire method is adequate to predict the thermal conductivity of small grains.

Gurgel and Klüppel (1996) studied the effective thermal conductivity of a packed bed of silicagel particles with different moisture contents by analyzing radial heat distribution in both transient and steady state conditions in the porous bed. They used the steady state measurements to find the thermal conductivity and the transient temperature recordings to find the thermal diffusivity in the packed bed by using inverse analysis. They found that the thermal conductivity increased lineary with the water content of the packed bed.

Singh (2004) investigated the effective thermal conductivity of highly porous materials numerically and suggested a numerical formulation that could estimate the thermal conductivity of the foams without any need to consider the sphericity level or any other factor in the formulation. He shows that the effective thermal conductivity is highly influenced by the ratio of the thermal conductivity of the solid and gas phases.

Wen and Ding (2006) report an experimental study on the steady state and transient two dimensional (axial and radial) heat transfer in a gas flowing through a column of glass balls. They found the effective thermal conductivity of the bed and convective heat transfer coefficient of the particle bed in the steady state conditions by using a numerical model based on minimizing the error between the experimental and numerical temperature distribution. They mention that their model can predict the axial temperature distribution in the packed bed fairly well, but it is not successful in simulating the radial temperature distribution.

Evitts et al. (2006) performed transient experiments to find the effective thermal conductivity of a packed bed of potash particles at different moisture contents. They used an inverse analysis in order to estimate the thermal conductivity by minimizing the difference between the experimental measurements and numerical outcomes. They report that there is a linear relation between the effective conductivity and moisture content of the potash bed. They used a steel ball as a heat source inside the potash bed and assumed that the thermal conductivity of the porous bed at the boundary of the solid heat source and the packed bed, was half of the effective conductivity of the potash bed. They point out that a 10% uncertainty in their assumption caused less than 5% uncertainty in the estimated value of the effective thermal conductivity.

Znaidia et al. (2009) investigated optimal experiment design and the measurements of the effective thermal conductivity of a porous medium made of spherical sand particles by using the transient hot-wire technique. They applied an inverse method based on minimizing ordinary least-square function in order to parameter estimation of the effective thermal conductivity. The estimated thermal conductivity was evaluated by comparison between their model and previous research studies.

de Matos Jorge et al. (2010) studied the response of a non-adiabatic bed of cylindrical particles to a step change in airflow rate, inlet temperature of the airflow, and temperature of the surrounding walls. They recorded the temperature changes by using ring shaped thermocouples at five different axial positions while the temperature was measured at five different radial positions in each axial position. They estimated a correlation for the radial effective thermal conductivity based on the steady state results and reported that the radial thermal conductivity is increased linearly with the increase in Reynolds number of the inlet air flow.

Solmuş et al. (2012) studied the influence of porous bed geometries, convective heat transfer coefficient, and the ratio of the thermal conductivity of the components of the porous bed on the transient temperature distribution in a bed of silicagel/water. They found that the temperature difference between the gas phase and the solid phase was not significant except during the early stages of the transient test. They found that the thermal conductivity of the solid phase had a significant influence on the heat and mass transfer in the packed bed. So to increase the heat transfer efficiency fins or other thermal enhancements can be used; however

increasing the convective heat transfer coefficient more than a certain value does not lead to any significant change in the temperature gradient.

A review of the previous research on effective thermal conductivity shows that the steady state methods are less successful, especially when a two dimensional heat transfer analysis is applied. Furthermore in steady state methods such as the hot wire method, it is necessary to assume that the temperature in the porous material is uniform, which cannot be applicable in all cases. Experimental steady state methods to measure thermal conductivity use a material with a known thermal conductivity to measure the heat flux, which can be a source of uncertainty.

Transient methods to predict the thermal conductivity which are based on an estimation of the thermal conductivity by comparing the experimental and numerical outcomes, show more success in predicting the effective conductivity. Applying a heat source (or sink) inside the porous bed in the transient methods causes two problems. The first one is the higher possibility of a significant influence of heat loss on the transient analysis; the second is the disturbances and non-uniformities in the structure of the packed bed at the boundary of the heat source (or sink). Therefore, it is expected that applying a transient experiment where the heat source (or sink) is at the surface boundary of the porous bed, would yield more accurate estimation of the effective thermal conductivity of the packed bed.

1.4 Silicagel Particles

Silicagel particles are used as the solid phase in the porous bed during transient tests. Silicagel is a granular porous solid material, formed from SiO_2, and has a crystalized porous structure. *ASHRAE Handbook* (American Society of Heating & Air-Conditioning, 1985) categorizes desiccants in two general types: liquid and solid. Solid desiccants have a high level of surface area per unit of mass. Silicagel is a solid desiccant with a microporous structure that provides a high internal surface area (up to $800\frac{m^2}{gr}$) (Pesaran and Mills, 1987), and no possibility of chemical reaction when exposed to fluids. This makes silicagel a high performance desiccant to be used in HVAC facilities such as energy recovery systems used to ventilate buildings (Besant & Simonson, 2003). Therefore, silicagel porous medium is one of the main subjects of transient energy transfer research about desiccants.

The internal porosity of silicagel particles can change the available surface area involved in convective heat transfer. A wide range of crystalized structures yield different values for the thermal conductivity of these silicagel particles during steady state tests. Hence the internal porosity in the silicagel particles makes this a challenging material to be studied.

Sun and Besant (2005) studied the temperature and relative humidity distribution in a packed bed of silicagel particles that were exposed to a heated airflow passing through the bed from top to bottom. They modeled the packed bed numerically by considering a non-thermal equilibrium model, assuming that the thermocouples inside the packed bed showed the average mean value of the temperatures of the gas and the solid. They found that these particles have a very large specific surface area, which causes a time delay in the humidity and temperature response of the packed bed. Furthermore, they showed that the internal surface area of the particles was only exposed to the water vapor over an extended time, which means that short transient tests with the airflows of low relative humidity cannot cause a significant uncertainty in the results.

Silicagel particles have an infinite lifetime if they are stored in the ambient condition. These particles can absorb water up to one third of their total mass (Sun, 2003), but they can be regenerated and reused by being heated in the oven in a temperature as low as 50℃ (Ng et al., 2001). Silicagel is non-toxic, non-flammable, and available in a wide range of sizes, which are suitable for different applications. Silicagel can be found in the form of beads and can be considered as spherical with a good approximation.

1.5 IHTP Analysis of Transient Tests

1.5.1 Background information

Interest in the theory and application of Inverse Heat Transfer Problem (IHTP) has grown in recent years. This method is used in nuclear applications, aerospace projects and almost every branch of engineering including mechanical and chemical. One of the most common applications of this method is to estimate thermophysical properties of substances or mechanical procedures. Knowing such properties of an industrial process, one can develop a numerical simulation of the phenomenon in order to control and modify the facilities and efficiency of the involved procedure.

Unfortunately, in most cases thermophysical properties change by time and position in the system, which makes the direct measurement of the mass and energy transport properties such as thermal conductivity, convective heat transfer coefficient, and mass diffusivity impossible or difficult. Steady state measurements designed to find these properties directly have some problems:

- Sometimes it takes a long time (from an hour to days) for a mechanical system to achieve steady state conditions, which are not absolute for any mechanical system.
- Steady state experiments are normally calibrated just to find a single property, assuming that other properties are already known.
- Final determination of an unknown property is a time-consuming process as experiments must be performed several times in order to estimate the uncertainty of the needed parameter.
- The reported value of a thermal property in steady state conditions may be not the same during the transient step, which is of primary interest in most studies aimed at control and modification of the procedure of energy or mass transfer.

Therefore, transient tests are less time-consuming and have less uncertainty as compared with steady state tests. As well, they yield better understanding of result distribution in both time and position dimensions in the system.

IHTP method is a numerical method that can estimate the unknown properties needed to analyze a system. This method is applicable for both steady state tests and transient tests, and can be applied to estimate more than one unknown parameter if the necessary assumptions are made. Using the IHTP solution, one can estimate the causes of the phenomenon (unknown parameter) by applying the effects of that phenomenon as inputs (temperature distribution).

Usually inverse analysis consists of an experimental test (transient test is preferred) that supplies the measurements of the input parameter (temperature in the heat transfer problems), a direct numerical modeling that simulates the transport problem, and a numerical algorithm that estimates the unknown parameters by decreasing the differences between the

experimental results and numerical simulation results. Using the sensitivity analysis, which is the first step of the IHTP analysis, one can find the best transient experiment design to discover the unknown parameters, or the type of unknown parameters that can be found using data from a transient test. Furthermore, the best positions for sensors to record changes, and the best time period of the transient experiment for use in the inverse solution can also be determined.

In conclusion, unknown properties of mechanical systems that are hard to determine by direct measurement can be determined with reasonable accuracy by using IHTP analysis.

1.5.2 Research review

The inverse method of analysis can be used to find the unknown properties of systems undergoing transient diffusion processes.

Raynaud (1999) compared the direct methodology and inverse analysis to determine thermophysical properties. He suggested seven steps in order to have complete parameter estimation, starting from the direct simulation of the problem to the verification of the inverse solution. He described the sensitivity analysis that should be performed before carrying out the transient experiments and illustrated with examples the importance of the sensitivity analysis to understand the physical behavior of the problem. He also suggested three different verification methods to examine the validity of the inverse solution.

Furthermore, he suggested "sequential-over-experiments" to increase the confidence in the parameter estimation. This method is about performing more than one experiment: the first to find the unknown parameters, and more to modify the estimation, examine the validity of the solution, and increase the confidence of the parameter estimation.

Huang & Yeh (2002) used an inverse algorithm to simultaneous estimate the time-dependent Biot number of the heat and mass transfer in the porous materials. They used an iterative algorithm to estimate the unknown parameters by comparing their direct numerical simulation with the analytical solution of the temperature and moisture distribution in the porous material. They show that the result of the inverse analysis is accurate enough even when the measurement errors are increasing.

Telejko and Malinowski (2004) used the inverse method for calculation of the thermal conductivity of a well- conducting solid (electrolytic iron). They used a finite element method (FEM) to find the temperature distribution inside the solid body and compared the temperature results with the mathematical solution of the problem to estimate the thermal conductivity in two cases: first assuming that it is independent of the time, and second assuming it changes with time. They compared their estimated values with a direct steady state experiment to find the thermal conductivity. They found good agreement between the estimation method and experiment.

Albouchi et al. (2005) developed an optimal design of an experimental method to determine the effective thermal conductivity of the powders used in coating. They used the study of the sensitivity coefficients to find the optimal duration of the experiment, and the optimal duration of the heating time involved in the experimental method. They estimated the effective thermal conductivity and effective thermal capacity of the glass powders by comparing the experimental data of the optimal experiment and numerical simulation.

Zueco et al. (2006) developed an inverse solution to estimate the thermal conductivity of a homogeneous material by using a neural network to modify the initial postulation in the solution. They simulated a cylinder under forced convection with air on the walls, and constant heat flux because of a hot wire mounted at the axes. They used the neural network method to better estimate the heat source as a function of the time. They conclude that the estimated thermal conductivity is close to the real value.

Blackwell and Beck (2010) introduced a technique for uncertainty analysis of a linear heat conduction problem by considering the uncertainty of the temperature measurements and known parameters. They performed the uncertainty propagation for a one-dimensional heat transfer in a planar stainless-steel slab under uniform heat flux to check the most effective known parameter in the inverse analysis. They present some ideas to include the uncertainty of the mounted thermocouples in the heat transfer domain, and uncertainty of their assumed and actual location in the inverse solution.

Kuye et al. (2010) developed an inverse study to determine the thermal conductivity and heat capacity of neem seeds. They defined a one-dimensional heat conduction problem in radial direction for temperature distribution in spherical neem particles by assuming that the particles were exposed to the hot dry air in a fluidized drying bed. They report that the

experimental temperature measurements from previous studies and numerical results are in good agreement with each other, so they conclude that IHTP can be used to find the thermophysical properties of particles.

Cui et al. (2012) used the inverse method as a method to find the thermal time-dependent properties in a transient heat conduction problem. The direct problem was the heat conduction on a plate with the heat flux at the top and bottom. They analyzed two cases: In one, the thermal capacity and thermal conductivity were defined as a function of the time; in the other they were independent variables. Furthermore, they used the sensitivity study to minimize the numerical computation time. They concluded that their method can provide accurate thermal properties with the same accuracy as the uncertainty measurements.

It is clear that many research studies have been done to estimate thermophysical properties of materials including porous media. Different inverse methods, different unknown parameters, different measured parameters, and different numbers of sensors are some of the variables in these studies.

1.6 Research Objectives

In this study, a methodology to find the thermal properties of packed particle beds as porous media is introduced. Transient heat transfer tests were performed on a packed bed of silicagel particles. More than one type of silicagel particles were tested to investigate the effects of the physical properties, such as particle size and density, on the transient heat transfer. The experiments were designed and developed based on the required type of heat transfer (convective or conductive).

The results of the transient tests were used in the IHTP analysis to estimate the effective thermal conductivity and convective heat transfer coefficient of a packed bed of silicagel particles. Confidence of the estimation algorithm was examined by comparing the results with the available studies and also by performing more transient and steady-state tests.

The objectives of this research study are:

1) To determine the physical properties (porosity, specific volumetric surface area, particle size, and permeability) of a dry packed bed of silicagel particles and the resulting uncertainties.

2) To develop a numerical model to simulate temperature distribution of the silicagel particle bed during energy transfer transient tests.

3) To develop a transient test to study the convective heat transfer in a heated particle bed when exposed to a dry airflow at the required flow rate. The effects of physical properties of the particles, and the volumetric flow rate of air on the convective heat transfer are investigated.

4) To develop a transient test to study the conductive heat transfer between a dry heated particle bed and an aluminum plate at the top of the packed bed while heat loss from the bed and plate to the surrounding is negligible. The effects of porosity and particle size on the conductive heat transfer are studied.

5) To design an experimental setup with a changeable inlet section to perform the transient convection and conduction tests. This setup must be capable of applying a single step temperature change to the inlet airflow as well as an instant change to the boundary of the packed bed to start the conduction test.

6) To develop an IHTP method to estimate the convective heat transfer coefficient and effective thermal conductivity of the packed bed, and determine the uncertainty of the estimation.

7) To validate the estimation method by comparing the estimated values with previous research, applying these values to simulate other transient tests, and comparing the values with the results of steady state measurements of the unknown parameters. Such validation will effectively prove that this methodology can be used to find the thermal properties of porous beds.

1.7 Overview of Thesis

Chapter 2 introduces the basics of the inverse heat transfer problem (IHTP) method. Necessary assumptions for application of this method are listed. The steps and the parameters required for a high level of confidence in inverse analysis are explained. The iteration algorithm used to estimate the unknown properties is illustrated. The uncertainty calculation of the IHTP method is presented, and the validation options used to examine the uniqueness of the IHTP analysis are introduced.

Chapter 3 presents the experimental procedure to perform the transient convective heat transfer tests on silicagel particles. Different sections of the experimental setup are introduced and illustrated. Necessary preparation and exact procedure of the convection transient test are explained. The direct numerical solution that can simulate the convection transient test is introduced and its algorithm is explained. Determined values of the stopping criteria that ensure the convergence of the inverse algorithm are introduced. The optimum transient test time period used in the IHTP analysis and the best sensor to be used in the inverse analysis are determined.

Chapter 4 shows the results of the convective heat transfer coefficient for two types of packed silicagel particle beds (differing particle size and internal structure). The convergence level of the inverse algorithm in each case is presented. Comparison is made between the experimental and numerical results using the estimated value of the convective heat transfer coefficient. A new correlation for the Nusselt number versus Reynolds number is presented and comparison between the new correlation and the most recent correlation is established.

Chapter 5 introduces the experimental setup used to perform the conduction transient tests on four different types of packed beds of silicagel particles. The assumptions made to determine the governing equations are explained, and the governing equations used in the direct numerical simulation to model the convection test, are presented. The algorithm of the direct numerical solution is explained and the stopping criteria applied in the inverse analysis are introduced. The optimum transient test time period and the optimum sensor for measuring inputs in the IHTP solution are introduced as well.

Chapter 6 shows the estimated values of the effective conductivity of the packed bed of silicagel particles. The effects of particle size on the estimated values are explained. Comparison of the experimental and numerical temperature distributions (using the estimated

value of effective conductivity) is established. Furthermore, residual function that shows the level of success in the inverse analysis is plotted for each sensor. Comparison is made between the theoretical models to estimate the thermal conductivity and the IHTP estimated values in order to examine the confidence of the inverse methodology. Furthermore, direct measurement of the effective thermal conductivity in steady state conditions is presented and comparison between the obtained and estimated values is made. Discussion is presented about the causes of the differences between these two methods. Furthermore, results of a different transient test on the packed silicagel bed are shown. This test is simulated numerically by using the estimated values of the thermal conductivity obtained from IHTP, and the comparison between the experimental and numerical results is presented to examine the validity of the IHTP results.

Chapter 7 presents the conclusions and summary of this research study and suggests ideas to improve the IHTP methodology to find the thermophysical properties of the packed bed of particles. Furthermore, suggestions for future studies in this field are explained.

The appendices include: (A) Calibration of the thermocouples and relative humidity sensors. (B) Measurement of the physical properties (Porosity, specific volumetric surface area, and particle size) and calculation of the measurement uncertainties. (C) Discretization of the governing equations and boundary conditions used to simulate the convective heat transfer and conductive heat transfer in the silicagel particle bed. (D) Sensitivity study of the grid size and time step that are applied in the direct numerical simulation.

CHAPTER 2 THEORY OF INVERSE HEAT TRANSFER PROBLEM (IHTP)

The inverse heat transfer problem (IHTP) method is an analytical/numerical method to estimate unknown heat transfer transport properties in a material that can be modeled as a continuum after a heat transfer change is made to one or more boundary conditions while some temperatures are measured at selected locations over a period of time when transient temperature changes will occur in the modeled continuum domain or region (e.g., a homogeneous, isotropic bed of particles) but the internal conduction and/or convection coefficients are not known a priori (i.e., the heat transfer problem is not well set with known internal properties and complete boundary and initial conditions – so classical analytic methods of solution cannot be applied). Without these internal transport properties, prediction or control of the time and spatial varying heat fluxes and temperature distributions is not possible for a region.

In this research, the IHTP technique uses the transient temperature recordings at a specified location to estimate properties such as convective heat transfer coefficient or conductive heat transfer coefficient, which cannot be found with the desired degree of accuracy by well-established classical methods (Ozisik & Orlande, 2000).

The IHTP analysis consists of two steps: a well-designed experimental test and a numerical simulation of the heat transfer process for the test coupled with an optimization technique to find or estimate the best fit for the unknown conduction or convection coefficient such that the fitted coefficient used in the simulation shows good agreement with the data. An experimental test consists of measuring the temperature of a specimen at one or more locations when it is subjected to transient temperature change in one or more boundary conditions thus causing a heating or cooling disturbance to diffuse through the test cell specimen (Raynaud, 1999). In general, this numerical procedure should be able to handle several measurements producing a continuous stream of data over a selected time period to estimate one or more internal or boundary properties simultaneously. Using the optimization method to determine the best estimate for the unknown property, the difference between the

measured temperature data and numerically simulated temperature data should be within the experimental measurement errors for the sensors used. Inverse heat transfer problems belong to an ill-posed class of problem meaning these problems are very sensitive to small random errors in the measured input data and this can lead to a lack of stability for any direct, well-posed problem solution. These problems involve time varying temperature changes (e.g., step, impulse and sinusoidal changes in one or more boundary conditions are commonly used).

The main purpose of the direct model is to determine the same temperature profile obtained from the transient test while all the parameters, boundaries, and initial conditions are known, so the direct numerical model is able to simulate the reality as closely as possible. The direct solution should be a well-posed standard heat transfer problem, which means it must satisfy three conditions (Hadamard, 1952):

- The solution must exist;
- The solution must be unique;
- The solution must be stable (not sensitive to small changes in input data).

The number of parameters that can be estimated simultaneously using IHTP depends on the amount and the quality of the available experimental data (Raynaud, 1999). IHTP are sensitive to random errors in the measured input data. Also they are ill- posed problems, because the uniqueness of the solution cannot always be proven (Ozisik & Orlande, 2000).

It is necessary to state the assumptions that can guarantee the uniqueness of the solution by applying constraints on the measurement errors. Beck (1979) introduced eight statistical assumptions that can be applied in actual experiments when:

a) The measurement errors are equal, which makes the standard deviations (σ_i) of the measurements constant and independent of the measurements.

b) The measurement errors are unbiased, which means they have a zero mean.

c) The errors regarding to different measurements are uncorrelated, which means they have no effect on each other.

d) Measured temperature is the only variable that has random errors, and other values applied in the IHTP are accurately known.

Inverse problems use optimization methods to minimize the differences between experimental measurements and numerical results. If all the statistical assumptions mentioned before are valid, the "Objective function" (S) is defined as the ordinary least squares norm that is the sum of the squared residuals (Ozisik & Orlande, 2000) and is formulated as

$$S = (Y - T)^T (Y - T) \qquad (2.1)$$

where Y and T are the measured temperature and IHTP analysis estimated temperature, respectively. In the case of just on sensor with transient measurements at times t_n, $n=1,...N$, the objective function can be reformulated as

$$S = (Y - T)^T (Y - T) = \sum_{n=1}^{N} (Y_n - T_n)^2 \qquad (2.2)$$

1.1 Sensitivity Coefficient

The sensitivity coefficient determines the level of sensitivity of the measured temperature to the unknown parameter or parameters. This parameter plays an important role in designing the optimum experimental process by determining the best sensors to be used in IHTP analysis, determining the unknown parameters that can be found simultaneously, and choosing the proper numerical method to be applied in IHTP solution.

The sensitivity coefficient is defined based on the sensitivity of the measured temperature with respect to the changes in the unknown parameter (Ozisik & Orlande, 2000), and it can be defined as the first derivative of measured temperature at time t_n with respect to the unknown parameter (Raynaud, 1999)

$$X(x_i, t_n, \alpha, \beta) = \frac{\partial T}{\partial \beta} = X|_{i,n} \qquad (2.3)$$

where x_i is the vector of position, t_n is the vector of time, α is the vector of known parameters, β is the unknown parameter and T is the temperature which can be found by using the direct numerical solution.

In a sensitivity matrix, each column represents the sensitivity coefficients of one unknown parameter and each row represents time nodes for a specific position. In the case of just one unknown parameter it can be defined as a vector

$$\hat{X} = \begin{bmatrix} X|_1 \\ X|_2 \\ \vdots \\ X|_{n-1} \\ X|_n \end{bmatrix} \qquad t = 1,2, \dots n \qquad (2.4)$$

The temperature is sensitive to changes in unknown parameters during the time periods when the sensitivity coefficient is large. Small values of sensitivity coefficients mean that there should be a big change in the unknown parameter in order to affect the direct numerical simulation. On the other hand, a large sensitivity coefficient means that temperature is changing a lot with a small change in the unknown parameter. As a result, the unknown parameter can be estimated accurately by using the inverse method. The sensitivity coefficient can also determine whether or not two or more unknown parameters can be estimated simultaneously. The sensitivity coefficients of any unknown parameter should not be linearly dependent on the sensitivity coefficients of other parameters. If the sensitivity coefficients of two or more unknown parameters are linearly dependent on each other in any time period of the experiment, they cannot be estimated simultaneously in that period. If the linear dependency happens for the whole experiment period, then designing other experiments to estimate the rest of the unknown parameters is necessary.

One of the other benefits of sensitivity coefficients is to be able to determine the effective sensor for the inverse solution. If there is more than one sensor applied in the experimental measurement, the sensor with higher sensitivity coefficients in the period of observation is the most reliable sensor for use in the inverse analysis. However, using more

sensors in the tests can be useful to validate the accuracy of the estimated parameters by comparing the experimental results and numerical results for those sensors.

Moreover, the sensitivity matrix can determine if the estimation is linear or not. In the linear IHTP problem the assigned values for the unknown parameters to be used in the sensitivity coefficient equation do not influence the magnitude of sensitivity coefficient. On the other hand, in the non-linear case the sensitivity coefficient changes by changing the value of the unknown parameter, so the assigned value for the unknown parameter and also the initial guess, which are used in the sensitivity analysis and the IHTP solution, should not be far from the reliable values of the unknown parameter.

One of the most common criteria in designing the experiment and choosing the proper IHTP numerical method is $X^T X$. In the case of one unknown parameter this matrix is a single number. The determinant of this matrix must be maximized, which means the sensitivity coefficients of the unknown parameters should be large and linearly independent (Raynaud, 1999). When the sensitivity coefficients are small, $|X^T X|$ is approximately zero, which means the problem is ill-conditioned, so IHTP methods, which are for well-conditioned problems cannot be used anymore.

Furthermore, the determinant of sensitivity matrix can help to find the proper time period of the experiment to be used in the inverse analysis, because the periods with large value determinants in them are the most reliable periods to be used in IHTP. In the cases in which one sensor is chosen for recording temperature measurements for the IHTP analysis, recording the whole experiment is not necessary, because only the recordings up to the time that provides a small value for the objective function can be used.

In most of the cases, it is hard to obtain the first derivative of the temperature with respect to the unknown parameter, so a finite differences method can be used to compute the sensitivity coefficient. The numerical sensitivity coefficient can be written as

$$X|_n = \frac{T(t_n, \beta + \delta\beta) - T(t_n, \beta - \delta\beta)}{2\delta\beta} \qquad (2.5)$$

In equation (2.5), $X|_n$ is the sensitivity coefficient, and $\delta\beta$ is the differential change in the unknown parameter. Central approximation is more accurate for use in the finite differences especially if high accuracy is demanded (Ozisik & Orlande, 2000). $\delta\beta$ should be small enough to have a valid linear approximation for the first derivation, thus it can be considered between $10^{-3}\beta$ and $10^{-2}\beta$ (Raynaud, 1999). The sensitivity coefficient is a scale of sensitivity of the temperature to the unknown parameter, so it is more convenient to reformulate the sensitivity coefficient to have the same unit as the temperature. Therefore, the reduced sensitivity coefficient is introduced to simplify the analysis and is formulated as

$$\bar{X}|_n = \frac{T(t_n, \beta + \delta\beta) - T(t_n, \beta - \delta\beta)}{2\delta\beta/\beta} \qquad (2.6)$$

Analysis of sensitivity coefficients and sensitivity matrices is important for every experimental design in IHTP. With their help, one can find the proper sensors to use in the inverse solution, the unknown parameters, which can be simultaneously estimated, and the numerical method that should be used in the IHTP.

2.1 The Levenberg- Marquardt Method for Parameter Estimation

After using the sensitivity analysis to create an optimum design for the experimental process, a numerical method should be developed to simulate the experiment and estimate the unknown parameters. The purpose of the numerical method in IHTP is to estimate the unknown parameters by minimizing the objective function. When the problem is not ill-conditioned, an iterative technique based on the Gauss-Newton method can be used. This method is called Levenberg-Marquardt and is useful for the IHTP with few unknown parameters (less than 20). It intends toward the Guess-Seidel method in the neighborhood of the minimum of the objective function and tends to the "steepest descent method" in the neighborhood of the initial guess, which is used to start the iteration(Ozisik & Orlande, 2000).

2.1.1 Direct problem

The first step in using the inverse method is to simulate the physical problem numerically, which is called the direct problem. The direct problem must include the

measured parameter (temperature), known parameters, and unknown parameters to simulate the physical phenomenon accurately. Governing equations should be derived and discretized to simulate the experiment. Also, boundary conditions and initial conditions should present the real physics of the conditions of the tests. The direct numerical simulation for each test used in the IHTP, will be explained in detail in the two following chapters.

2.1.2 Iterative procedure

The second step in the numerical modeling of IHTP, is to introduce the objective function (equation (2.2)), and the unknown parameter. The estimated temperatures $T_i(\beta)$ are computed by using the direct simulation at the position of the sensor or sensors and the estimation of the unknown parameter obtained at each iteration.

The third step is to use the iterative method to find the modified estimation for the unknown parameter. The iteration method consists of a numerical procedure to suggest a new value for the unknown parameter at each iteration, and a stopping criterion to check if the estimation is satisfying or not. To minimize the objective function, the first derivation of the objective function with respect to the unknown parameter should be zero:

$$\frac{\partial S(\beta)}{\partial \beta} = 0 \qquad (2.7)$$

In the case of a non- linear problem, $T(\beta)$, the estimated temperature vector, can be linearized by using equation (2.3) and applying the Taylor series expansion (Ozisik & Orlande, 2000)

$$T(\beta) = T(\beta^k) + X^k(\beta - \beta^k) \qquad (2.8)$$

$T(\beta^k)$ is the estimated temperature vector at iteration *k*, and X^k is the sensitivity matrix at iteration *k*. Substituting equation (2.1) in equation (2.7) and using equation (2.8), an iterative procedure is obtained to find the unknown parameter

$$\beta^{k+1} = \beta^k + [(X^k)^T X^k]^{-1}(X^k)^T[Y - T(\beta^k)] \qquad (2.9)$$

β^{k+1} is the new estimation of the unknown parameter. As can be seen the necessary condition to use equation (2.9) is to have a non- singular $X^T X$ matrix that needs to have a non-zero determinant. In the case of non- linear equations, some difficulties may appear because of the lack of convergence near the final estimated value for unknown parameter. The Levenberg- Marquardt method introduces two parameters in the iterative procedure as below

$$\beta^{k+1} = \beta^k + [(X^k)^T X^k + \mu^k \Omega^k]^{-1} (X^k)^T [Y - T(\beta^k)] \quad (2.10)$$

where μ^k is a positive scalar, which is called "damping parameter" and Ω^k is a diagonal matrix (when there is just one unknown parameter Ω^k=1). $\mu^k \Omega^k$ is applied to damp the instabilities at the beginning of the iteration when the $X^T X$ matrix is more likely to be singular. So the Levenberg-Marquardt method tends to the steepest descent method" near the initial guess, and near the final estimation of the unknown parameter when μ^k is getting too small it tends to the Gauss-Seidel Method (Beck & Arnold, 1977)

2.1.3 Stopping criteria

Criteria should be set to stop the iteration procedure. The first criterion is satisfying the convergence of the iteration procedure which means two successive estimations of the unknown parameter should have very small difference (Dennis & Schnabel, 1983)

$$|\beta^{k+1} - \beta^k| < \varepsilon_1 \quad (2.11)$$

where ε_1 is a small number and must be determined by the investigator (typically 10^{-3}) (Raynaud, 1999).

The second criterion checks if the objective function is small enough, which means the experimental results and IHTP results are in good agreement.

$$S(\beta_{estimated}) < \varepsilon_2 \quad (2.12)$$

When two stopping criteria are satisfied, it can assure that the iterative procedure has converged to a valid final estimation.

2.2 Numerical Algorithm

The following steps are taken to estimate the unknown parameter by using the Levenberg-Marquardt IHTP method.

1- Insert the constant variables which are: time vector (t=1:Nmax), damping parameter ($\mu = 0.001$), and diagonal matrix($\Omega = 1$).

2- Import the measurement matrix (experimental temperature profile).

3- Set the stopping criteria:

- Objective function (S)< ε_2
- IHTP Convergence criterion=ε_1

4- Consider the first estimation for the unknown parameter.

5- Calculate the objective function for the current estimation

6- Check the objective function with the stopping criterion; if the stopping criterion is satisfied it means that the first estimation is accurate enough and no more iteration is needed.

7- If the stopping criterion is not satisfied the iteration method will start as follows:

- Calculate the sensitivity matrix
- Start the iterative method to find a new estimation

8- The validity of the estimation will be checked with the stopping criterion for the new estimation and the iteration will continue until the stopping criterion is satisfied.

9- The program output will determine the final estimated value for the unknown variable.

A flow chart of the IHTP solution can be seen in Figure 2-1.

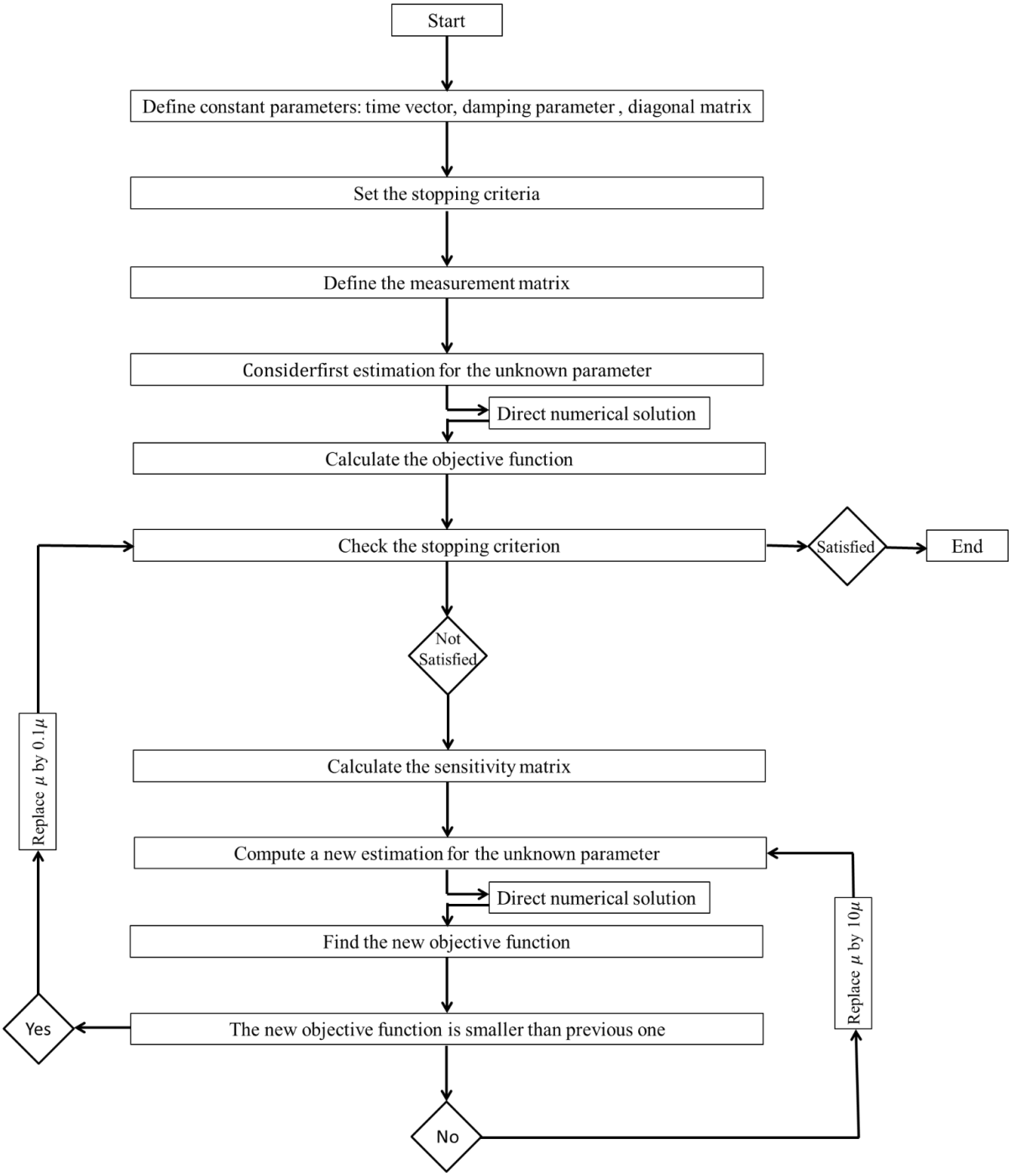

Figure 2-1 Designed IHTP algorithm in Matlab

2.3 Uncertainty Analysis

The uncertainty analysis in the inverse method can be performed by statistical analysis to find the accuracy of the estimation. If the eight statistical assumptions are valid then the relative uncertainty of the estimated parameter can be found as

$$\frac{U(\beta)}{\beta} = (X^T X)^{-1} U^2 \qquad (2.13)$$

where *U* is the uncertainty of the temperature measurement. Equation (2.13) can be derived from the covariance matrix of the unknown parameter (Znaidia et al., 2009). It is noted that this uncertainty comes along with the assumption that states there is no uncertainty in the assigned values of the known parameters.

2.4 Validity of the Model

The quality of the IHTP analysis can be examined with different tools. The reliability of the IHTP analysis will determine if the estimated value of the unknown parameter is valid and applicable in future studies or not. The first method is the residual function. The residual is the difference between the measured temperature and the computed temperature found by applying the estimated parameter at each data point (Znaidia et al., 2009). The residual function is written as

$$r_i = T_{meas,i} - T_i(\beta_{estimated}) \qquad (2.14)$$

where $T_{meas,i}$ is the measured temperature at each data point, $T_i(\beta_{estimated})$ is the calculated temperature, and *I* represents the time *i*=1,2,…,N. Residual function can be plotted versus time for each sensor. The magnitude of the residual function should be in the same order as the measurement uncertainties and it should oscillate around zero. The absence of any of these properties will show a poor numerical simulation or inefficient experimental process.

Using the temperature measurements obtained from the other installed sensors is another tool to validate the IHTP analysis. As mentioned, sensitivity study can determine the effective sensors in the inverse solution. On the other hand, the measurements of the sensors,

which have low sensitivity to the unknown parameter, can be usefully compared with the numerical temperature profile for the position of each sensor. Plotting the residual function and calculating the sum of least squares for each sensor can investigate the validity of the estimation method.

Other tools that can be used to examine the quality of an IHTP solution include performing other experiments and numerically simulating them while applying the estimated unknown parameter in the simulation, and comparing the numerical and experimental results. Comparison between the estimated value of the unknown parameter and previous studies and theoretical models of the unknown parameter is another tool to investigate the validity of the IHTP analysis.

CHAPTER 3 IHTP ESTIMATION OF CONVECTIVE HEAT TRANSFER (THEORY AND MODELING)

IHTP analysis was used to find the convective heat transfer coefficient in a randomly packed bed of silicagel particles. An experimental setup was designed to study transient convective heat transfer between the dry heated packed bed and dry airflow at room temperature. Two types of silicagel packed beds were used in the test. A numerical method was developed to simulate the transient test, and an inverse solution was applied to find the convective heat transfer coefficient of the packed bed.

3.1 Transient Tests

Transient tests were designed and developed to study the transient convective heat transfer between the dry particle bed and dry airflow. Two types of silicagel particles were used to fill the packed bed. Table 3-1 lists thermal and physical properties of each type of silicagel particle. Before each experiment, particles were heated in the oven for 24 hours to ensure they are dry and clean. After that they were packed in two layers of plastic bags to be in contact with the room temperature air and at the same time stay dry and clean.

In each test, one type of silicagel particles was used to fill the packed bed. The porous bed was a randomly unshaken packed bed, because the particles were poured in the empty bed through a funnel without any shaking process. The top surface of the particle bed was smoothed by hand to have a definable boundary with a depth that is uniform within one particle diameter.

When the experimental setup was assembled, dry airflow at 65℃ entered the packed bed from the top to heat up the particles and exited from the bottom. The particles were exposed to the hot airflow until the whole packed bed reached the same temperature as the hot airflow. The transient test started by performing a single temperature step change of the airflow passing through the packed bed. The inlet section of the test cell could rotate freely, which made it possible to set another airflow line carrying dry air at the room temperature at

the entrance of the packed bed. Exposing dry airflow at a certain Reynolds number to the heated packed bed at 65℃, one can study the transient convective heat transfer between the porous bed and the airflow.

Table 3-1 Properties of the silicagel particles used in the convection transient tests

Particle	Transparent silicagel (Sigma-Aldrich)	Blue silicagel (Fisher Scientific)
Size (*mm*)	$2.36<d_p<2.80$	$1.00<d_p<2.00$
Average diameter (*mm*)	2.58	1.60
Bulk density ($\frac{kg}{m^3}$)	N/A	2200
Pure solid density ($\frac{kg}{m^3}$)	2190 (Sun, 2003)	N/A
Pure solid thermal conductivity ($\frac{W}{m.K}$)	1.00 (Incropera & DeWitt, 2002)	1.00 (Incropera & DeWitt, 2002)
Pure solid specific heat capacity ($\frac{J}{kg.K}$)	700.0 (Incropera & DeWitt, 2002)	700.0 (Incropera & DeWitt, 2002)

3.1.1 Experimental Setup

A compressor (Devilbiss-WAT-5062) supplied the airflow that passed through the particle bed. The airflow was dried by a pre-dryer installed just after the compressor at the beginning of the airflow line. The airflow was then divided into two separate lines: The first line is called the heating line, which sent the airflow through a heater (Omegalux-AHP-7561) to increase and maintain the temperature and then to the entrance of the packed particle bed. The heated air passed through the packed bed until the particles reached steady state conditions, heated thoroughly to the needed temperature (65℃). The second line was the transient test line, which delivered dry airflow at room temperature to the heated packed bed. Each airflow line contained a flow meter (MKS-200 *lpm* for the heating line and 400 *lpm* for the transient test line) and a flow controller to provide the needed flow rate.

A test cell was designed to guide the airflow to the particle bed through an inlet section, hold the silicagel particles as a packed bed, and conduct the airflow out of the packed bed through an outlet section. Figure 3-1 shows a schematic view of the experimental setup in the stage when the packed bed was being heated in order to start the transient test.

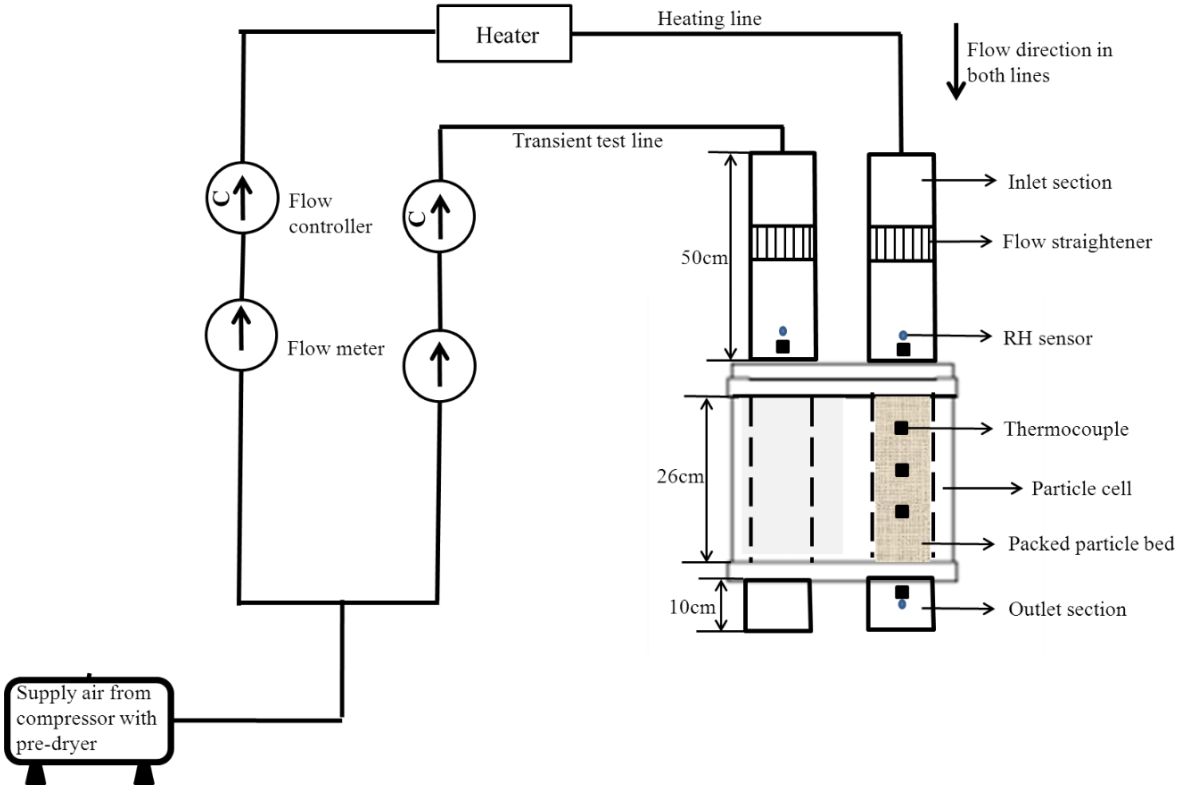

Figure 3-1 A schematic view of the test setup, heating the packed bed before starting the transient test

The test cell consisted of three sections; inlet section, particle cell, and outlet section. The inlet section itself consisted of three different parts: inlet pipes, rotating plate, and clamping plate. Figure 3-2 shows a view of the test cell.

Two PVC inlet pipes with an inner diameter of 101.16 *mm* and a length of 50.00 *cm* were each connected to one airflow line. Therefore, one pipe was for the heated dry airflow and was insulated with 1 *cm* fiberglass insulation, while the other pipe was for the transient test line (dry airflow at room temperature). Each pipe had three flow straighteners installed at the middle of the inside to provide a uniform flow regime to go through the particle bed. A thermocouple and a relative humidity sensor at the end of each pipe measured the temperature and relative humidity of the airflow, respectively.

A rotating plate was attached to the bottom end of the inlet pipes. This plate was connected to a clamping plate with a pin. 4 *inches* (101.16 *mm*) in diameter holes on both the rotating and clamping plates let the designated airflow go through the particle cell. The pin connection let the rotating plate rotate freely on the clamping plate between two stop signs

180 degrees apart. This rotation, which took less than 1 second, allowed a temperature step change to start the transient test. Four tall bolts fastened the clamping plate to the experiment table so it could hold the inlet section, particle cell, and outlet section tightly together when the test cell was assembled on the table.

The particle cell was a polystyrene insulation block with two identical cylindrical spaces that could be assembled in line with the inlet pipes in the test cell. The one on the left was the particle bed, which had a thin stainless steel screen at the exit to hold silicagel. The one on the right provided a by-pass for the airflow not directed to the particle bed at a given moment. Each cylinder had the same diameter as the inner diameter of the inlet pipes (101.16 *mm*), and the height of the particle cell (26 *cm*). The polystyrene block with these two cylindrical spaces, provided a 2 *cm* insulation guard around the packed bed while the surface of the particle bed was covered with aluminum foil. Therefore, the particle bed was an adiabatic and impermeable porous bed.

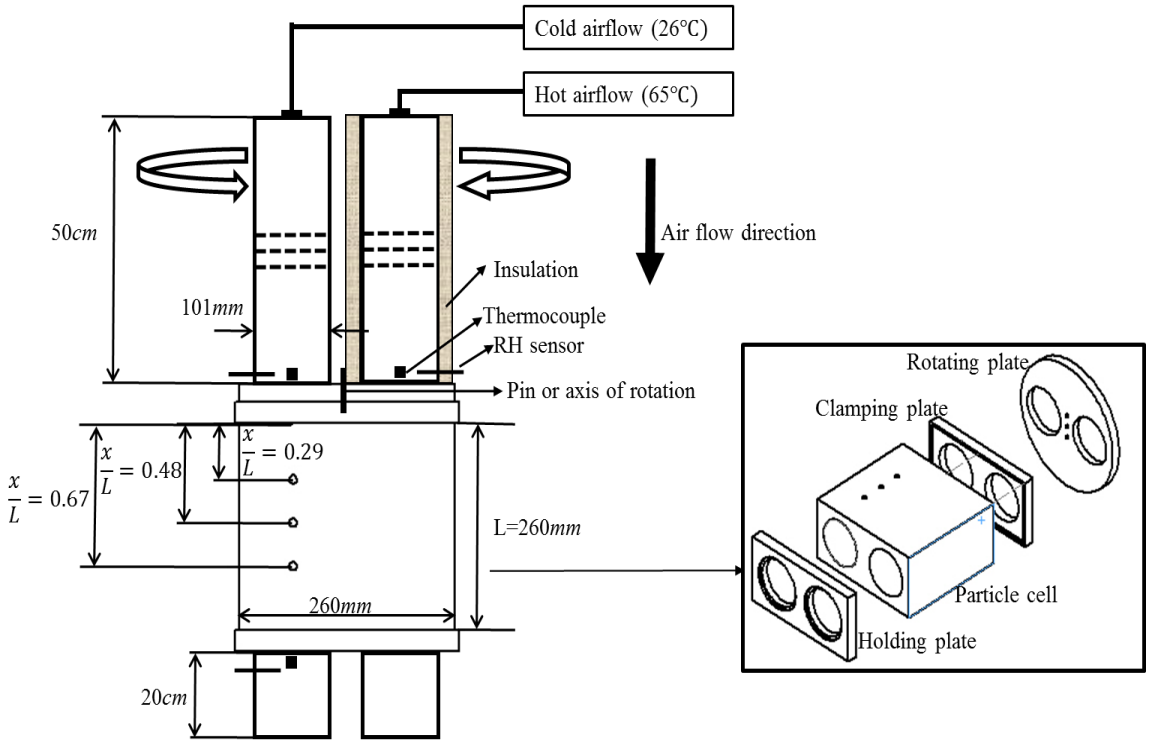

Figure 3-2 Schematic view of the test cell; inlet section, particle cell, outlet section, positions of the temperature and relative humidity sensors.

Three sets of T-type thermocouples (outer diameter of 2 *mm*), each set consists of three thermocouples, were installed in three different axial positions in the particle bed. The packed bed was accessible through three sides of the polystyrene block, so for each selected height one hole was drilled in the block on each side to be able to install the thermocouples and access them whenever necessary. On each side, the centers of the holes were aligned in the axial direction. Therefore, thermocouples in each set had the same axial coordinate while distributed randomly in radial coordinate.

The outlet section consisted of two PVC pipes attached to a PVC plate. The outlet section plate was mounted on the experiment table which had a hole to let the outlet pipes have an unblocked end. The particle cell and the inlet section could be assembled on the outlet section. Two outlet pipes guided the exiting air flows out of the particle cell. A thermocouple and a relative humidity sensor were installed at the beginning of the left outlet pipe, which was aligned with the particle cell, to measure the temperature and relative humidity of the airflow coming out of the particle bed.

3.1.2 Experimental procedure

The transient convection test involved heat transfer from the dry heated packed bed of silicagel particles to the dry airflow at room temperature, which passed through the packed bed at a certain Reynolds number. This convective heat transfer started with a temperature step change at the airflow passing through the particle bed. Before starting the experiment, the particle bed was fully filled with clean and dry silicagel particles. Properties of the particle bed for each type of silicagel particles are listed in Table 3-1. Interested readers can refer to Appendix 2 for details about finding the physical properties.

The experimental process included the following steps:

- Turned on the compressor. The dry airflow started to go through the heated and transient test lines.
- Lined up the transient test flow line with the particle bed by using the rotating plate to keep the particles in dry condition.
- Adjusted the flow rate at 150 *lpm* in the heating line.
- Turned on the heater and adjusted the power to 75 *V*.

- Waited for the airflow in the heating line to reach to 65℃.
- Turned the rotating plate to expose the particle bed to the heated airflow.
- Waited three hours for the particle bed to be heated and have a uniform temperature all along the bed.
- Adjusted the airflow in the transient test line to have needed Reynolds number.
- Turned the rotating plate 180 degrees to have a temperature step change and start the transient heat transfer test.
- Recorded the temperature change at three different positions in the particle bed during the transient test.
- Waited for the particle bed to reach steady state conditions, which was having the same temperature as the inlet dry airflow at room temperature.

3.2 Direct Problem Solution

Transient heat transfer between a heated, randomly packed bed of silicagel particles and a dry airflow at room temperature was simulated numerically. This numerical simulation can be used in IHTP analysis in order to estimate the convective heat transfer coefficient of the silicagel particle bed. Assumptions must be applied in order to develop the governing equations and boundary conditions, so the transient convective heat transfer can be modeled.

3.2.1 Assumptions

Applied assumptions the simulation are listed in the following:

1- It is assumed that the packed particle bed is a homogeneous porous medium, which means that there is no difference in physical properties of any two arbitrarily chosen positions in the packed bed.

2- It is assumed that the packed bed is an isotropic porous medium, which means it has identical values of properties no matter which direction it is.

3- Silicagel particles are porous particles, so each particle consists of two phases: a pure solid phase (SiO_2), and an internal gaseous phase in the internal pores. The small thermal capacity of the internal gaseous phase in comparison with the thermal capacity of the pure solid phase ($\frac{(1-\varepsilon_i)\rho_{silica}C_{p_{silica}}}{\varepsilon_i\rho_g C_{p_g}} = 1717$) makes the energy storage in the internal gaseous phase negligible in comparison with the pure solid phase. Therefore, it is assumed that the internal gaseous phase and the pure solid phase are in quasi-equilibrium with each other during the transient test. As a result, they can be volume-averaged together.

It can be concluded that the heat transfer happens in two main domains of the particle bed: the solid phase, which consists of the pure solid (SiO_2) phase-internal gaseous phase, and the external gaseous phase, which is the air flowing through the available voids between the particles. Figure 3-3 shows a view of these two phases. Also, the heat transfer between the solid phase and gaseous phase happens in the form of convection at the external surface of the particles, which is the interface between the solid domain and external gaseous domain.

4- It is assumed that the external gaseous phase behaves as an ideal gas at atmospheric standard pressure (101 *kPa*). Also, the external gaseous phase is a continuous isotropic phase.

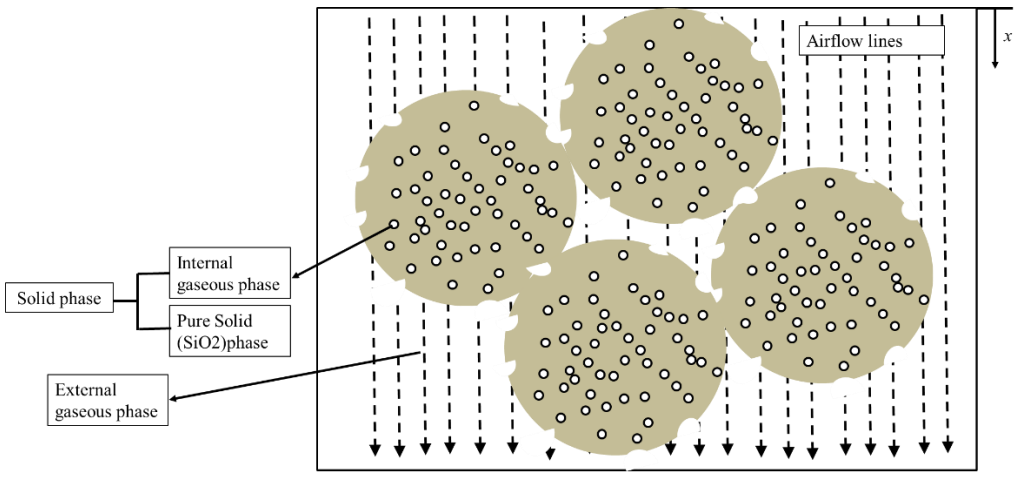

Figure 3-3 A schematic view of the involved phases in the randomly packed bed of silicagel particles.

5- A 2 *cm* polystyrene guard around the particle bed made the heat transfer from the particle bed to the surrounding environment negligible. As a result it is assumed that the particle bed is adiabatic and impermeable.

6- For the spherical particle bed the entrance (or exit) effect is in the size of one particle diameter (Kaviany, 1995). Considering the length of the packed bed (L=26 *cm*) and the particle diameter (d_p =2.58 *mm*), $\frac{d_p}{L} = 0.01 \ll 1$ is small enough to ignore the entrance effect in the particle bed. Also, for the spherical mono- sized particle bed the wall effect occurs in the half particle diameter distance from the wall (Ismail et al., 2002). Considering the diameter of the cylindrical particle bed (D=101.16 *mm*), the non-uniformities of the flow regime due to the wall effects can be neglected.

7- Each silicagel particle is considered as a sphere. The Biot number of a spherical particle is calculated as

$$Bi_{d_p} = h_t({}^{d_p}/_{6})/k_p \qquad (3.1)$$

where h_t is the convective heat transfer coefficient, $\frac{d_p}{6}$ is the volume to surface area ratio for a spherical particle, and k_p is the thermal conductivity of the particle. Considering the particle bed as a mixture of solid phase and internal gaseous phase in thermal equilibrium, the thermal conductivity can be calculated as (Kaviany, 1995)

$$k_p = \varepsilon_i k_g + (1 - \varepsilon_i) k_{silica} \qquad (3.2)$$

where k_g and k_s are thermal conductivity of the pure (SiO_2) solid phase and gaseous phase, respectively. The convective heat transfer coefficient can be calculated by using the correlation introduced by Nie et al. (2011)

$$\frac{Nu_{d_h}}{Pr^{1/3}} = (0.0491 \pm 0.0236) Re_{d_h}^{(0.8572 \pm 0.0937)} \qquad (3.3)$$

where Nu_{d_h} is the Nusselt number based on the hydraulic diameter, Pr is the Prandtl number, and Re_{d_h} is the Reynolds number based on the hydraulic diameter. Considering the highest Reynolds number used in the tests and the highest corresponding Nusselt number in (3.3), the biggest possible Biot number for the largest particle size ($d_p = 2.58\,mm$) is 0.01, which is smaller than 0.1. Therefore, it can be assumed that each silicagel particle has a uniform temperature distribution.

8- It is assumed that at each time node the solid phase (porous particle) and the external gaseous phase had a temperature difference less than 1 *K* with each other. The validity of this assumption increases by moving from the inlet (top of the particle bed) to the bottom. Also, the validity of this assumption increases as the time goes in the transient test. Therefore, it can be assumed that the thermocouples measured the temperature of the solid phase during the transient test.

9- Silicagel particles were heated in the oven for 24 hours before the experiment to be completely dried. Furthermore, a pre-dryer at the exit of the compressor decreased the relative humidity of the airflow to less than 5%. Therefore, it can be assumed that there was no moisture transfer between the airflow and the particle bed and only heat transfer was happening in the particle bed. Also, two relative humidity sensors, one at the inlet and the other at the exit of the particle bed, recorded the relative humidity of the airflow. Figure 3-4 shows the relative humidity changes of the airflow versus time at the inlet and outlet of the particle bed. As can be seen, the relative humidity both at the inlet and outlet was less than 5% at all times.

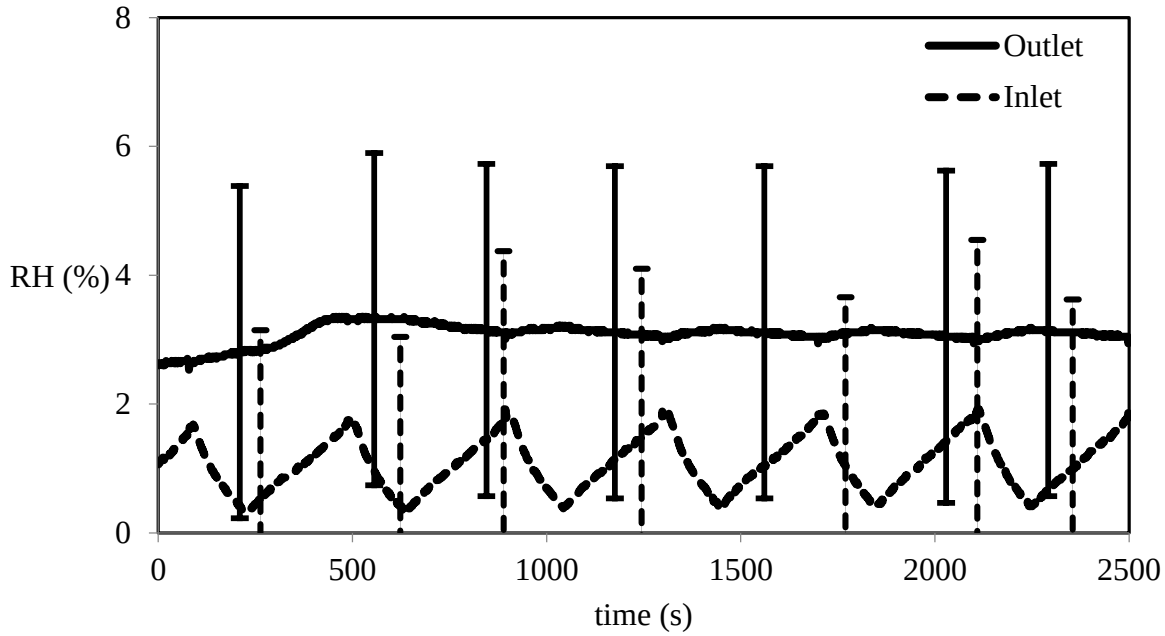

Figure 3-4 Relative humidity changes of the airflow versus time at the inlet and outlet of the dry packed bed of the silicagel particles ($d_p = 2.58mm$), Re_{d_h}=82, $T_{bed|0}$=65℃, $T_{air|inlet}$=25℃.

10- It is assumed that the main energy transfer between the airflow and the particle bed was happening in the flow direction (axial direction), *x*, and there was no heat transfer in the radial direction. As mentioned before, three different positions along the particle bed were chosen in order to record the temperature changes. Three thermocouples at each height were distributed randomly to record the temperature at each height.

Figure 3-5 shows the radial position of the thermocouples that were at the same height ($\frac{x}{L} = 0.48$) during the transient test, and Figure 3-6 shows their corresponding temperature profiles. As can be seen, temperature recordings are in the uncertainty bounds of each other which agrees with the assumption of no radial heat transfer in the particle bed.

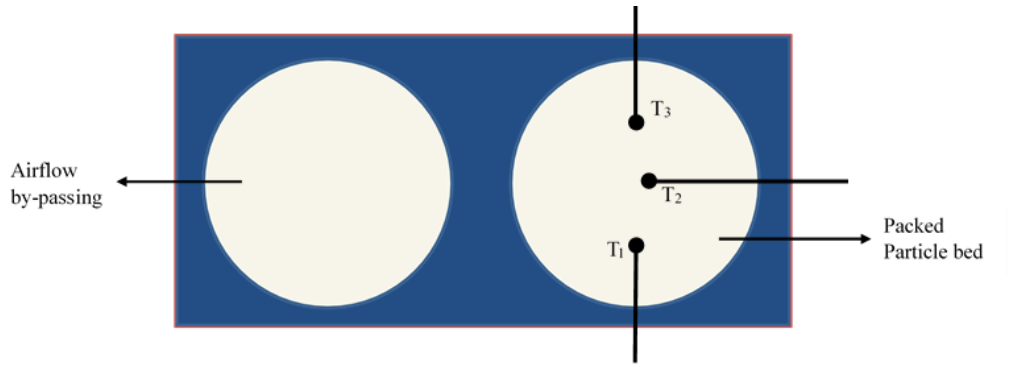

Figure 3-5 Schematic view of the cross section of the particle cell at $\frac{x}{L} = 0.48$ with the randomly distributed thermocouples (T_1, T_2, and T_3) at this height.

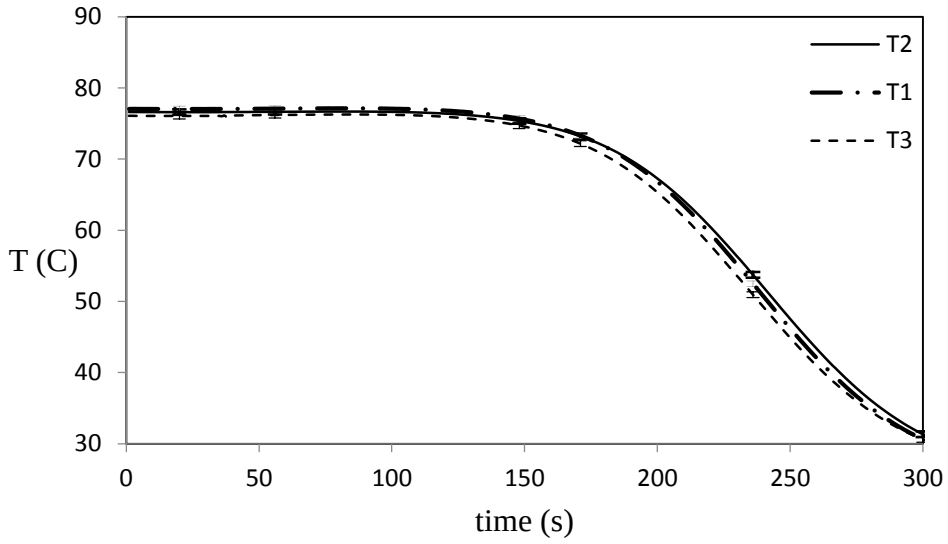

Figure 3-6 Temperature profiles of the three thermocouples shown in Figure 3-5 for the first 300s of the transient test, dry packed bed of the silicagel particles ($d_p = 2.58mm$), Re_{d_h}=73.47, $T_{bed}|_0$=65℃, $T_{air}|_{inlet}$=25℃.

3.2.2 Governing equations

The direct problem must be numerically solved in order to be used in the inverse analysis. As mentioned before, the direct problem is convective heat transfer between the solid phase (pure solid (SiO_2) phase and the internal gaseous phase) and the external gaseous phase, which is the available voids between the silicagel particles. Applying the porous media

theory (Kaviany, 1995) and the assumptions that were made in the previous section, the governing equation are listed as follows:

A. Energy transfer in the solid phase

Heat transfer between the heated solid phase and the external gaseous phase at room temperature was in the form of convection. Also, the heat transferred in the solid phase in the form of conduction. Therefore, the energy transfer equation for the solid phase is

$$\frac{\partial}{\partial t}\left(\rho_s C_{p_s}(1-\varepsilon_e)T_s\right) = \frac{\partial}{\partial x}\left(k_{eff,s}\frac{\partial T_s}{\partial x}\right) + A_{sf,v}h_t\left(T_{g,e}-T_s\right) \quad (3.4)$$

where ρ_s is the effective density of the solid phase ($\frac{kg}{m^3}$), C_{p_s} is the effective specific thermal capacity of the solid phase ($\frac{J}{kg.K}$), $k_{eff,s}$ is the effective thermal conductivity of the solid phase ($\frac{W}{m.K}$), and ε_e is the external porosity of the packed particle bed (Appendix B). Also, T_s is the temperature of the solid phase (*K*), $T_{g,e}$ is the temperature of the external gaseous phase (*K*), $A_{sf,v}$ is the specific external surface area per unit volume of the silicagel particles ($\frac{m^2}{m^3}$) (Appendix B), and h_t is the convective heat transfer coefficient of the spherical silicagel particle bed ($\frac{W}{m^2K}$) which is considered as the unknown parameter, and will be found by using the IHTP analysis. *x*(*m*) and *t*(*s*) represent the axial position and time, respectively.

Kaviany (1995) introduced equations to calculate the theoretical values of the effective heat capacity and effective density of a porous medium, which can be used to calculate the density and heat capacity of the solid phase.

$$\rho_s = (1-\varepsilon_i)\rho_{silica} + \varepsilon_i\rho_{g,i} \quad (3.5)$$

$$C_{p_s} = \left[(1-\varepsilon_i)C_{p_{silica}}\rho_{silica} + \varepsilon_i\rho_{g,i}C_{p_g}\right]/\rho_s \quad (3.6)$$

ρ_{silica} and $C_{p_{silica}}$ are the density and the specific thermal capacity of the pure silica, respectively. Also, ε_i is the internal density of the silicagel particles which can be calculated

by using the information obtained from the BET analysis (Appendix B). $\rho_{g,i}$ and $C_{p_{g,i}}$ are the density and the specific thermal capacity of the gaseous phase, respectively. As mentioned before, the pure solid phase and the internal gaseous phase were in thermal equilibrium with each other. Thermal capacity of the dry gaseous phase can be considered as the thermal capacity of the dry air at room temperature which is $1005\frac{J}{kg.K}$ (Incropera & DeWitt, 2002). Applying the ideal gas law for the internal gaseous phase, one can find the density of the internal gaseous phase as

$$\rho_{g,i} = \frac{P}{R\,T_s} \tag{3.7}$$

where R is the ideal gas constant which is $287(\frac{J}{kg.K})$.

Thermal conductivity of the silicagel particles can be found by using the correlation introduced by Tavman (1996) for a randomly packed particle bed.

$$k_{eff,s} = k_{silica}^{(1-\varepsilon_i)} k_g^{\varepsilon_i} \tag{3.8}$$

where k_s is the thermal conductivity of the pure solid phase. Also, k_g is the thermal conductivity of the dry air at room temperature which is $0.0257\frac{W}{m.K}$ (American Society of Heating & Air-Conditioning, 1985).

B. Energy transfer in the external gaseous phase

When airflow at room temperature and at a certain Reynolds number passed through the particle bed, convection heat transfer happened at the interfacial surface area between the gaseous phase and the silicagel particles. Considering that the external gaseous phase was a continuous phase and ignoring the conductive heat transfer in comparison with the convective heat transfer in this phase (because of the small value of thermal conductivity of dry air), it can be concluded that the change in the energy level of the external gaseous phase is mainly due of the convection.

Assuming a control volume around the gaseous phase, the energy transfer in the gaseous phase is

$$\frac{\partial}{\partial t}\left(\rho_{g,e} C_{p_{g,e}} \varepsilon_e T_{g,e}\right) + \frac{\partial}{\partial x}\left(\rho_{g,e} C_{p_{g,e}} U_d T_{g,e}\right) = A_{sf,v} h_t \left(T_s - T_{g,e}\right) \qquad (3.9)$$

where $T_{g,e}$ is the temperature of the external gaseous phase, $C_{p_{g,e}}$ is the specific heat capacity of the dry air at room temperature, and U_d is the interfacial velocity of the airflow. Considering the external gaseous phase as an ideal gas, its density ($\rho_{g,e}$) is

$$\rho_{g,e} = \frac{P}{R\, T_{g,e}} \qquad (3.10)$$

C. Boundary conditions

Airflow entered the packed particle bed in a specific constant Reynolds number and at room temperature, recorded as 25℃. Therefore, the temperature of the external gaseous phase at the inlet was equal to the temperature of the inlet air, which stayed constant during the transient test. Also, it is assumed that there was no heat conduction for the silicagel particles at the inlet of the particle bed, which means the temperature gradient of the solid phase at the inlet of the particle bed was zero.

$$x = 0: \quad \frac{\partial T_s}{\partial x} = 0 \qquad (3.11)$$

$$x = 0: \quad T_{g,e} = T_{inlet} \qquad (3.12)$$

It is assumed that there was no heat flux in either the gaseous phase or the solid phase at the outlet of the packed particle bed (x=L), so the temperature gradient at this position for both phases was zero.

$$x = L: \quad \frac{\partial T_s}{\partial x} = 0 \tag{3.13}$$

$$x = L: \quad \frac{\partial T_{g,e}}{\partial x} = 0 \tag{3.14}$$

D. Initial conditions

It is assumed that both airflow and packed particle bed were dry at the beginning and during the transient test. Also, both phases were in steady state conditions at the beginning of the transient test.

$$t = 0: \quad T_s = 65℃ \tag{3.15}$$

$$t = 0: \quad T_{g,e} = 25℃ \tag{3.16}$$

3.3 Direct Problem Simulation Method

The nonlinear, coupled partial differential equations must be discretized in order to develop a numerical code in Matlab (Appendix C). All the known and unknown parameters must be defined as two dimensional vectors (in time and axial position) in the Matlab program. A time step of 1.00 *s* with 1001 total time grids (1000 *s* by considering the first time grid for initial conditions, t=0), and a grid mesh of 2.6 *mm* with 101 total grid points were used in the simulation. The first grid point is considered as the inlet boundary (x=0), and the last grid point is considered as the outlet boundary(x=260 *mm*).

The energy equations of the solid phase and the gaseous phase leave the main unknown variables in the numerical direct problem as temperature of the gaseous phase ($T_{g,e}$), and temperature of the solid phase (T_s). Secondary unknown variables that can be estimated based on the primary unknown variables are: density of the gaseous phase ($\rho_{g,e}$),

density of the solid phase (ρ_s), density of the internal gaseous phase ($\rho_{g,i}$), and specific heat capacity of the solid phase (C_{p_s}). Furthermore, the "known" parameters are: total porosity of the particle bed (ε), internal porosity of the particle bed (ε_i), external porosity of the particle bed (ε_e), total pressure of the gaseous phase (P), thermal conductivity of the solid phase ($k_{eff,s}$), specific heat capacity of the gaseous phase ($C_{p_{g,e}}$), and specific external surface area per unit volume of the silicagel particles ($A_{sf,v}$). The convective heat transfer coefficient (h_t) is the estimated value at each iteration of IHTP analysis.

An iteration method was used to find the temperature distribution in the particle bed at each time. Starting from the first time node, initial conditions were assumed as the first guess for the temperature vector. Estimating secondary unknown variables and applying the known parameters, a new estimation for the temperature vector can be obtained. A relaxation factor is defined in order to modify the new estimation at each iteration and speed up the convergence:

$$T|^{k+1} = T|^{k} + R_{factor} \times (T|_i^{k+1} - T|^{k}) \qquad (3.17)$$

where R_{factor} is the relaxation factor, equal to 0.1, $T|^{k}$ is the temperature vector in the previous iteration (k), $T|^{k+1}$ is the temperature vector in the current iteration (k+1), and $T|_i^{k+1}$ is the temperature vector obtained from the vector solver in the current iteration.

The convergence of the iteration procedure of estimating the temperature distribution in the particle bed can be examined by using a convergence criterion defined as

$$\left|\frac{T|^{k+1} - T|^{k}}{T|^{k}}\right| < Covergence\ Criterion \qquad (3.18)$$

where *k+1* and *k* are the previous iteration and current iteration, respectively, and the convergence criterion is considered as 10^{-5}. When the convergence criterion is satisfied, the estimation of the temperature profile is acceptable, so the iteration process for the temperature distribution of the particle bed at the next time node can be started.

The estimated temperature distribution was used as the initial guess to start the iteration procedure to guess the temperature distribution at the next time step. Following the same process of iteration, estimating the secondary unknown variables and applying the known parameters, estimation for the temperature distribution was calculated and the iteration process continued until it satisfied the convergence criterion. Therefore, the temperature profile at any position of the packed bed during the transient test can be simulated. Figure 3-7 shows the algorithm used in the direct solution of convective heat transfer in the randomly packed bed of silicagel particles.

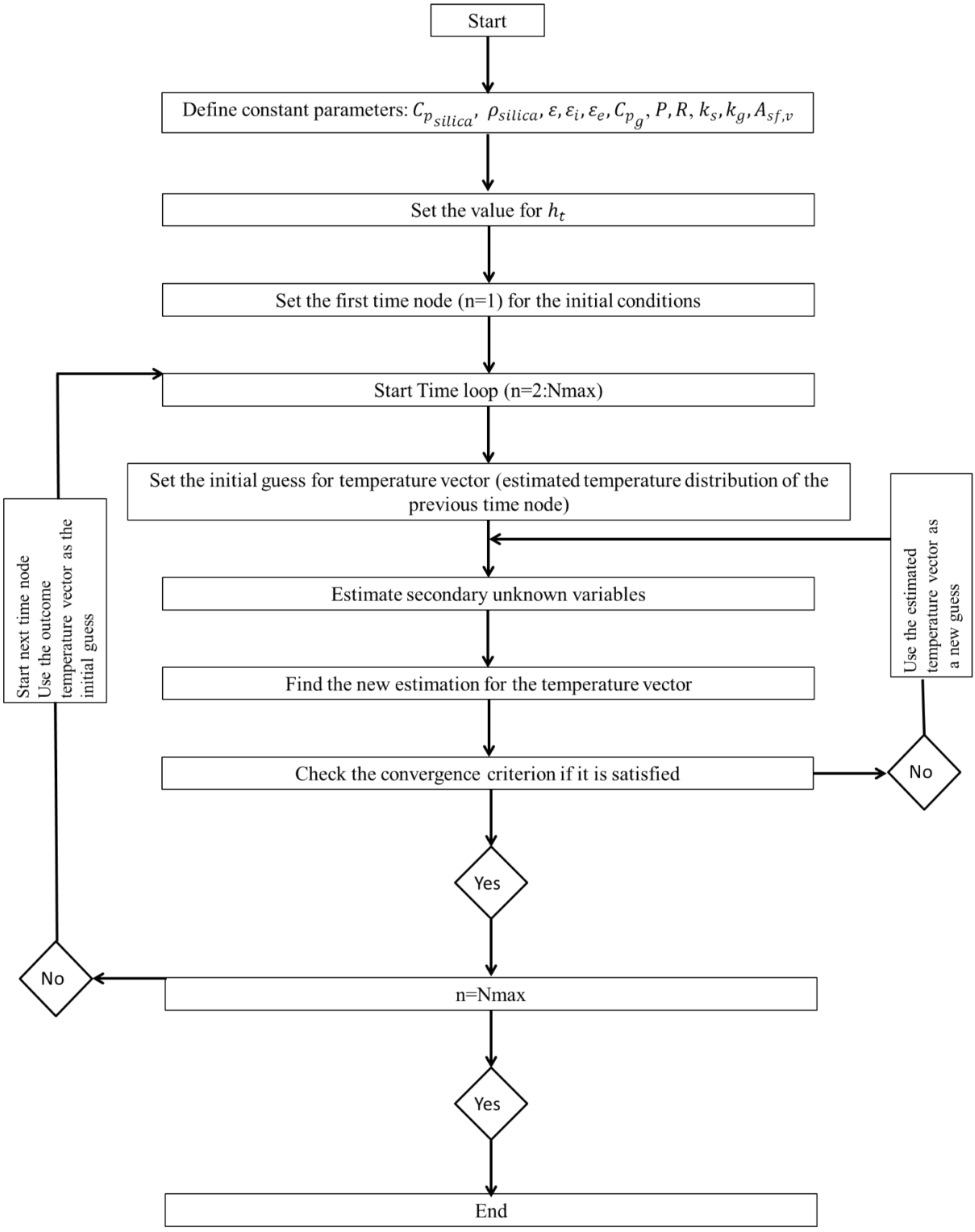

Figure 3-7 Matlab Algorithm used to solve the direct problem

3.4 Inverse Problem Simulation

Three different axial positions were available that could be used as the measured temperature vector in the inverse solution. Sensitivity of the unknown parameter (h_t) to each of these sensors must be studied in order to find the sensor that yields the best measurement. Sensitivity coefficients of each sensor were calculated versus time at each desired Reynolds number. The convective heat transfer coefficient, which is required in the direct problem in order to find the sensitivity coefficient, was calculated using equation (3.3). Figure 3-8 shows the sensitivity coefficients of the temperature sensors for the transparent silicagel particle bed in a typical Reynolds number.

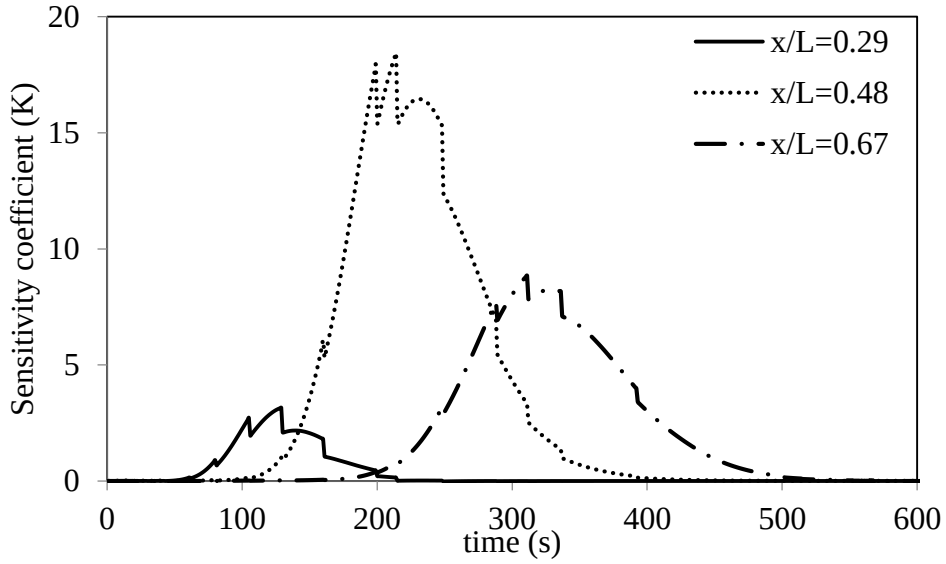

Figure 3-8 Sensitivity coefficients of the temperature sensors, dry packed bed of the transparent silicagel particles ($d_p = 2.58\ mm$), Re_{d_h}=58.80, $T_{bed}|_0$=65℃, $T_{air}|_{inlet}$=26℃.

The best sensor for the IHTP analysis is one with the highest sensitivity coefficients. A sensitivity coefficient is considered high if it deviates from zero with a magnitude greater than 1(Raynaud, 1999). Among these three sets of sensors, the one at the middle of the particle bed ($\frac{x}{L}$=0.48) had the highest sensitivity coefficients over a time period that covers the time ranges when the sensitivity coefficients of the two other sensors were large. Therefore, the thermocouple set at the middle of the packed bed could be used to provide the measured temperature vector in the IHTP analysis. The two other sensors could still be used to compare

the experimental temperature distribution with the numerical temperature distribution, calculated using the estimated unknown parameter, in order to examine the validity of the IHTP analysis. The same conclusion was obtained for the other desired Reynolds numbers used in the transient tests.

Figure 3-9 shows the sensitivity coefficients of the thermocouple sets for the packed bed of blue silicagel particles, and illustrates that similar to the transparent silicagel bed, the thermocouples set at the middle of the bed made the best sensor for IHTP analysis.

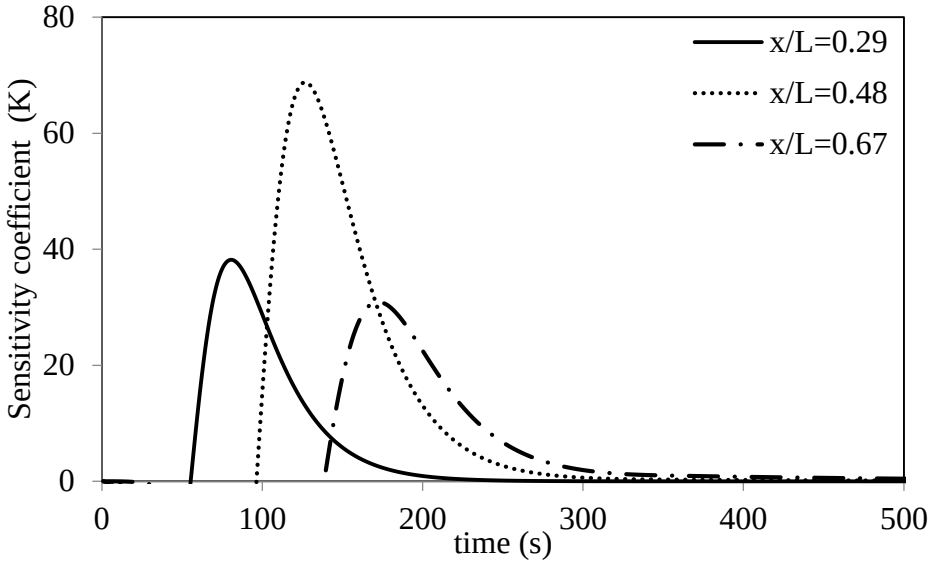

Figure 3-9 Sensitivity coefficients of the temperature sensors, dry packed bed of the blue silicagel particles ($d_p = 1.60\ mm$), Re_{d_h}=62.1, $T_{bed}|_0$=65℃, $T_{air}|_{inlet}$=26℃.

The time period of the transient test, which must be considered for the IHTP analysis, can be found by analyzing the determinant of the sensitivity matrix (CHAPTER 2). Figure 3-10 illustrates the determinant of the sensitivity matrix versus time for the temperature sensor at $\frac{x}{L} = 0.48$, which is the one to be used in the inverse solution. Clearly, the determinant of the sensitivity matrix increases with time and, as expected, with the increase in the number of measurements due to additional information for estimating the unknown parameter. On the other side, the greatest increase in the determinant happened in the first 400*s* of the transient test. As a result, this became the most suitable duration for use in the inverse solution, since the value of the determinant had already become reasonably large and this duration was not too long. The same result can be concluded for the randomly packed bed of blue silicagel particles as well.

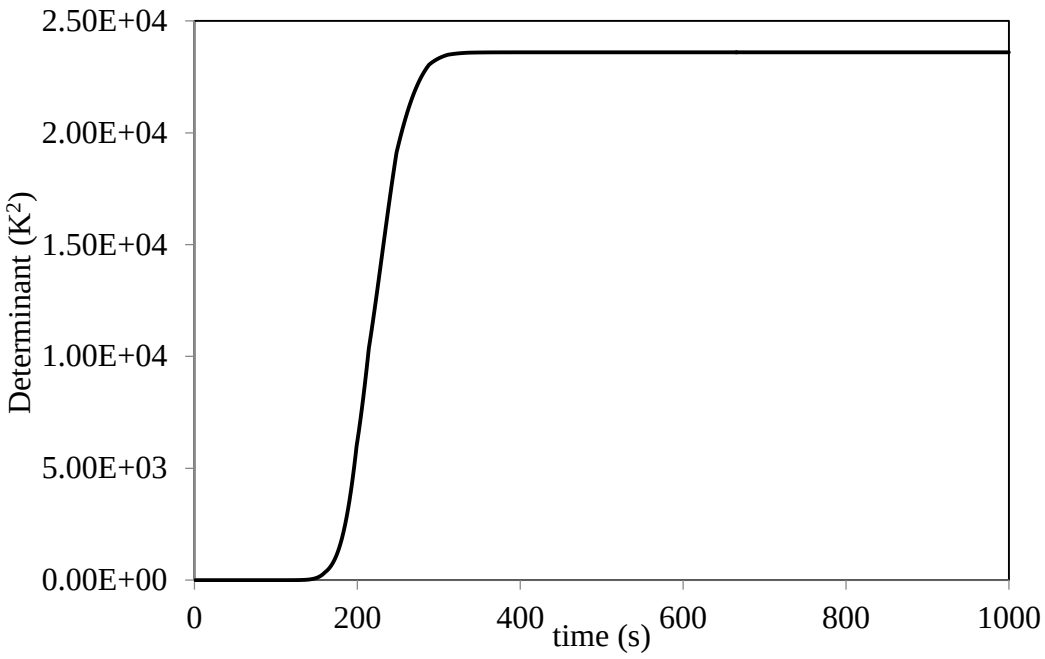

Figure 3-10 Determinant of the sensitivity matrix versus time, dry packed bed of the transparent silicagel particles ($d_p = 2.58mm$), Re_{d_h}=58.80, $T_{bed}|_0$=65℃, $T_{air}|_{inlet}$=26℃.

The convective heat transfer coefficient is estimated by using the Levenberg-Marquardt IHTP method. The first estimation of the unknown parameter is calculated from equation (3.3) in each specific Reynolds number. The iteration method explained in CHAPTER 2 is applied for this non- linear inverse problem. Considering $0.5\,K$ as the maximum accepted residual to ensure the agreement between measured temperature and simulated temperature at each time, and a typical 400 temperature recordings, the stopping criteria used to check the convergence and accuracy of the iteration are

- Objective function (S)<100 K^2
- IHTP Convergence criterion=0.001.

CHAPTER 4 IHTP RESULTS OF COVECTIVE HEAT TRANSFER COEFFICIENT

Transient heat transfer between a dry heated packed bed of silicagel particles and dry airflow at room temperature was studied at different Reynolds numbers. Convection was the dominant form of heat transfer between the particles and the airflow passing through the packed bed. Using the convective heat transfer coefficient of the packed bed (h_t) as the unknown parameter, a numerical model was developed to simulate the transient convective heat transfer test, and then IHTP analysis was applied to estimate the unknown parameter based on minimizing the difference between the experimental and numerical temperature distribution in the packed bed.

Estimated h_t was used to simulate temperature distribution in the packed bed in two different axial positions during the transient tests. Numerical results were compared with the experimental outcomes to check the stability of the IHTP estimation.

Furthermore, a new correlation between the Nusselt number based on the hydraulic diameter and Reynolds number based on the hydraulic diameter was investigated, and comparison between the new correlation and the previous correlations was made in order to examine the validity of the correlation.

4.1 IHTP Analysis Result

Two types of particles were used in the packed bed to perform the transient convection heat transfer tests (Table 3-1). The convective heat transfer coefficient was estimated for each type of particle bed in the possible range of Reynolds numbers.

A Reynolds number based on hydraulic diameter can be calculated as

$$Re_{d_h} = \frac{U_p d_h}{\nu} \tag{4.1}$$

where Re_{d_h} is the Reynolds number base on hydraulic diameter, $U_p = \frac{U_D}{\varepsilon_e}$ is the pore velocity ($\frac{m}{s}$) in which U_D is the interfacial velocity of the airflow (m) , d_h is the hydraulic diameter (m), and ν is the kinematic viscosity of dry air, which is assumed as$15.68\times10^{-6}\,\frac{m^2}{s}$ at room temperature.

The hydraulic diameter of the porous bed is

$$d_h = \left[\frac{2\varepsilon_e}{3(1-\varepsilon_e)}\right] d_p \qquad (4.2)$$

where ε_e is the external porosity of the packed bed and d_p is the particle diameter (m).

Table 4-1 lists the range of the flow rates in which the transient tests were performed for each type of the particle bed.

The transient temperature profile at $\frac{x}{L} = 0.48$ was used as the measurement vector in the IHTP analysis. The convective heat transfer coefficient of the packed bed was estimated for each Reynolds number by minimizing the objective function, which is the difference between the measured temperature profile and the simulated temperature profile. The best estimation of the convective heat transfer coefficient was obtained when the objective function was less than the criterion chosen for the objective function ($100K^2$) in the inverse analysis.

Table 4-1 Facial velocity, flow rate, and hydraulic Reynolds numbers which were used in the convective transient tests for each type of the particle bed.

Volumetric flow rate (lpm)	Face velocity ($\frac{m}{s}$)	Re_{d_h}	Relative Uncertainty, $\frac{U(Re_{d_h})}{Re_{d_h}}$ (%)	Re_{d_h}	Relative Uncertainty, $\frac{U(Re_{d_h})}{Re_{d_h}}$ (%)
		Transparent silicagel particles ($d_h = 0.85mm$)		Blue silicagel particles ($d_h = 1.67mm$)	
320	0.666±0.008	109	54	116	14
280	0.583±0.008	96	54	102	14
240	0.500±0.008	82	54	87	14
200	0.416±0.008	68	54	73	14
160	0.333±0.008	55	55	58	14
120	0.250±0.008	41	55	44	15

Table 4-2 lists the estimated convective heat transfer coefficient at each Reynolds number for the transparent silicagel particles. Also, the objective function and the convergence error are listed in each case.

Table 4-2 Estimated value of convective heat transfer coefficient and its relative IHTP uncertainty, objective function of inverse analysis and convergence error of inverse analysis for each flow rate, packed bed of transparent silicagel particles, $T_{bed}|_0$=65℃, $T_{air}|_{inlet}$=26℃.

Reynolds number (Re_{d_h})	h_t ($\frac{W}{m.K}$)	U(h_t)/h_t (%)	Objective function (K^2)	Convergence error
41	15.69	1.32	89	0.0001
55	18.88	1.67	87	0.0001
68	29.39	1.12	94	0.0001
82	50.26	1.96	96	0.0001
96	58.72	1.03	95	0.0001
109	70.68	1.12	30	0.0001

As illustrated, an increase in the volumetric flow rate resulted in a higher convective heat transfer coefficient in the packed bed because of the higher rate of heat transfer between the silicagel particles and airflow. This result is in agreement with Nie et al. (2011) who found the convective heat transfer coefficient for a packed bed of urea particles at different Reynolds numbers. Furthermore, the values of the objective function for each flow rate are in the acceptable range (less than $100K^2$). Relative uncertainty of the convective heat transfer coefficient represents the effect of the measurement errors on the estimated value.

Figure 4-1 to Figure 4-6 show the normalized temperature distribution in the packed bed for the transient tests and their corresponding numerical model at each Reynolds number. The estimated values of convective heat transfer coefficient, obtained from IHTP, were used in the simulation. Normalized temperature is defined as

$$T_{normalized}|_i = \frac{T_i - \mathrm{T_{air}}|_{\mathrm{inlet}}}{T_{bed}|_0 - \mathrm{T_{air}}|_{\mathrm{inlet}}} \qquad (4.3)$$

where T_i is the temperature at *t*=*i* in the particle bed at each position (*K*), $T_{bed}|_0$ is the initial temperature of the packed bed (65℃), and $T_{air}|_{inlet}$ is the temperature of the inlet airflow (26℃).

As shown, the temperature of the solid phase decreased during the transient test because of the convective heat transfer between the packed bed and the dry airflow. By moving from the inlet (top) to the outlet (bottom) of the packed bed, the time needed to begin a visible transient temperature change increased. Furthermore, as the Reynolds number (flow rate) of the airflow increased, the time required for the transient test decreased because of the higher convective heat transfer rate.

As the flow rate got further from the upper and lower bounds of the range of the flow meter (Re_{d_h}=109 as maximum, and Re_{d_h}=41 as minimum), the agreement between the numerical and experimental results grew because of the reduced possibility of errors in the flow measurement.

Also, the strongest agreement between experimental and numerical temperature profiles for each axial position happens during the rapid temperature change ($0.4<T_{normalized}|_i<0.8$), because thermocouples have higher sensitivity coefficients in comparison with the rest of the transient test. Obviously, in the rest of the transient test deviation between the simulated temperature profile and experimental temperature profile does not play a key role in the IHTP estimation of convective heat transfer coefficient.

There is less agreement between the experimental and numerical temperature profiles for $\frac{x}{L} = 0.67$ because of the increase in the value of possible error sources such as heat loss in the packed bed.

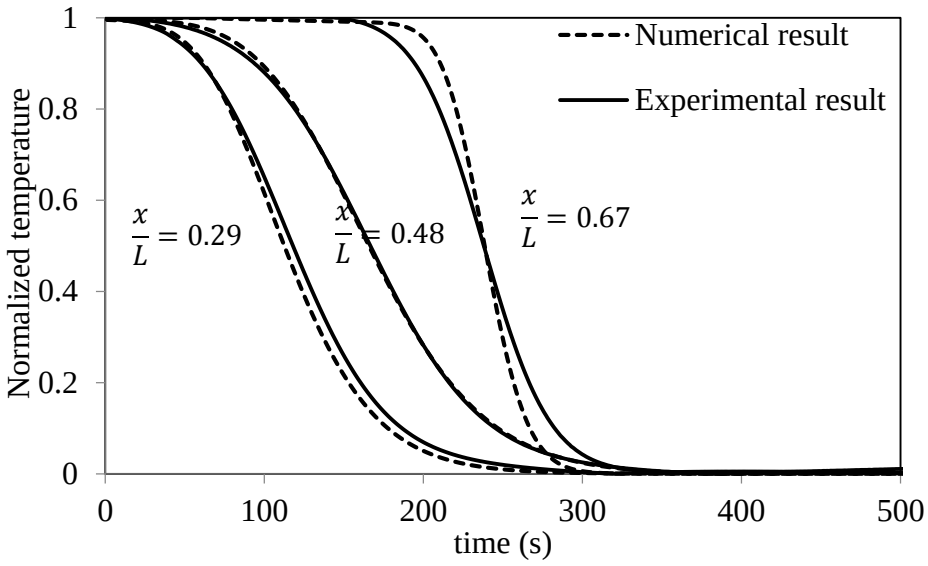

Figure 4-1 Experimental and numerical temperature distribution in three different axial positions in the packed bed, Transparent silicagel particles, Re_{d_h}=109, 2.36*mm*<d_p<2.80*mm*, $T_{bed}|_0$=65℃, $T_{air}|_{inlet}$=26℃.

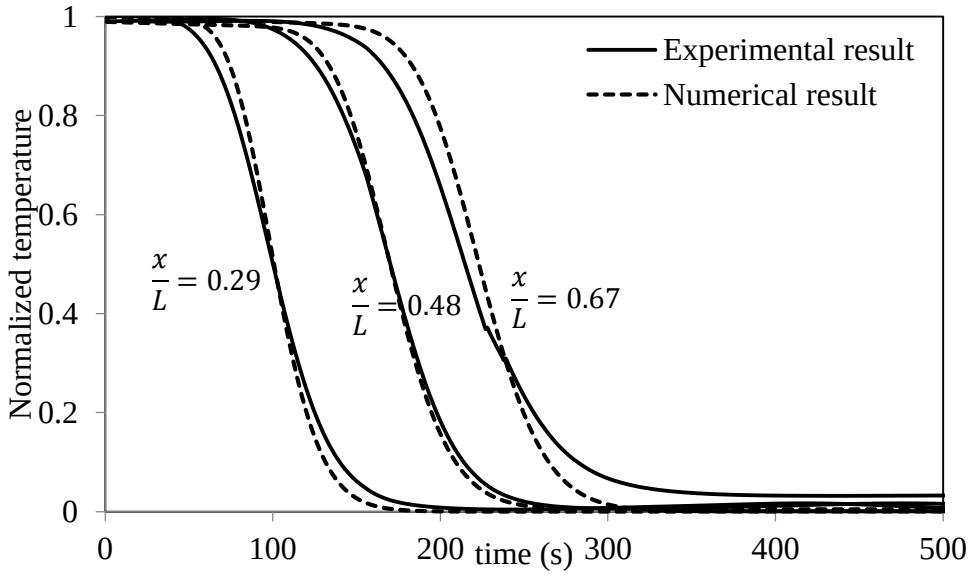

Figure 4-2 Experimental and numerical temperature distribution in three different axial positions in the packed bed, Transparent silicagel particles, Re_{d_h}=96, 2.36*mm*<d_p<2.80*mm*, $T_{bed}|_0$=65℃, $T_{air}|_{inlet}$=26℃.

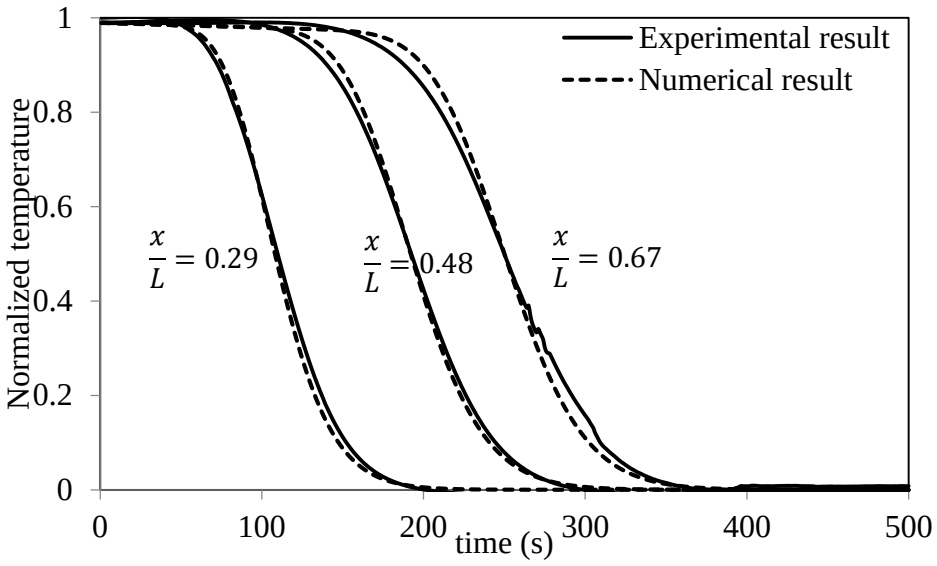

Figure 4-3 Experimental and numerical temperature distribution in three different axial positions in the packed bed, Transparent silicagel particles, Re_{d_h}=82, 2.36*mm*<d_p<2.80*mm*, $T_{bed}|_0$=65℃, $T_{air}|_{inlet}$=26℃.

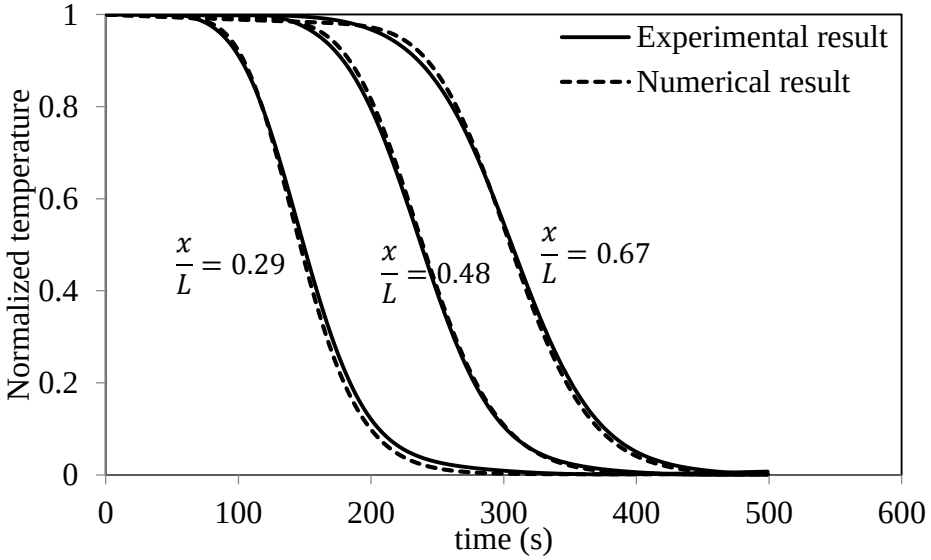

Figure 4-4 Experimental and numerical temperature distribution in three different axial positions in the packed bed, Transparent silicagel particles, Re_{d_h}=68, 2.36*mm*<d_p<2.80*mm*, $T_{bed}|_0$=65℃, $T_{air}|_{inlet}$=26℃.

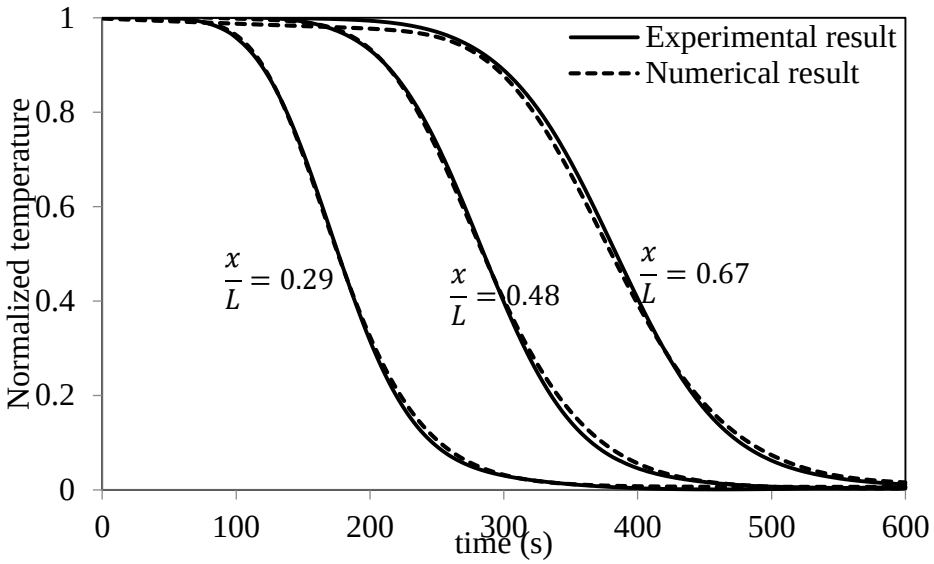

Figure 4-5 Experimental and numerical temperature distribution in three different axial positions in the packed bed, Transparent silicagel particles, Re_{d_h}=55, 2.36*mm*<d_p<2.80*mm*, $T_{bed}|_0$=65℃, $T_{air}|_{inlet}$=26℃.

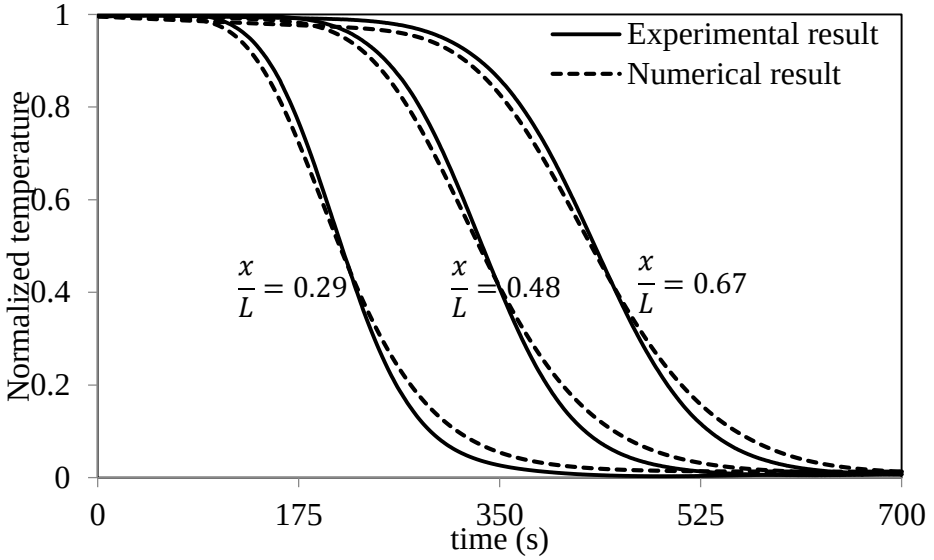

Figure 4-6 Experimental and numerical temperature distribution in three different axial positions in the packed bed, Transparent silicagel particles, Re_{d_h}=41, 2.36*mm*<d_p<2.80*mm*, $T_{bed}|_0$=65℃, $T_{air}|_{inlet}$=26℃.

There is less agreement between the experimental and numerical temperature profiles for $\frac{x}{L} = 0.67$ because of the increase in the value of possible error sources such as heat loss in the packed bed.

Table 4-3 lists the estimated convective heat transfer coefficients for the packed bed of blue silicagel particles. As can be seen both the objective function and the convergence error satisfy the stopping criteria in the IHTP analysis. Clearly, an increase in flow rate results in an increase in the convective heat transfer coefficient because of the higher convective heat transfer rate between the solid phase and external gaseous phase.

Table 4-3 Estimated value of convective heat transfer coefficient and its relative IHTP uncertainty, objective function of inverse analysis and convergence error of inverse analysis for each flow rate, packed bed of blue silicagel particles, $T_{bed}|_0$=65℃, $T_{air}|_{inlet}$=26℃.

Reynolds number (Re_{d_h})	h_t ($\frac{W}{m.K}$)	U(h_t)/h_t (%)	Objective function (K^2)	Convergence error
44	13.57	1.56	97	0.0001
58	15.07	1.18	92	0.0001
73	16.68	1.78	99	0.0001
87	21.96	1.56	99	0.0001
102	39.62	1.14	37	0.0001
116	55.05	1.62	98	0.0001

The same flow rates used for the transparent silicagel particles were used for the packed bed of blue silicagel particles as well. A different hydraulic diameter resulted in different Reynolds numbers for the blue silicagel bed compared with the transparent one. Blue silicagel particles are a smaller size than transparent ones, which results in a smaller convective heat transfer coefficient at each flow rate. The higher specific external surface area of the smaller particles is the reason for their lower convective heat transfer coefficient compared with the larger particles.

Figure 4-7 to Figure 4-12 illustrate the experimental and numerical temperature distribution in the packed bed of blue silicagel particles. The same discussion made for the results for the transparent silicagel packed bed can be applied here as well. At each Reynolds number, the best agreement between the numerical and experimental results is for $\frac{x}{L} = 0.48$.

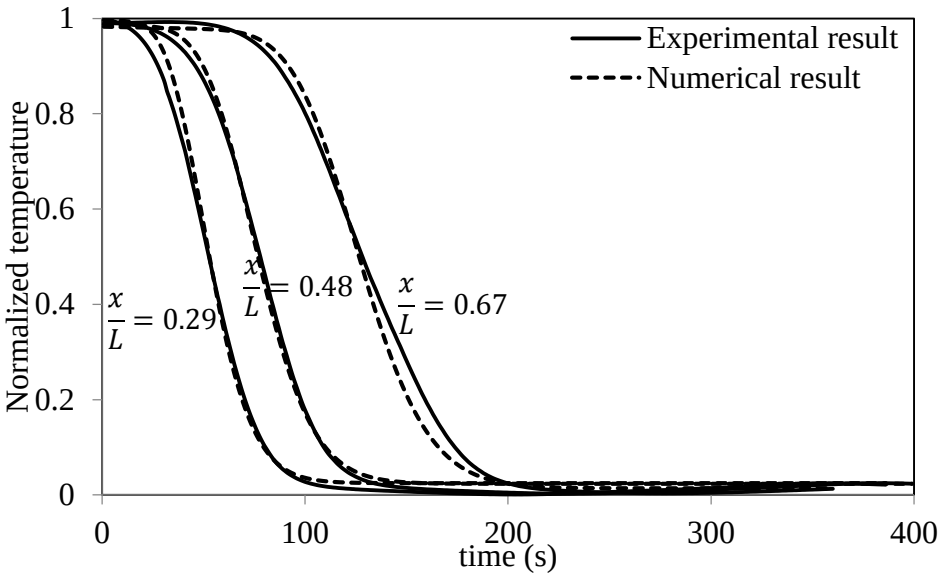

Figure 4-7 Experimental and numerical temperature distribution in three different axial positions in the packed bed, blue silicagel particles, Re_{d_h}=116, 1.00*mm*<d_p<2.00*mm*, $T_{bed}|_0$=65℃, $T_{air}|_{inlet}$=26℃.

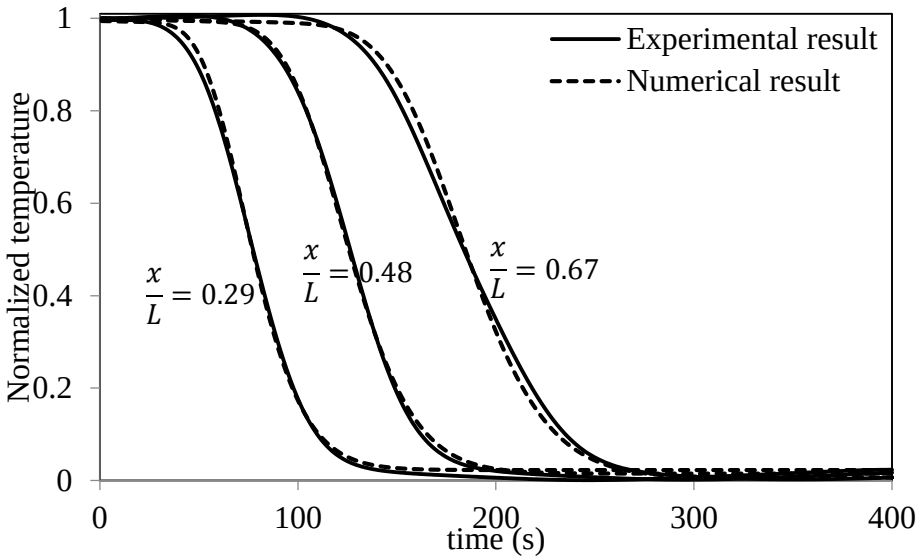

Figure 4-8 Experimental and numerical temperature distribution in three different axial positions in the packed bed, blue silicagel particles, Re_{d_h}=102, 1.00*mm*<d_p<2.00*mm*, $T_{bed}|_0$=65℃, $T_{air}|_{inlet}$=26℃.

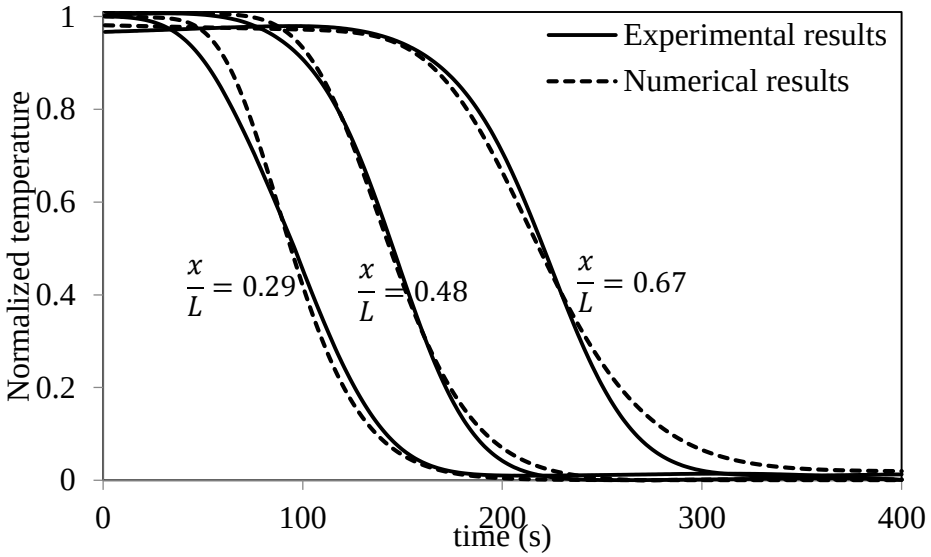

Figure 4-9 Experimental and numerical temperature distribution in three different axial positions in the packed bed, blue silicagel particles, Re_{d_h}=87, 1.00*mm*<d_p<2.00*mm*, $T_{bed}|_0$=65℃, $T_{air}|_{inlet}$=26℃.

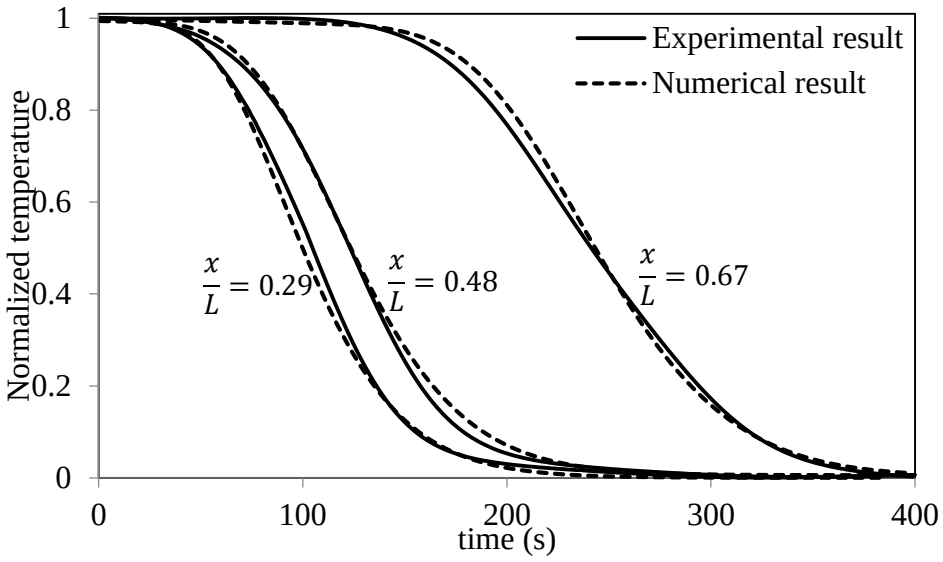

Figure 4-10 Experimental and numerical temperature distribution in three different axial positions in the packed bed, blue silicagel particles, Re_{d_h}=73, 1.00*mm*<d_p<2.00*mm*, $T_{bed}|_0$=65℃, $T_{air}|_{inlet}$=26℃.

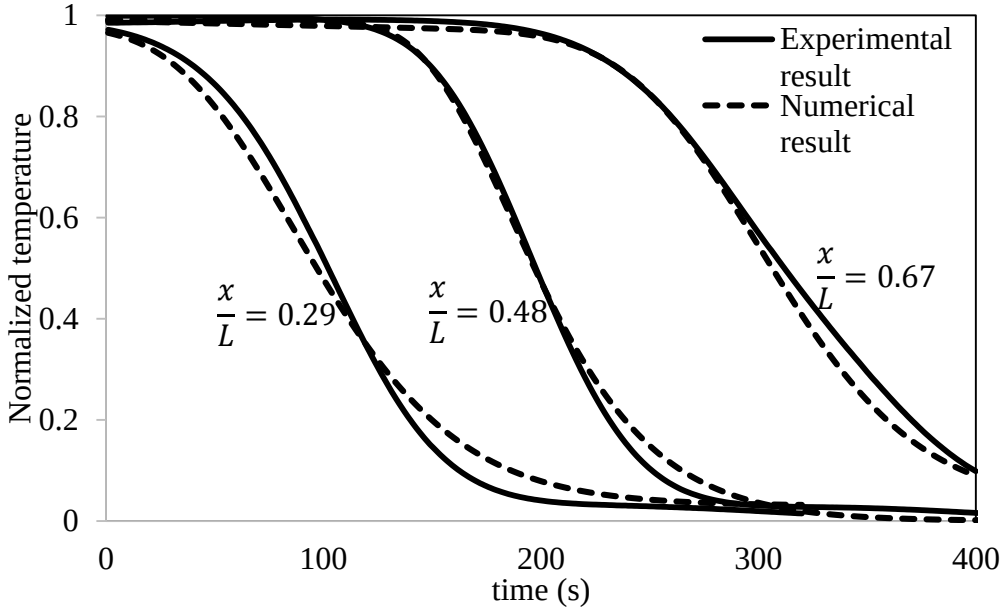

Figure 4-11 Experimental and numerical temperature distribution in three different axial positions in the packed bed, blue silicagel particles, Re_{d_h}=58, 1.00*mm*<d_p<2.00*mm*, $T_{bed}|_0$=65℃, $T_{air}|_{inlet}$=26℃.

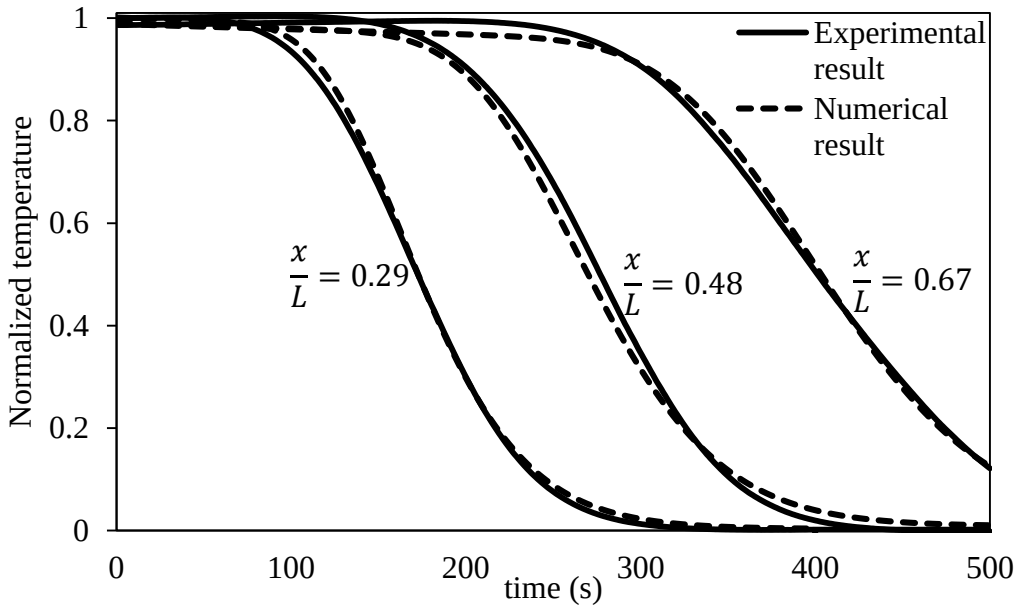

Figure 4-12 Experimental and numerical temperature distribution in three different axial positions in the packed bed, blue silicagel particles, Re_{d_h}=44, 1.00*mm*<d_p<2.00*mm*, $T_{bed}|_0$=65℃, $T_{air}|_{inlet}$=26℃.

4.2 A New Correlation for the Convective Heat Transfer Coefficient

Different studies have been done to find the convective heat transfer coefficient between the airflow and porous bed for different particle sizes and bed geometries. Differences between some of these correlations are in the range of 50% to 100%, especially for low Reynolds numbers (Re_{d_h}<20). In this part a new correlation for the Nusselt number (dimensionless convective heat transfer) is presented, and is compared with one of the latest correlations (Nie et al., 2011). The form of this correlation is

$$\frac{Nu_{d_h}}{Pr^{1/3}} = CRe_{d_h}^{n} \qquad (4.4)$$

where C and n are constants. As shown, Nusselt number is a function of Reynolds number, Prandtl number, and the geometry of the flow channel (Nie, 2010). All the dimensionless variables are based on the hydraulic diameter, so the Reynolds number is defined by equation (4.1) and the Nusselt number is

$$Nu_{d_h} = \frac{h_t d_h}{k_g} \tag{4.5}$$

where k_g is the conductivity coefficient for the external gaseous phase ($\frac{J}{m.K}$), d_h is the hydraulic diameter, and h_t is convective heat transfer coefficient. Also, the Prandtl number is defined as

$$Pr = \frac{\nu}{\rho_g c_{P_g}} \tag{4.6}$$

where ν is the kinematic viscosity of dry air ($\frac{m^2}{s}$), ρ is the density of the dry air and c_P is the specific heat capacity of the dry air. It can be assumed that for a narrow temperature change of the airflow, *Pr* is constant and equal to the Prandtl number of the dry air at room temperature which can be calculated as 0.724.

Figure 4-13 is a plot of Nusselt number versus Reynolds number for blue silicagel particles for both the curve fit and the estimated convective heat transfer coefficients. The correlation gives C=0.000134±0.00069 and n=2.155± 1.103 in equation (4.4) while the R^2=0.918, and the correlation uncertainty is t×SEE=1.5457 at the 95% confidence level. Figure 4-14 shows the correlation for the packed bed of transparent silicagel particles in which C=0.00093±0.00200, n=1.697±0.477, R^2=0.975, and the correlation uncertainty is t×SEE=0.2234 at the 95% confidence level.

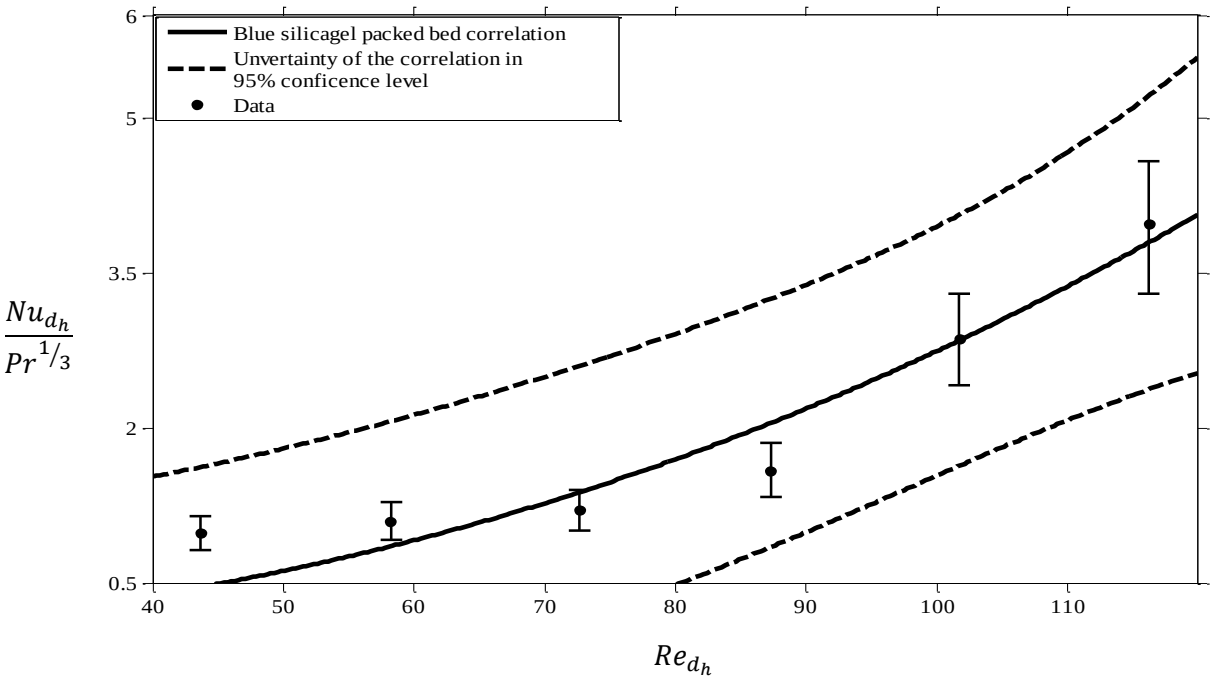

Figure 4-13 Experimental data and correlation of Nusselt number versus Reynolds number for bed of blue silicagel particles.

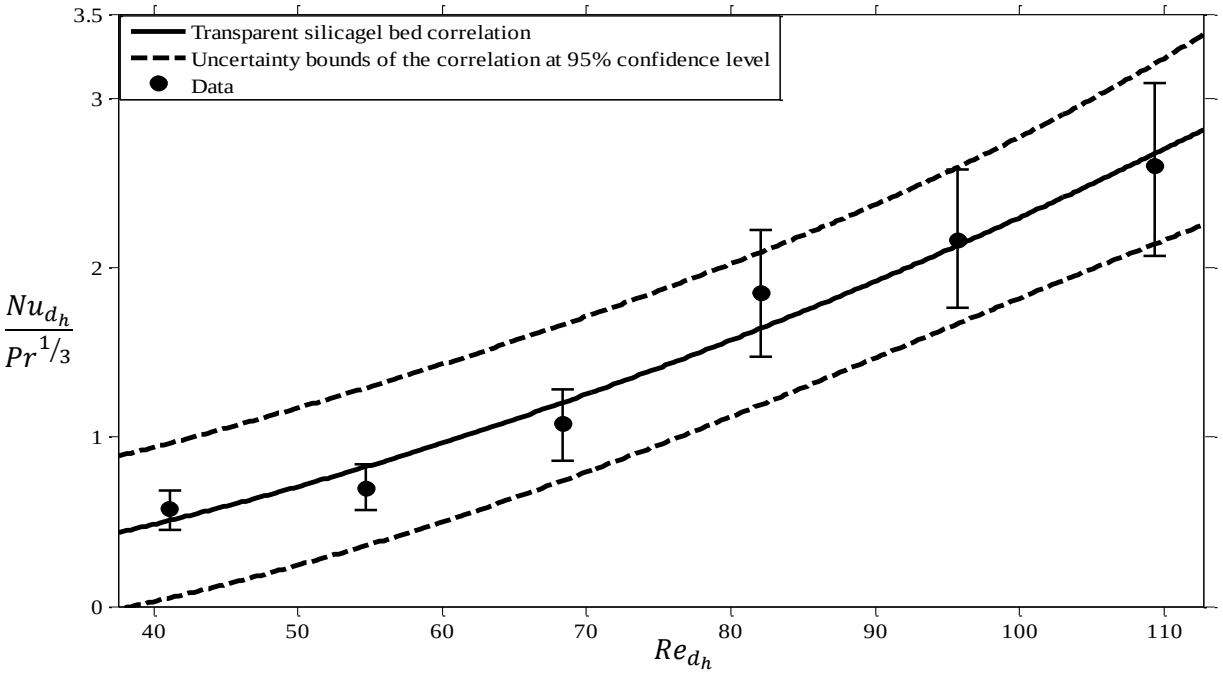

Figure 4-14 Experimental data and correlation of Nusselt number versus Reynolds number for bed of transparent silicagel particles

To obtain a unique correlation for all types of particles, data for these two types of particles were combined together to yield the following correlation for the range $40<Re_{d_h}<120$.

$$\frac{Nu_{d_h}}{Pr^{1/3}} = (0.00119 \pm 0.00273)\, Re_{d_h}^{(1.647\pm0.501)} \qquad (4.7)$$

For this correlation, R^2=0.920, and the uncertainty bound is ±2.357 at the 95% confidence level. Figure 4-15 compares the new correlation with the latest empirical correlation by Nie et al. (2011) for spherical solid particles (glass, steel, and lead) for the same range of Reynolds numbers based on the hydraulic diameter. This figure illustrates that their correlation lies in the uncertainty bounds of the new correlation. The differences between these two correlations can be because of the differences in the structures of the tested particles. The internal porosity of the silicagel particles makes the available surface for the heat transfer between the solid phase and external gaseous phase larger, which may cause an underestimate of the convective heat transfer coefficient. Also, the particles they used were in the range of 1.00 *mm* to 3.20 *mm*, which is different from the tested particle size in this study (1.00 *mm* to 2.80 *mm*). Furthermore, the porosity range of the particle beds in Nie et al. (2011) was 0.30 to 0.40 in comparison with the porosity of the silicagel packed beds which was in the range of 0.60 to 0.70.

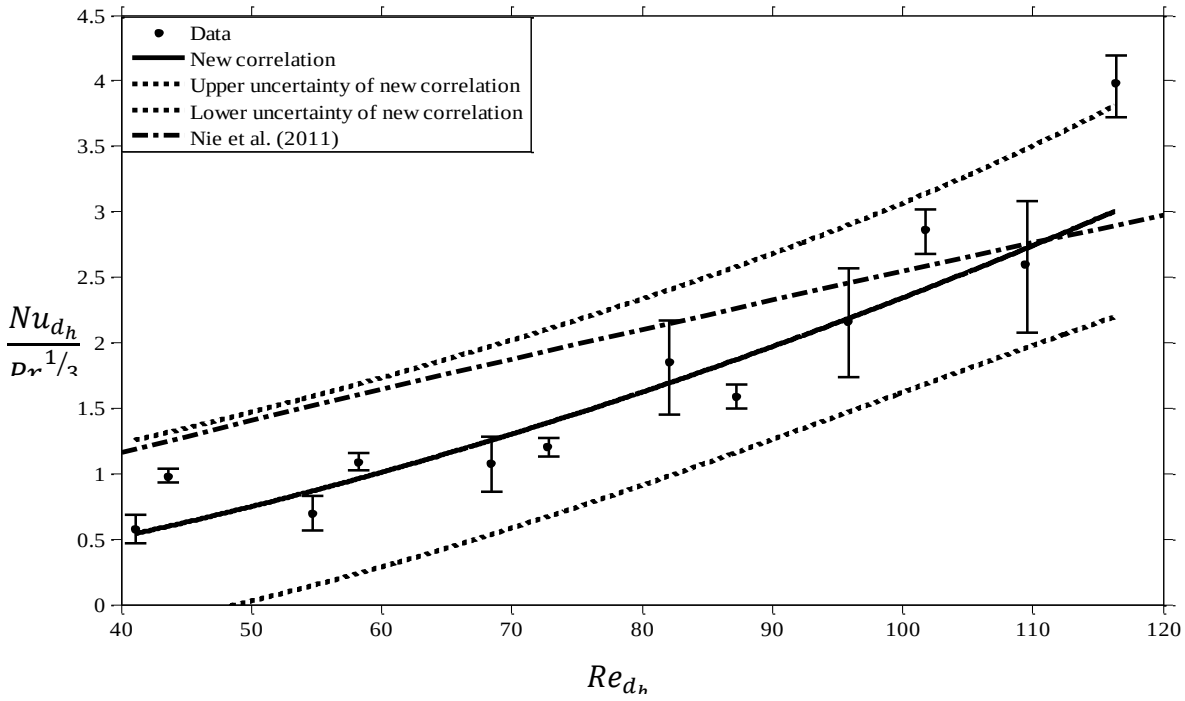

Figure 4-15 Comparison of the correlations for $\frac{Nu_{d_h}}{Pr^{1/3}}$ v.s Re_{d_h}

In summary, it can be concluded that the new correlation can estimate the convective heat transfer coefficient of the packed bed of spherical particles (especially in the case of particles with internal porosity) with a good uncertainty, which is in agreement with the latest correlation.

CHAPTER 5 IHTP OF EFFECTIVE THERMAL CONDUCTIVITY (THEORY AND MODELING)

Inverse heat transfer problem (IHTP) analysis is used to determine the effective thermal conductivity of randomly packed bulk particle test beds. An experimental set cell has been designed to obtain transient temperature test data that is used in the IHTP method. The estimated values for the effective thermal conductivity are compared with selected correlations of effective thermal conductivity in porous media. Using a manufactured thermal conductivity measuring device, steady-state test data are used to calculate the effective thermal conductivity of a particle bed directly and these measured data are compared with the data obtained during from the transient tests using the IHTP analysis for the same particles. Thermal conductivity values obtained from these steady-state tests are compared in numerical simulations of transient test conditions of packed particle beds.

5.1 Experimental Setup

An experimental setup similar to the facility used for the convective heat transfer tests was used to perform the thermal conductivity test on a packed bed of silicagel particles. Four different samples of silicagel particles were used to fill the packed bed. Table 5-1 shows the type of the packed bed, particle diameter range, and porosity of each.

In each test, one type of silicagel particles as listed in Table 5-1 was used to fill the particle bed and estimate effective thermal conductivity. Also, a mixture of transparent silicagel and blue silicagel with the same mass fraction was used as a randomly packed bed to be tested to estimate its effective thermal conductivity. The porosity of this packed particle bed, consisting of a mixture of blue and transparent silicagel particles, can be found by using a method introduced by Chen et al. (2004).

The experimental facility used to execute the conduction test is the same one used to perform the convection test with a changed inlet section. One inlet pipe of the inlet section supplied the hot airflow to be exposed to the particle bed, while the other inlet pipe was cut in

half to hold the aluminum plate in a good contact with the top of the particle bed and the insulation at the top of the aluminum plate.

Table 5-1- Different types of silicagel particles used in the packed bed

#	Particle type	Particle size (mm)	Porosity
1	Transparent silicagel	2.36 mm<d_p<2.80 mm	0.62
2	Transparent silicagel	2.00 mm<d_p<2.36 mm	0.63
3	Blue silicagel	$d_{p(average)}$ =1.6 mm	0.69
4	Equal mass fraction of #1 and #3	$\frac{1}{2}[(2.36\ mm < d_p < 2.80\ mm) + (d_{p(average)} = 1.6\ mm)]$	0.62

First, the randomly packed particle bed was exposed to a hot dry airflow until the whole particle bed had the same temperature as the hot airflow. The transient test started by turning the inlet section 180 degrees, so the cooled aluminum disk could be put in good contact with the top of the particle bed. Insulation at the top of the aluminum disk and around its perimeter reduced its heat exchange with its surroundings to a small fraction of that exchanged with the particles. The experiment could be terminated any time after the temperature wave or disturbance had passed the selected bed position when the temperature profile could be used in IHTP analysis. Three sets of thermocouples recorded the temperature change of the particle bed in three different positions while the packed bed was insulated in all directions and was just in touch with the aluminum plate. Figure 5-1 shows a schematic view of the experimental setup used for the transient step change conduction test.

The same compressor used for the transient convection tests was used to provide the dry air supply for the conduction experiments. An airflow meter (MKS, 200SLM) was used to measure and provide the needed flow rate, and a flow controller was installed in the supply line to adjust the airflow. Again, the same heater used in the convection tests was used in these experiments to heat the airflow to 60℃ and keep the airflow at that constant temperature. A thermocouple at the end of the airflow inlet pipe monitored the temperature of the inlet airflow during the heating process of the packed bed.

Three different heights in the particle bed were chosen to monitor the temperature. One set of three thermocouples was installed at each height to record the temperature while the radial arrangement of the thermocouples in each set was the same as in the convection transient tests. The first set of thermocouples was at 5 *mm* ($\frac{x}{L} = 0.98$) from the bottom of the particle bed to record the temperature changes furthest from the inlet where it took more time for the packed bed to reach the same temperature as the hot airflow. When the bottom of the packed bed was at the airflow temperature, a uniform temperature in the whole bed could be assumed and the step change could start the transient test.

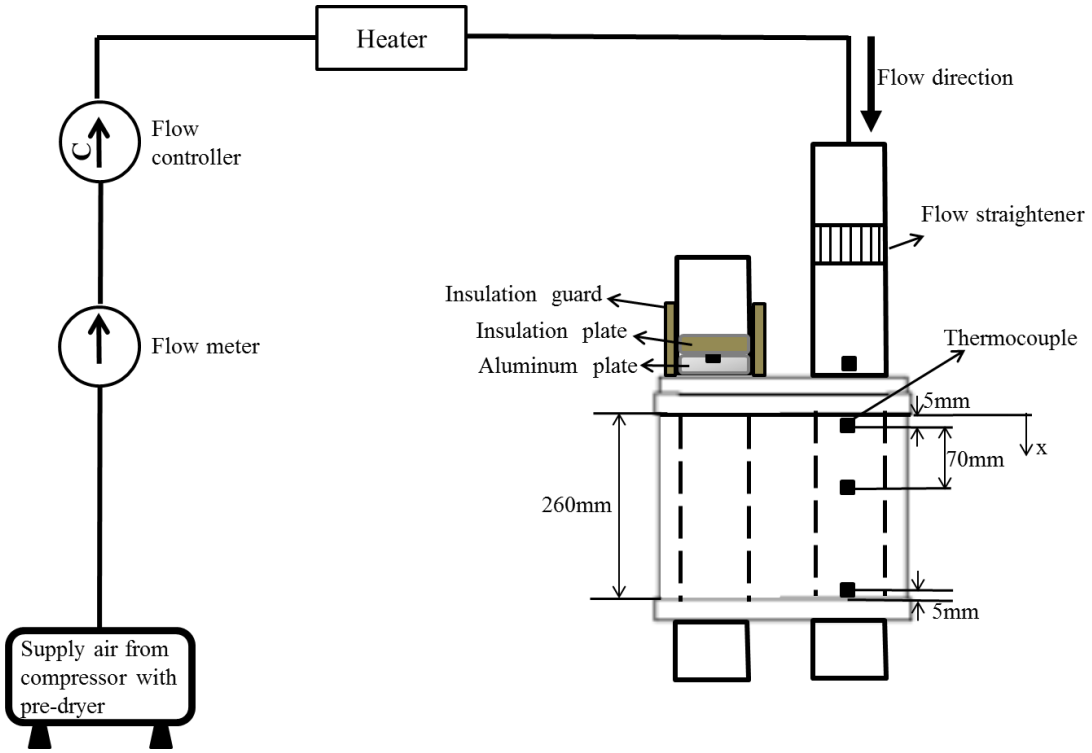

Figure 5-1 Schematic view of the experimental setup used for estimation of effective thermal conductivity of the silicagel particle bed using IHTP method.

The second set of the thermocouples was at 5 *mm* ($\frac{x}{L} = 0.02$) below the top of the particle bed. The temperature recordings at this position during the transient test have been used as the measurement vector in the IHTP analysis.

The third set of the thermocouples was at 75 *mm* ($\frac{x}{L} = 0.29$) lower than the top of the particle bed. It was used to examine the validity of the final estimation of the effective conductive heat transfer coefficient by comparing the temperature profile obtained from the

numerical model (using the estimated thermal conductivity) with the temperature profile obtained from the transient measurements.

An aluminum plate 40 *mm* thick and 100 *mm* (4 *inches*) in diameter was held in the other inlet pipe, which was cut in half to have an open end. An insulation plate of the same diameter (inner diameter of the shortened inlet PVC pipe) and 50 *mm* thick was attached to the top of the aluminum plate to prevent heat transfer from the plate to the surrounding. The inlet pipe was insulated to also prevent heat exchange from the aluminum plate. A thermocouple was mounted at the center of the aluminum plate (2 *cm* in depth) to record the temperature changes of the plate. Once the particle bed was thoroughly heated by the hot airflow, a step change was performed by turning the inlet section 180 degrees putting the aluminum plate in good contact with the particles at the top of the bed. At the same time an insulation plate was mounted at the beginning of the outlet section to prevent any heat loss from the bottom of the particle bed. Figure 5-2 shows a view of different sections of the test cell.

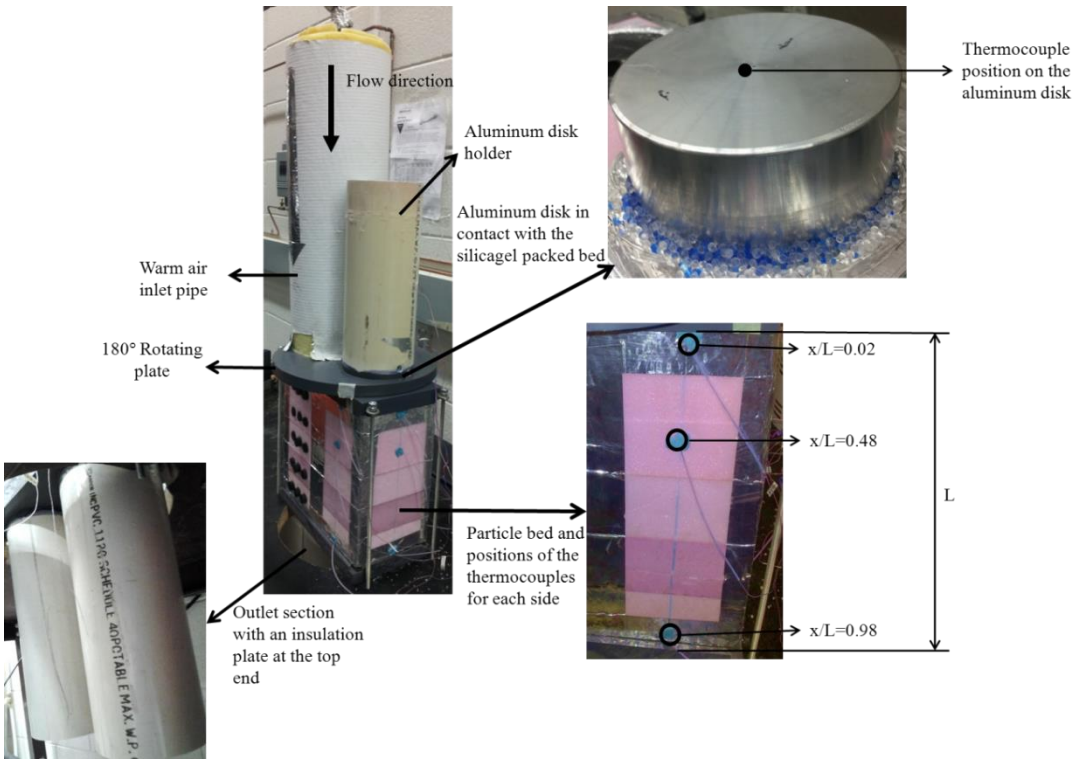

Figure 5-2 Different parts of the experimental test cell

The following presents the procedure of the experiment.

1. Dried the silicagel particles for 24 hours in the oven.

2. Sealed the particles in two layers of plastic bag to prevent moisture transfer from the surroundings to the particles and simultaneously decrease the temperature of the particles to room temperature.

3. Filled the particle cell with the chosen silicagel particles for the transient test and assembled the test cell.

4. Heated the airflow to $60\pm1℃$ and set the flow rate to 240 *lpm* to allow the particle bed temperature to become uniform throughout.

5. Recorded the temperature at the bottom of the particle bed ($\frac{x}{L} = 0.98$) and let the packed bed be exposed to the hot airflow until the thermocouple showed the same temperature as the temperature of the airflow.

6. Rotated the inlet section (rotating plate) to perform the step change. This put the aluminum plate in good contact with the particles at the top of the particle bed and the transient test started.

7. Recorded the temperatures of the aluminum plate and the packed particle bed for first 1000 seconds in two positions: 5 mm lower than the top of the bed to be used in the IHTP analysis, and 75 mm lower than the top of the bed to be used to validate the accuracy of the IHTP model.

5.2 Assumptions

Local volume averaging (LVA) is used to simulate the transient conductive heat transfer between the randomly packed silicagel particle bed and the aluminum plate numerically. The LVA method requires defining the representative elementary volume (REV). The REV is the smallest volume that yields the proper local averaged properties at each point of the particle bed and it has two main phases: solid phase, which is the pure silicagel (SiO_2), and gaseous phase, which consists of the internal gaseous phase (inside the particles) and the external gaseous phase (the available void space between the particles).

Kaviany (1995) described the requirements for the length scale of REV in porous media as below

$$K^{1/2} \ll d \ll l \ll L \qquad (5.1)$$

where K is the permeability of the porous bed (m^2), d is the particle size (m), l is the length of the REV (m), and L is the length characteristic of the particle bed (m). He also determined the range of each length parameter to be applied for the validity of the REV

$$K^{1/2} \sim O(10^{-2} d)$$

$$d \sim O(1mm - 1cm)$$

$$l \sim O[(1 - 10)d]$$

$$L \sim O[(10 - 100)l]$$

Considering the transparent silicagel particle with the $2.36\ mm < d_p < 2.8\ mm$ and average diameter of 2.58 *mm* as the biggest particle size used in the packed particle bed, the average permeability of this particle bed was $4.27 \times 10^{-9}\ m^2$ (Appendix B). The required lengths for the REV to be applied and their validity analysis are listed in Table 5-2.

By considering the biggest particle size in the packed bed and choosing the l in the range of 0.003-0.025 *m*, the length characteristic of the particle bed was acceptable to allow use REV and LVA in simulating the energy transfer transient test in the packed bed of silicagel particles. Even considering the other particles in the bed with smaller particle

diameter, making the l for the REV even smaller, the validity of using LVA in the packed particle bed is still proven.

Table 5-2 Local volume requirements for the packed bed of transparent silicagel particles (2.36 mm<d_p<2.80 mm)

Parameter	K	d	L	L
Value (m)	4.27×10^{-9}	2.58×10^{-3}	0.003-0.025	0.26
Required range	$K^{1/2}\sim O(10^{-2}d)$	$d\sim O(1\ mm - 10\ mm)$	$l\sim O[(1-10)d]$	$L\sim O[(10-100)l]$
Is it in the required range?	Yes	Yes	Yes	Yes

Usage of the LVA method simplifies the governing equations that are applied to simulate the heat transfer transient test.

In addition to the LVA assumption, some physical assumptions can be defined in order to apply possible restriction and boundaries to the governing equations making them more straightforward.

1- It is assumed that the cylindrical particle bed was insulated enough on the walls and the heat loss from the particle bed to the surrounding environment around the walls was negligible in comparison with the heat exchange from the particle bed to the aluminum disk.

   Also, the insulation plate that was mounted at the bottom of the particle bed at the moment of step change ensured that the heat transfer from the bottom of the particle bed to the surrounding was negligible. The only heat transfer at the boundaries of the packed particle bed was from the heated particle bed to the aluminum plate at the top of the packed bed.

2- It is assumed that the aluminum disk at the top of the particle bed was insulated on the boundaries except at the bottom where it was in contact with the packed particle bed. Therefore, the heat transfer from the aluminum plate to the surrounding during the heating process was negligible. The insulation plate at the top of the aluminum plate prevented heat loss from the metal plate to the surroundings. Furthermore, the aluminum plate was surrounded with the PVC pipe which was insulated with the 2 *cm* fiberglass insulation, so heat transfer between the disk and surrounding air was negligible. As a result the only possible heat transfer for the aluminum disk was from the heated particle bed.

3- It is considered that the heat transfer from the heated packed particle bed to the aluminum plate was in axial direction and the radial temperature change in the cylindrical particle bed was small enough to be ignored.

4- The silicagel packed bed is considered as an isotropic porous medium. It is assumed that the thermal conductivity and the porosity were not changing spatially in the particle bed except at the boundaries where the packed bed was in contact with the aluminum plate. The porosity of the porous medium at the contact with the solid surfaces was higher than the porosity in other positions of the particle bed (Kaviany, 1995). Studies show that this effect is negligible at distances greater than half the size of the particle diameter (Evitts et al., 2006). By assuming the biggest particle (d_p=2.58mm) was used in the tests, the distance, which is influenced by the contact between the aluminum disk and the packed bed, was 1.3mm, implying the porosity would not change the effective thermal conductivity beyond this distance.

5- It is assumed that the temperature inside the silicagel particle was uniform meaning it did not vary with the position in the particle. The validity of this assumption comes from the analysis of Biot number (Bi) of the silicagel particle, which is discussed in chapter3.

6- It is assumed that the temperature profile in the aluminum plate was uniform, which means it did not change spatially during the heat transfer from the packed bed to the plate. Three thermocouples were installed in three different positions in the aluminum plate for one of the transient conduction tests. Figure 5-3 shows the exact position of these three thermocouples in the aluminum plate. Figure 5-4 shows the temperature

profile of these three thermocouples during the test. This shows that the temperature difference between these three points at each time is less than the uncertainty of the thermocouples.

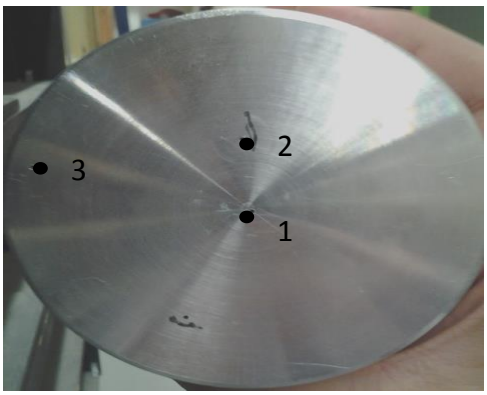

Figure 5-3- a top view of aluminum plate with the position of three thermocouples in different depth as: 2*cm* in depth for T_1, 3*cm* in depth for T_2, 1*cm* in depth for T_3.

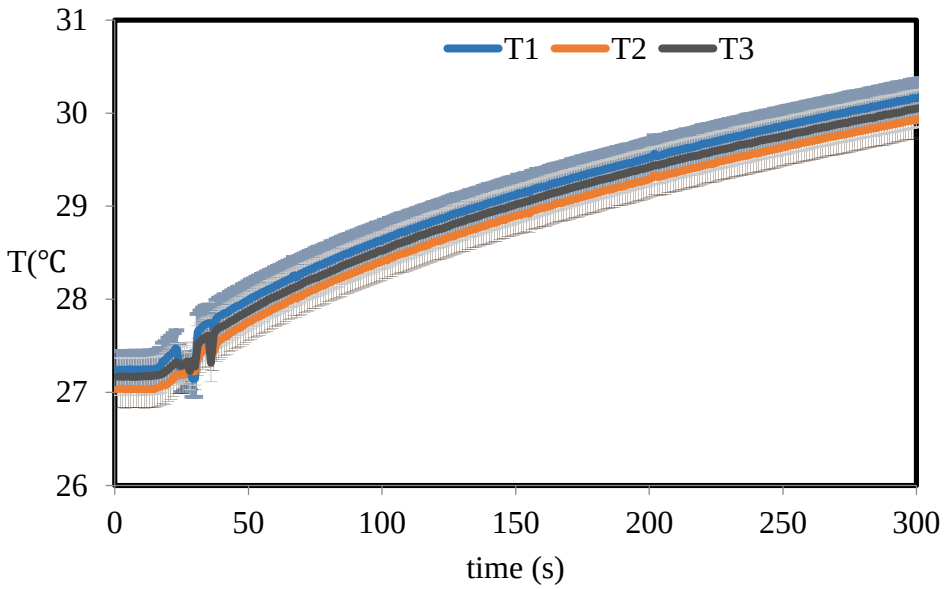

Figure 5-4- Temperature profile of three thermocouples at three random position in the aluminum plate as shown in Figure 5-3 (heated packed bed of transparent silicagel particles ($d_p = 2.58mm$)

7- It is assumed that the particle bed consisted of two different phases. The solid phase is considered a continuous phase and included the solid part of the particles (SiO_2). The gaseous phase included the external gaseous phase between the particles and the internal gaseous phase in the pores of each silicagel particle. The gaseous phase was treated as an ideal gas. It is considered that the local temperature difference between solid phase and gaseous phase was negligible, so it is assumed that both phases were in local thermal equilibrium with each other. It is noted that there was no airflow going through the particle bed during the conduction test and there was no internal energy source for the solid gaseous phases separately (Vadasz, 2005). As a result, all the phases had the same temperature and pressure at any time in the packed particle bed.

8- It is considered that there was no condensation on the aluminum plate because of the decrease in the temperature of the particle bed. Assuming the initial temperature of the packed particle bed was 60℃, considering that the relative humidity of the particle bed was a maximum of 10%, and the pressure in the particle bed was atmospheric pressure, the dew point of the air was 18℃, which is less than the minimum temperature of the aluminum plate (room temperature) during the conduction test. It can be concluded that the temperature of the gaseous phase was not low enough to let condensation occur on the surface of the aluminum plate, which was in contact with the packed particle bed.

9- It is assumed that the heat was transferred from the packed bed to the aluminum plate by conduction heat transfer meaning radiation and convection are negligible in the analysis. The initial temperature of the packed bed was 60℃, which was not high enough to consider radiation as a form of heat transfer from the packed bed to the aluminum plate.

The packed bed consisted of a solid phase as silica (SiO_2) and a gaseous phase as dry air. The presence of the air as the gaseous phase made a potential for natural convection while there was a heat sink at the top of the particle bed. Nield and Bejan (2006) performed studies on the natural convection in a porous packed bed that was being heated from the bottom to the top and found that there is a critical Rayleigh number (Ra_c), lower than which the heat transfer in the particle bed is solely from conduction. The $Ra_{c,}$ based on their study, is 39.48, and the Ra for a porous particle bed is defined as below:

$$Ra = \frac{\rho_g g \beta K L \Delta T}{\mu \alpha_{eff}} \quad (5.2)$$

where ρ_g is the density of the air as a gaseous phase ($\frac{kg}{m^3}$), g is the constant of gravity ($\frac{m^2}{s}$), β is the thermal volume expansion factor for air ($\frac{1}{K}$), K is the permeability of the packed bed ($\frac{1}{s^2}$), L is the height of the particle bed (m), ΔT is the temperature difference between the packed bed and heat sink (K), μ is the dynamic viscosity of the air ($\frac{kg}{m.s}$), and α_{eff} is the effective thermal diffusivity of the particle bed ($\frac{s}{m^2}$). Table 5-3 lists the Ra for both transparent and blue silicagel particle beds.

Clearly the Ra of each packed particle bed is much smaller than the critical Ra defined for the porous particle bed by Nield and Bejan (2006). Therefore, the only significant heat transfer phenomenon was the conduction; the natural convection that happened in the particle bed can be neglected.

Table 5-3 Ra for the two types of packed silicagel particle bed

Particle	Permeability (m^2)	Effective thermal diffusivity ($\frac{s}{m^2}$)	Ra
Transparent silicagel ($d_p = 2.58mm$)	4.27×10^{-9}	4.62×10^{-4}	0.147
Blue silicagel ($d_p = 1.6mm$)	1.60×10^{-9}	3.70×10^{-4}	0.069

5.3 Governing Equations:

The governing equations can be derived based on the porous media theory (Kaviany, 1995) and by applying the assumptions made in the previous section. Governing equations are used to simulate the conduction transient test numerically. This numerical simulation is called direct problem and its objective is to find the temperature profile of the packed bed of silicagel particles in the two different axial positions in the bed ($\frac{x}{L} = 0.02$ and $\frac{x}{L} = 0.29$) . The results of the simulation are compared with the outcomes of the experimental tests and the unknown parameter, which is the effective thermal conductivity of the packed bed can be estimated by minimizing the objective function. The governing equations used to simulate the direct problem numerically are presented in following.

5.3.1 Porous bed energy equation

It is considered that the heated particle bed was insulated on all the surroundings except at the top that was in contact with the aluminum disk. It is assumed that the energy transfer in the particle bed was conduction heat transfer solely. Also, it is assumed that the particle bed was in local thermal equilibrium in each REV. As a result the change of the energy storage in the particle bed can be written as below (Kaviany, 1995)

$$\frac{\partial}{\partial t}\left(\rho_{eff} C_{p_{eff}} T\right) = \frac{\partial}{\partial x}\left(k_{eff} \frac{\partial T}{\partial x}\right) \qquad (5.3)$$

where ρ_{eff} is the effective density of the porous particle bed ($\frac{kg}{m^3}$), $C_{p_{eff}}$ is the effective heat capacity of the packed bed ($\frac{J}{kg.K}$), and k_{eff} is the effective thermal conductivity of the packed bed of silicagel particles ($\frac{W}{m.K}$). Also, *t* represents the time (*s*) and *x* (*m*) is standing for the axial position in the particle bed considering the top of the particle bed as x=0 and the bottom of the particle bed as x=0.26mm. Also, *T* is the temperature in the considered control volume (*K*).

The effective density of the particle bed can be found using the following equation:

$$\rho_{eff} = (1-\varepsilon)\rho_{silica} + \varepsilon\rho_g \qquad (5.4)$$

where ε is the porosity of the particle bed as listed in Appendix B, ρ_{silica} is the density of the silicagel, also listed in Appendix B, and ρ_g is the density of the gaseous phase.

$$\rho_g = \frac{P}{RT} \qquad (5.5)$$

where P is the atmospheric pressure (*Pa*), R is the constant of ideal gas ($\frac{j}{kg.K}$), and T is the temperature (*K*).

The effective heat capacity of the particle bed can be calculated by using the relation between the thermal capacities of different phases in the porous media (Kaviany, 1995)

$$C_{p_{eff}} = \left[(1-\varepsilon)C_{p_{silica}}\rho_{silica} + \varepsilon\rho_g C_{p_g}\right]/\rho_{eff} \qquad (5.6)$$

where $C_{p_{silica}}$ is the thermal capacity of the silica, and C_{p_g} is the thermal capacity of the gaseous phase in the particle bed.

K_{eff} is the unknown parameter, which is sought using the IHTP method and is considered independent of the position in the particle bed except at the boundary at the top of the packed bed, which is in contact with the aluminum plate.

5.3.2 Energy change in the Aluminum plate (Boundary condition at x/L=0)

The aluminum plate at the top of the particle bed was insulated on all the surroundings except at the bottom, which was in contact with the heated particle bed, so the energy in the aluminum plate was changing because of the heat flux from the particle bed to the plate. The energy equation at the top boundary of the particle bed is an equality between the heat flux from the particle bed and the energy change of the aluminum plate.

$$C_{p_{Al}} m_{Al} \frac{\partial T_{Al}}{\partial t} = A_c k_{eff_c} \frac{\partial T}{\partial x}|_{x=0} \qquad (5.7)$$

where $C_{p_{Al}}$ is the specific heat capacity of the aluminum plate ($\frac{J}{kg.K}$), m_{Al} is the mass of the aluminum plate (kg), A_c is the contact area between the aluminum plate and the particle bed, which is the same as the section area of the particle bed (m^2), and T_{Al} is the temperature of the aluminum plate (K). Also, $\frac{\partial T}{\partial x}|_{x=0}$ is the temperature gradient at the top of the particle bed, and k_{eff_c} is the effective thermal conductivity at the contact surface of the aluminum plate and the particle bed.

The porosity of the particle bed at the interfaces and walls is higher than the rest of the bed, and this microscopic boundary is valid within the distance of half particle size from the boundary. As a result, if the conductivity of the gaseous phase was less than the solid phase ($k_s > k_g$), the thermal conductivity at the boundary (k_{eff_c}) is considered smaller than the effective thermal conductivity for the rest of the particle bed. Prat (1989) showed that the macroscopic governing equations cannot determine the temperature profile in the porous bed without an error. As a result, the microscopic boundary condition must be considered for the packed bed when it is interfaced with another medium at the boundary. The effect of the boundary will be higher when the difference between the thermal conductivity of the solid phase and thermal conductivity of the gaseous phase is large. Prat (1990) studied the heat transfer between a porous medium and an external fluid when the local conductivity effect at the boundary of the external fluid and the porous media was not negligible and found a correlation considering the microscopic temperature change at the boundary. His correlation was for the fluid-porous medium contact in which the interface cannot be determined precisely. Ofuchi and Kunni (1965) introduced a correlation for the effective thermal conductivity of the particle bed. They found that the effective thermal conductivity of the particle bed at the interface of the packed bed and the solid surface is half of the thermal conductivity of the particle bed. They ran experiments to validate their correlation for five different particles and five different fluids including air as the fluid phase and found that their estimation could bring agreement to the experimental and numerical results. Evitts et al. (2006) found the thermal conductivity of a packed bed of potash particles by using IHTP method. They used a steel ball at the center of the packed bed and considered that the thermal

conductivity at the interface was 55% of the effective thermal conductivity of the packed bed. They found that a 10% change in the effective conductivity at the boundary changed the estimated value of the effective thermal conductivity by less than 5%.

Based on the discussed previous studies, in this work, the thermal conductivity at the boundary is considered 50% of the effective thermal conductivity of the packed bed

5.3.3 Heat flux at the bottom of the bed (Boundary condition at x=L)

An insulating polystyrene plate with a thickness of 4cm and a radius equal to the radius of the particle bed was used at the bottom of the particle bed. As a result, it can be considered that the heat loss from the bottom of the particle bed was negligible, and there was no heat flux at the bottom end of the particle bed.

$$\frac{\partial T}{\partial x}|_{x=L} = 0 \qquad (5.8)$$

5.4 Inverse Analysis

The effective thermal conductivity of the particle bed as the unknown parameter is found by using the inverse heat transfer problem analysis. The general steps to find the unknown parameter are as follows:

1- Discretizing the nonlinear partial differential governing equations.

2- Writing a direct numerical solution to be able to find the temperature profile at any arbitrary position in the particle bed, and considering an initial guess for the unknown parameter, which is the effective thermal conductivity coefficient.

3- Using the inverse numerical solution to estimate the effective thermal conductivity.

A complete review of discretization of the governing equations can be found in Appendix C. Each of the mentioned steps are discussed in the following.

5.4.1 Direct Numerical Solution

The partial differential equations are solved by developing a program in Matlab to find the temperature distribution in the particle bed. 101grid points are used to simulate the transient test with a grid size of 2.6 *mm* (considering the first spatial grid as the interface of the packed bed and aluminum plate). The first 1000 seconds of the experiment with the time step of 1*second* is simulated. Therefore, the number of time nodes (Nmax) is 1001 by considering t=0*s* as the first node, which is the initial condition. The chosen values of the grid size and time step are based on the sensitivity analysis of these two parameters, which can be found in Appendix D.

The same method mentioned in Chapter 3 is used to develop the Matlab program based on defining known and unknown variables as a two dimensional vector (time and position). Also, effective thermal conductivity is defined as

$$k_{eff} = COEF_k \times (\varepsilon k_g + (1-\varepsilon)k_s) \qquad (5.9)$$

where $COEF_k$ is the unknown variable that must be found by using the inverse solution. If the initial guess for $COEF_k$ is considered as 1 that makes k_{eff} equal to the theoretical value for the effective thermal conductivity of the porous media (Kaviany, 1995).

Applying the known parameters and estimated value for the effective thermal conductivity, the temperature profile at different positions in the particle bed can be obtained. The iteration method that was used to find the temperature profile in the analysis of convective heat transfer coefficient is used to find the temperature profile in the conduction problem as well. A relaxation factor is chosen to modify the iteration process and is equal to 0.1, and the value of the convergence criterion is assumed as 10^{-5}. A flow chart of the Matlab code used to solve the direct problem is shown in Figure 5-5.

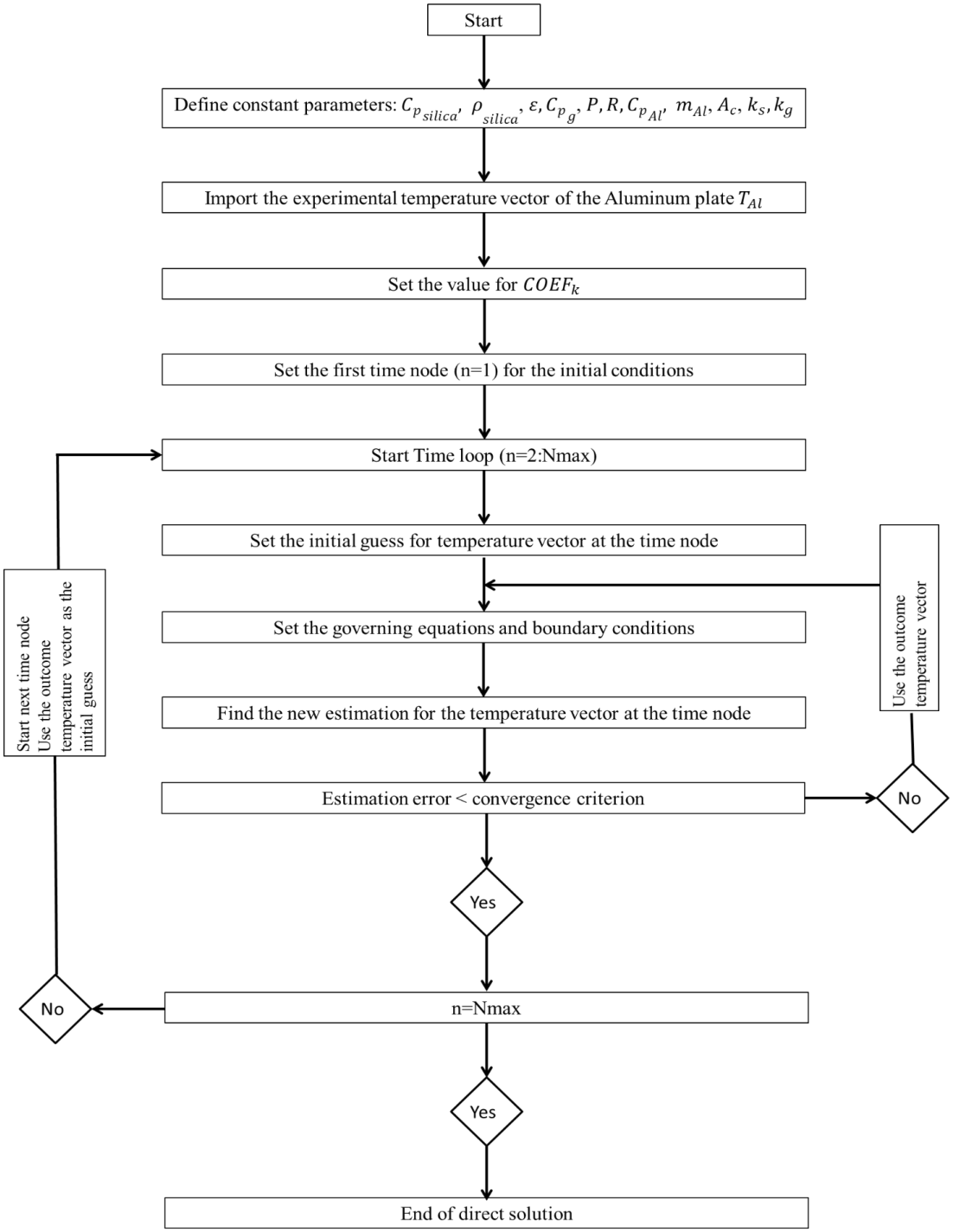

Figure 5-5 Numerical algorithm used to solve the direct problem

5.4.2 IHTP numerical solution

Three sets of sensors were installed in three different axial positions in the packed particle bed. Sensitivity analysis of these three positions can show the set with the most useable measurements for use in the inverse solution. Sensitivity coefficients of these three

axial positions were calculated for each type of packed particle bed. The value of the effective thermal conductivity of the packed bed was calculated by using equation (5.9) for use in the direct problem. Figure 5-6 illustrates the sensitivity coefficients of each set of sensors. As shown, sensitivity coefficients of the second sensor ($\frac{x}{L} = 0.02$) had small magnitudes at the beginning of the experiment, and again after 800*s* of the transient test. Sensitivity coefficients of the third sensor ($\frac{x}{L} = 0.98$) were small at the first 500*s* of the transient test. On the other side, the first sensor, closest to the aluminum plate, had large sensitivity coefficients for the whole duration of the experiment, especially for the first 500*s* of the test when the heat loss was still small and the dominant energy transfer in the packed bed was the conductive heat transfer to the aluminum disk. Therefore, the first sensor is the most preferred one to be used in the IHTP analysis. Furthermore, the two other sensors can be used to examine the validity of the inverse solution. The same conclusion can be made for the other types of particle packed beds as well.

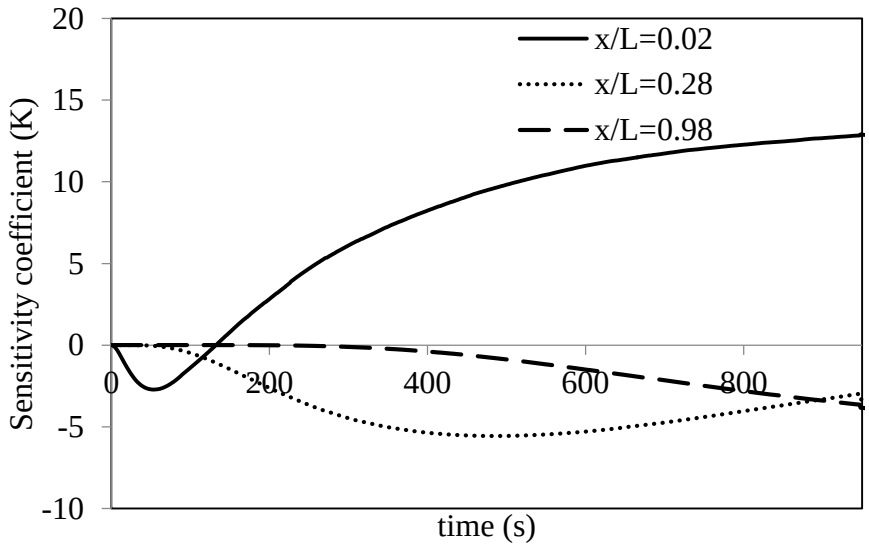

Figure 5-6 Sensitivity coefficients of temperature sensors versus time, dry packed bed of silicagel particle particles (2.36mm<d_p<2.80mm), T_{bed}=59℃, T_{Al}=24℃.

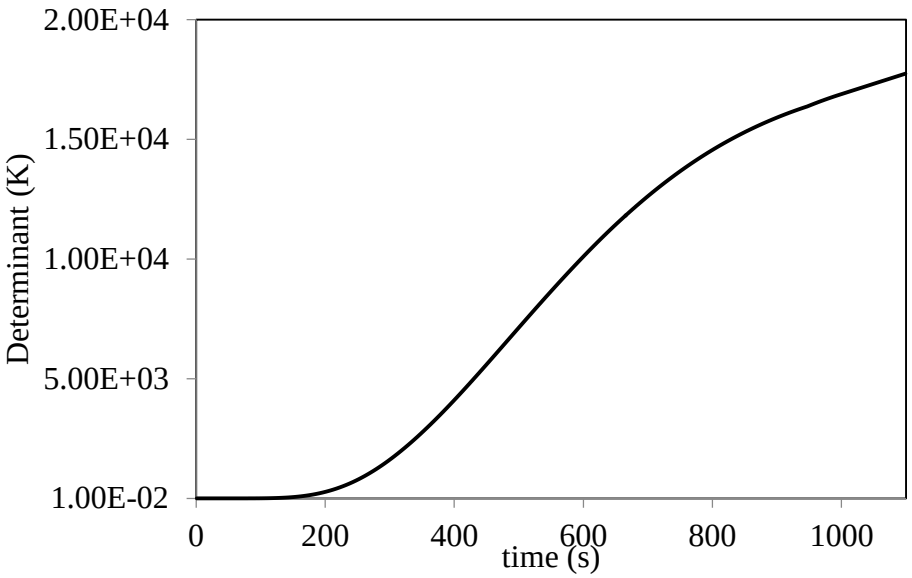

Figure 5-7 Determinant of the sensitivity matrix versus time, dry packed bed of silicagel particle particles (2.36mm<d_p<2.80mm), T_{bed}=59℃, T_{Al}=24℃ for$\frac{x}{L} = 0.02$.

As mentioned in Chapter 2, the proper duration of the transient test to provide adequate measurements for the inverse analysis can be found by determining the period during which the sensitivity matrix grows the most. As illustrated Figure 5-7, the determinant of sensitivity matrix at $\frac{x}{L}$=0.02 has the largest growth for the first 1000*s* of the transient test. This means this time period can be used as the suitable duration for the IHTP analysis.

The initial guess to start the iteration in IHTP is $COEF_k$=1, and the stopping criteria that are considered to determine the convergence of the inverse procedure are:

- Objective function (S)<$100K^2$
- IHTP Convergence criterion=0.001

Interested readers can refer to Chapter2 to see more detailed description of the IHTP solution.

CHAPTER 6 RESULTS OF ESTIMATION OF EFFECTIVE THERMAL CONDUCTIVITY

The final estimation of the effective thermal conductivity in the particle bed is presented and the comparison with the previous models is established. Also, the IHTP estimated values, which are the output of the transient test, are compared with the outcomes of an experimental device that is used to find the thermal conductivity of solid materials in a steady state test. The estimated values of effective thermal conductivity are used to numerically simulate a different transient conduction test in order to investigate the validity of the IHTP estimation. In each case, the reasons for any possible difference between the outputs of the mentioned methods and the IHTP analysis are discussed.

6.1 IHTP Results

Four different types of particles were used in the experiments and a numerical simulation was used to model the transient experiments. The temperature profile of the aluminum plate that was exposed to the heated dry packed bed and the temperature profile of the packed bed at $\frac{x}{L} = 0.02$ for the first 1000 seconds of the experiment are shown in Figure 6-1. Uncertainty bounds of each temperature profile are shown in the figure as well.

As it can be seen the temperature of the heated bed (T_{bed}=60℃) was decreasing while the temperature of the aluminum plate (initially at room temperature) was increasing. The temperature gradients in the porous bed and the aluminum plate were not the same because the thermal capacities of the packed bed and aluminum plate were different.

The temperature profile of the packed bed in three different positions of the particle bed during the transient test is shown in Figure 6-2.

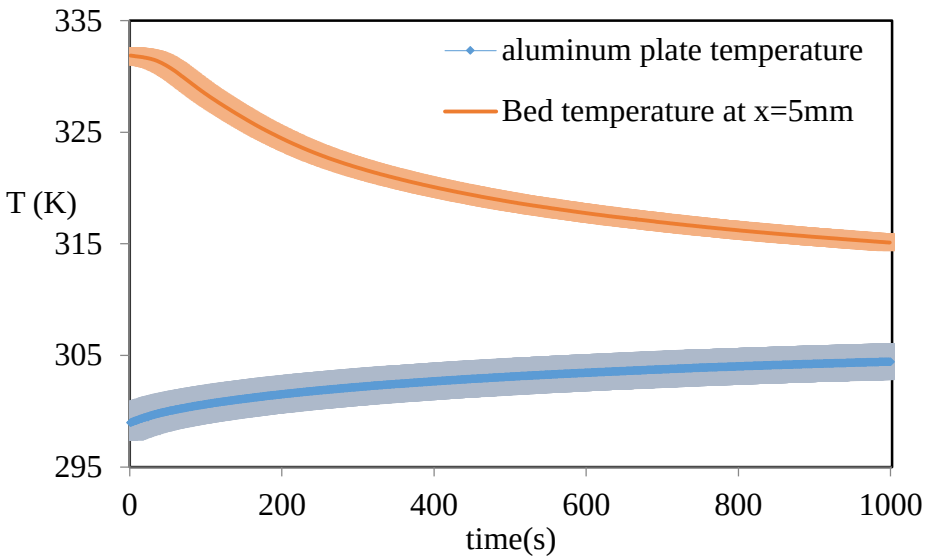

Figure 6-1 Temperature profile of the aluminum plate with the uncertainty bounds and temperature profile of the packed bed at x/L=0.02 with the uncertainty bounds, dry packed bed of silicagel particle particles (2.36 mm<d_p<2.80 mm).

It can be seen that the temperature was changing faster at the top of the bed that was closer to the aluminum plate, which was acting as a heat sink for the particle bed. As the time passed the temperature gradient was decreasing at $\frac{x}{L}$=0.02, which means it was getting close to the steady state condition. At the beginning of the transient test, the temperature change at $\frac{x}{L}$=0.29 was at a slower rate in comparison with the temperature change at the top of the bed, and the temperature gradient was decreasing during the time as the porous bed was approaching steady state condition. The temperature change at the bottom of the bed ($\frac{x}{L}$=0.98) was slower in comparison with the middle or top of the bed.

The temperature profile of the aluminum plate was used to simulate the energy transfer in the particle bed numerically. The numerical temperature profile and experimental temperature profile were compared to define the objective function. An estimation is called appropriate when the stopping criteria are satisfied, which means that the convergence error should be smaller than 0.001 and the objective function should be smaller than 100(K^2). The estimated values for the effective thermal conductivity for each type of packed particle bed and the uncertainties are listed in Table 6-1.

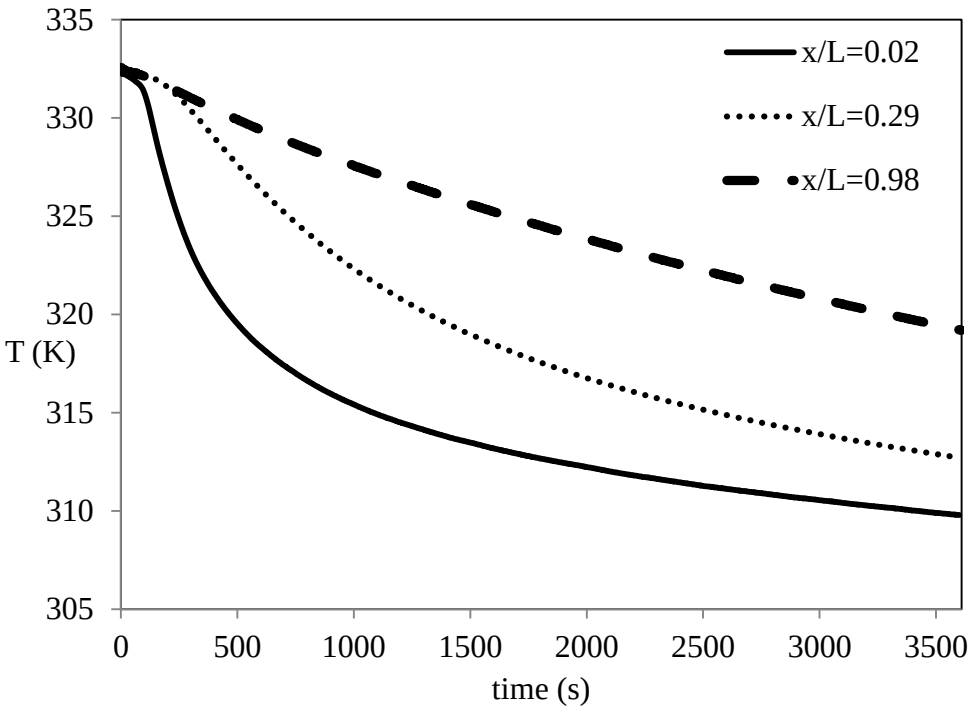

Figure 6-2 Temperature changes of the packed bed in three different positions versus time for the first hour of the experiment, dry packed bed of silicagel particle particles (2.36mm<d_p<2.80mm), T_{bed}=59℃, T_{Al}=24℃.

It is apparent from the thermal conductivities of the transparent particles that thermal conductivity is larger as the particle size is decreasing. As the particle size gets smaller the contact points between the particles increase, which results in a better conduction rate and larger value of thermal conductivity. The thermal conductivity of the blue silicagel particles has the smallest value among different particles because of the different chemical structure of the blue silicagel particles. The cobalt component with 10% of the weight fraction makes these particles different from the transparent silicagel particles. Cobalt has a lower thermal conductivity than silica, which results in a decrease in thermal conductivity of the blue silicagel in comparison with the transparent particles. Also, the thermal conductivity of the randomly packed bed of mixed transparent and blue silicagel is a value between the thermal conductivities of these two particles.

Table 6-1 Effective thermal conductivity, uncertainty of estimated effective conductivity, objective function, and convergence error for each type of the packed particle bed

Particle[1]	COEF k	Estimated effective thermal conductivity ($\frac{W}{m.K}$)	Relative uncertainty of the effective thermal conductivity (%)	Objective function (K^2)	Convergence error
Transparent silicagel $2.36<d_p<2.80$	0.59	0.234	1.97	83.50	0.00001
Transparent silicagel $2.00<d_p<2.36$	0.62	0.239	1.54	27.83	0.00001
Blue silicagel d_p= 1.6mm	0.55	0.180	0.84	2.88	0.00001
Mixed sample ½[$(2.36<d_p<2.80)$ + (d_p= 1.6mm)]	0.58	0.230	1.66	45.87	0.00001

Values of relative uncertainty for each type of the packed bed are listed in Table 6-1 as well. The relative uncertainty which shows the ratio of the uncertainty of the IHTP numerical model to the estimated value of unknown parameter, is in direct relation with the uncertainty of the measurements. It also has an inverse relation with the sensitivity matrix of the unknown parameter. Higher sensitivity to the effective thermal conductivity in the IHTP model will result in lower uncertainty in the outcome of IHTP. It can be seen that the relative uncertainty is increasing by the increase in the objective function.

[1] All the ranges of the particle size are in (mm)

The convergence error which is the difference between two successive iterations is listed in Table 6-1 for each particle bed as well. As illustrated, both objective function and convergence error are in a range that satisfies the stopping criteria.

The quality of the estimation is analyzed by comparing the experimental temperature profile and the numerical temperature profile obtained by applying the estimated value for the effective thermal conductivity. As mentioned before the estimation method is based on modifying the numerical temperature profile to fit with the experimental temperature profile at the position of the sensor chosen for the IHTP analysis ($\frac{x}{L} = 0.02$). Figure 6-3 to Figure 6-6 show the numerical and experimental temperature profiles for each type of particle bed at x/L=0.02. All the temperature profiles are for the first 1000 seconds of the experiment which was used in the IHTP solution.

The temperature of the particle bed was decreasing during the test because of the conductive heat transfer from the heated particle bed to the aluminum plate, which was initially at room temperature. The temperature gradient was small at the beginning because of the thermal capacity of the volume of the particle bed located between the aluminum plate and x/L=0.02. The particle bed with a higher porosity will have a smaller time delay to show a temperature drop at each point.

As the time proceeded the temperature changed in a higher rate because of the temperature difference between the particle bed and aluminum plate. When the temperature difference between the aluminum disk and the particle bed reduced, the rate of temperature change decreased until the time that the plate and the particle bed arrived at a steady state condition. The randomly packed bed of the smaller transparent silicagel particles had a larger temperature drop in comparison with the larger particles, because there were more contact points between the smaller particles.

As can be seen in most of the moments the numerical temperature profile is in good agreement with the experimental temperature profile. The differences arise because of the uncertainties in the known parameters, which are the porosity, and thermal capacity of the packed bed, used in the numerical analysis.

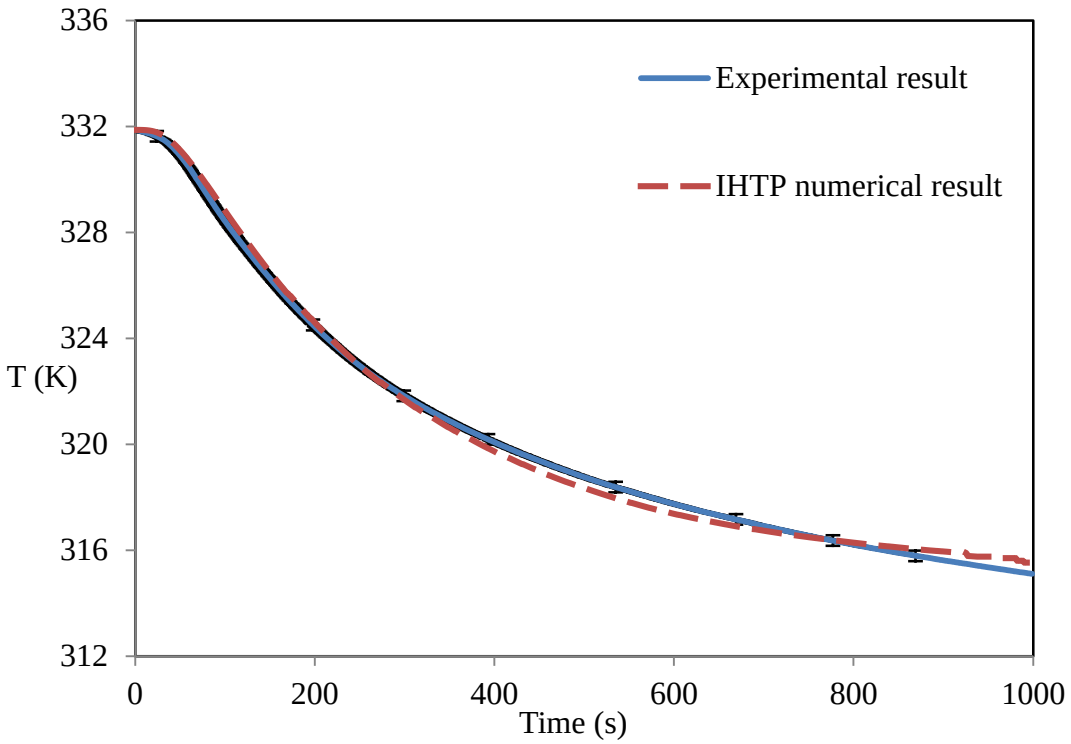

Figure 6-3- Experimental and IHTP numerical temperature profiles at x/L=0.02 for the transparent silicagel (2.36mm<d_p<2.80mm), Conduction test, dry heated packed bed, T_{bed}=59℃, T_{Al}=24℃.

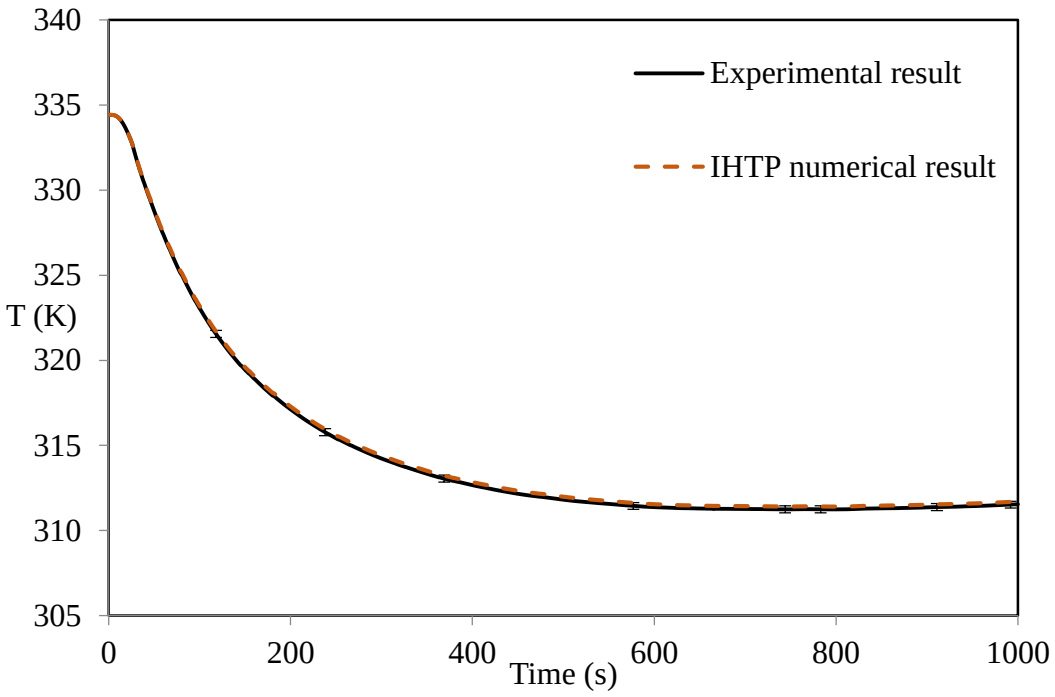

Figure 6-4- Experimental and IHTP numerical temperature profiles at x/L=0.02 for the transparent silicagel (2.00mm<d_p<2.36mm), Conduction test, dry heated packed bed, T_{bed}=60℃, T_{Al}=24℃.

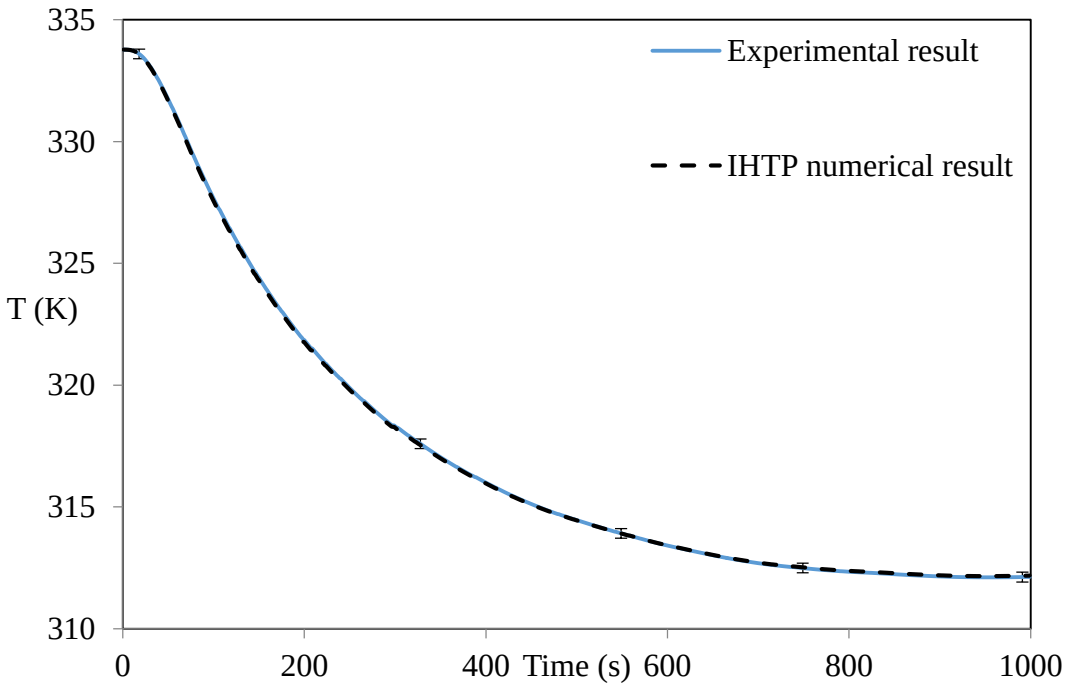

Figure 6-5- Experimental and IHTP numerical temperature profiles at x/L=0.02 for the blue silicagel ($d_{p(average)}$=1.6mm), Conduction test, dry heated packed bed, T_{bed}=61℃, T_{Al}=24℃.

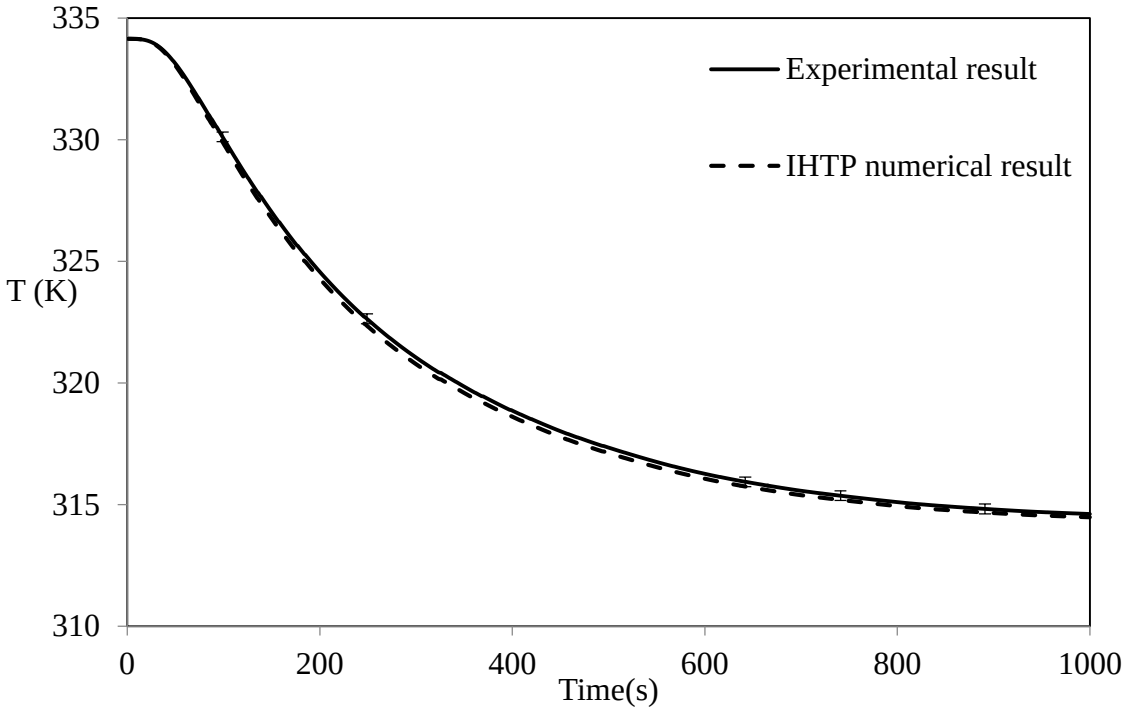

Figure 6-6- Experimental and IHTP numerical temperature profiles at x/L=0.02 for the mixture of silicagel particles (½[(2.36<d_p<2.80)+ (d_p= 1.6mm)]), Conduction test, dry heated packed bed, T_{bed}=61℃, T_{Al}=24℃.

Figure 6-7 to Figure 6-9 show the residual function versus time for each type of silicagel particle bed at x/L=0.02. As mentioned before in Chapter 2, residual function is the difference between the measured temperatures and simulated temperatures. The residual at each time node of the simulation is less than 0.5℃. The same initial conditions in both experimental and numerical simulations lead to the residual equal to zero at the beginning. Over time, because of the uncertainties in the values of porosity and thermal capacity used in the numerical analysis the residuals deviate from zero. Possible difference between the assumed position and exact position of the sensor in the packed particle bed can be another reason for this deviation.

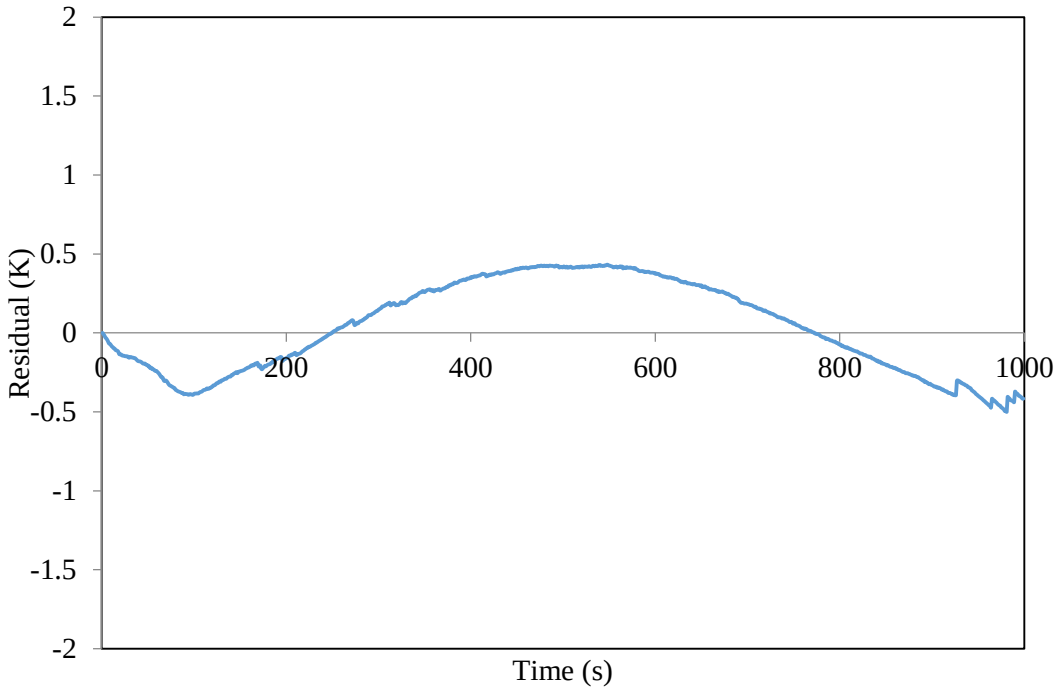

Figure 6-7 Residual function for x/L=0.02, transparent silicagel (2.00mm<dp<2.36mm), Conduction test, dry heated packed bed, T_{bed}=61℃, T_{Al}=24℃.

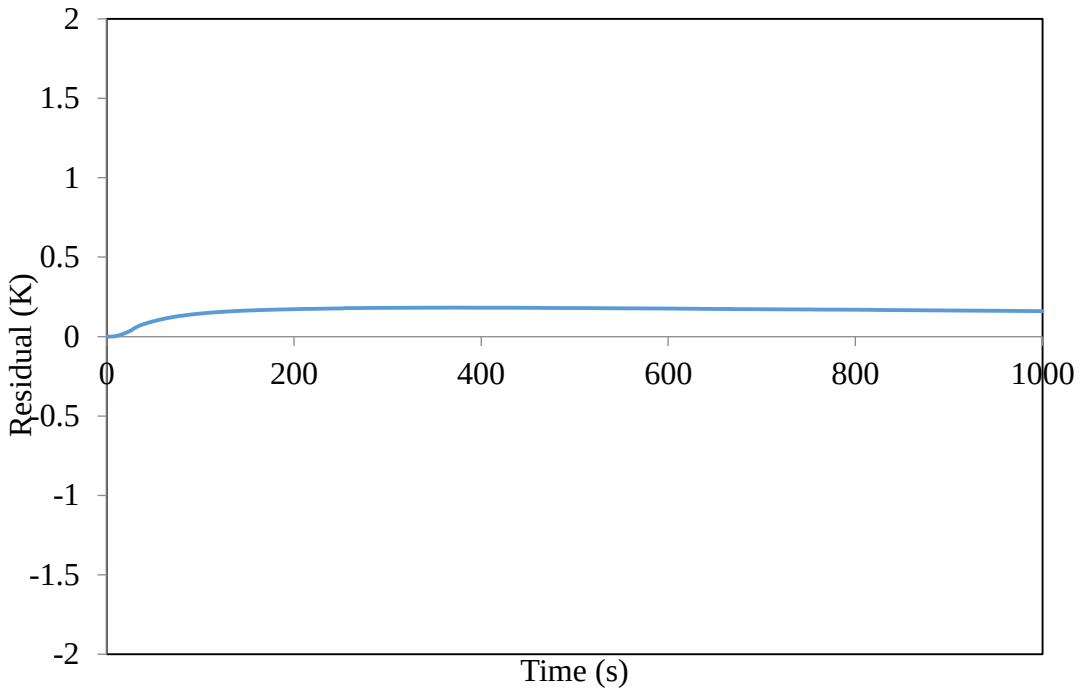

Figure 6-8 Residual function for x/L=0.02, transparent silicagel (2.00mm<dp<2.36mm), Conduction test, dry heated packed bed, T_{bed}=60℃, T_{Al}=24℃.

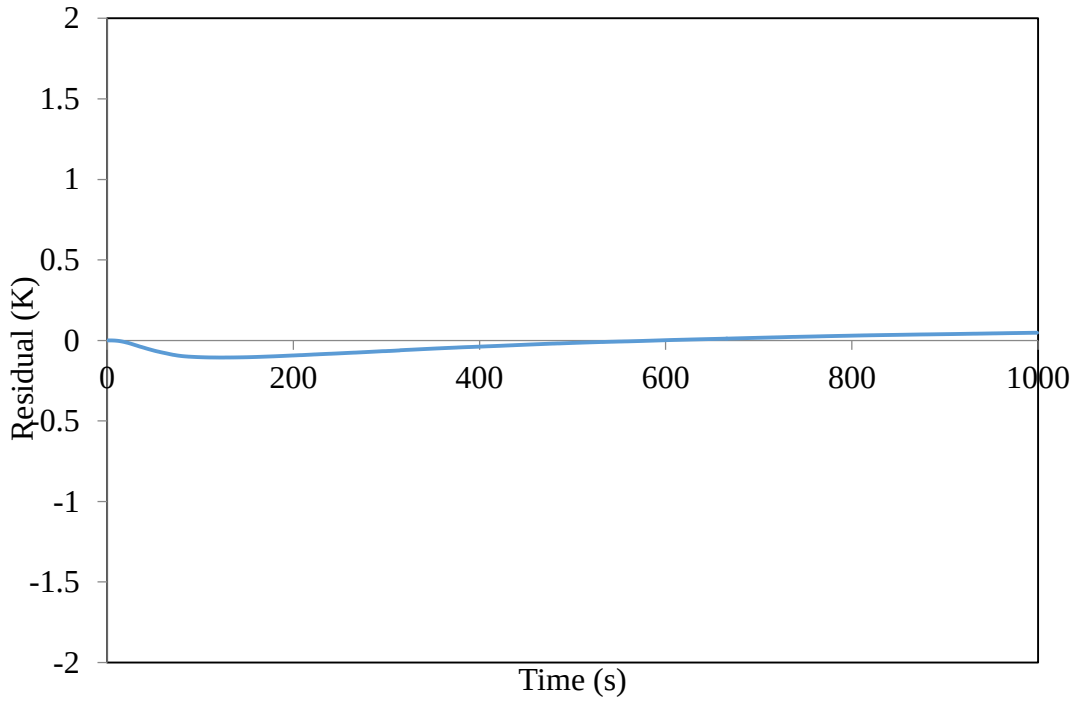

Figure 6-9 Residual function for x/L=0.02, blue silicagel ($d_{p(average)}$=1.6mm), Conduction test, dry heated packed bed, T_{bed}=61℃, T_{Al}=24℃.

Figure 6-10 to Figure 6-13 show the experimental and numerical temperature profiles at $\frac{x}{L} = 0.29$ for each type of particle bed. The temperature gradient was small at the beginning of the transient test because of the thermal capacity of the volume of the packed bed, which was above the chosen position ($\frac{x}{L} = 0.29$). Also, because this sensor was further from the aluminum disk the temperature gradient was also small for the first 1000*s* of the experiment when compared with the temperature drop at $\frac{x}{L} = 0.02$ in the same time period.

Comparison between the experimental and numerical results shows that they are in good agreement with each other, so applying the estimated effective thermal conductivity from IHTP analysis in the numerical simulation was successful.

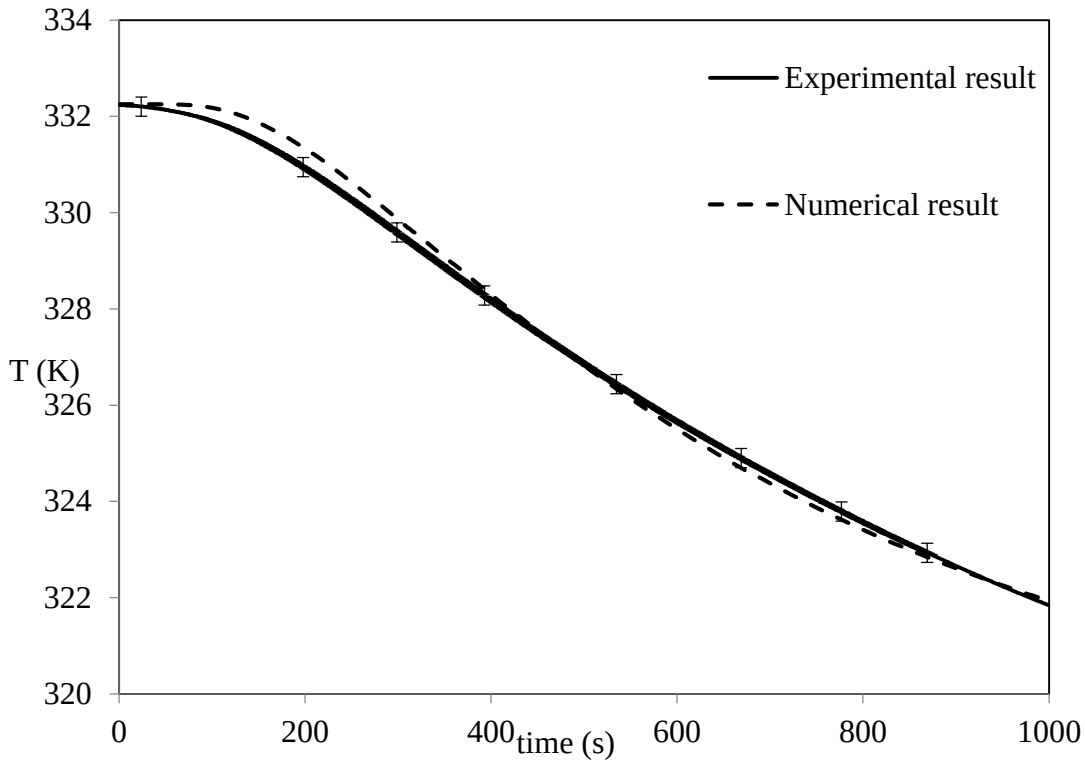

Figure 6-10 Experimental and IHTP numerical temperature profiles at x/L=0.29 for the transparent silicagel (2.36mm<d_p<2.80mm), Conduction test, dry heated packed bed, T_{bed}=59℃, T_{Al}=24℃.

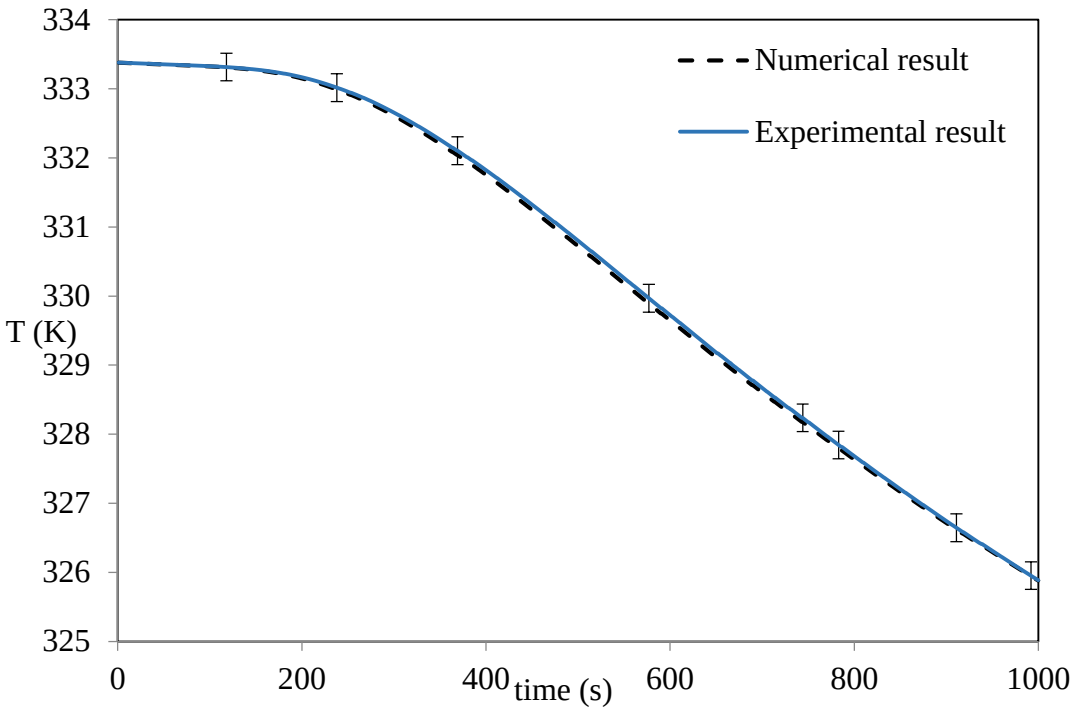

Figure 6-11 Experimental and IHTP numerical temperature profiles at x/L=0.29 for the transparent silicagel (2.00mm<dp<2.36mm), Conduction test, dry heated packed bed, Tbed=60℃, TAl=24

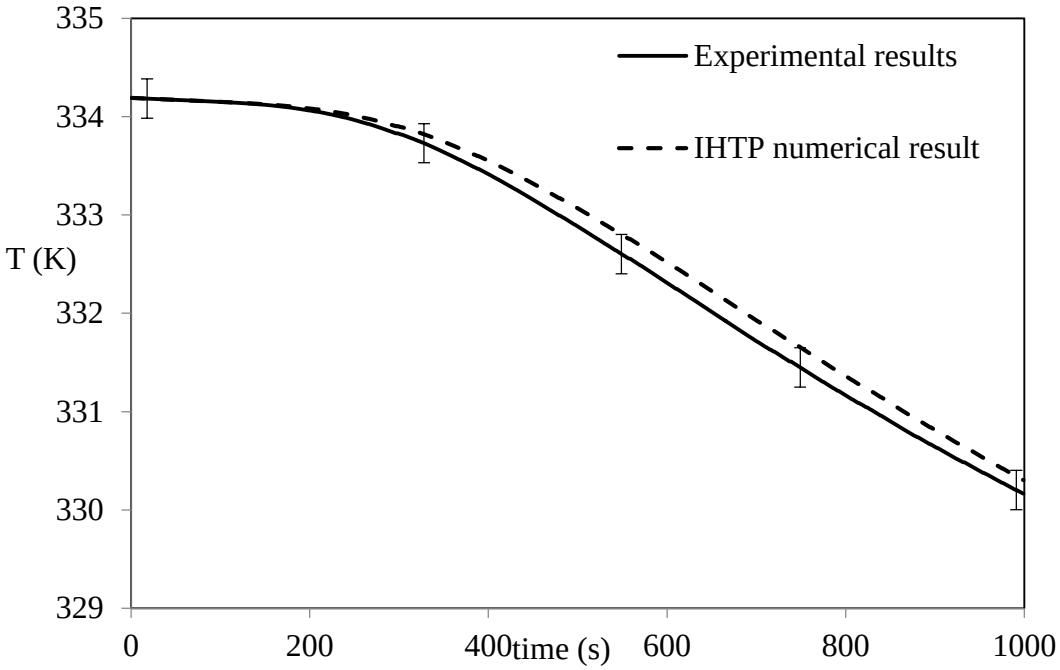

Figure 6-12 Experimental and IHTP numerical temperature profiles at x/L=0.29 for the blue silicagel (d_p(average)=1.6mm), Conduction test, dry heated packed bed, T_{bed}=61℃, T_{Al}=24℃.

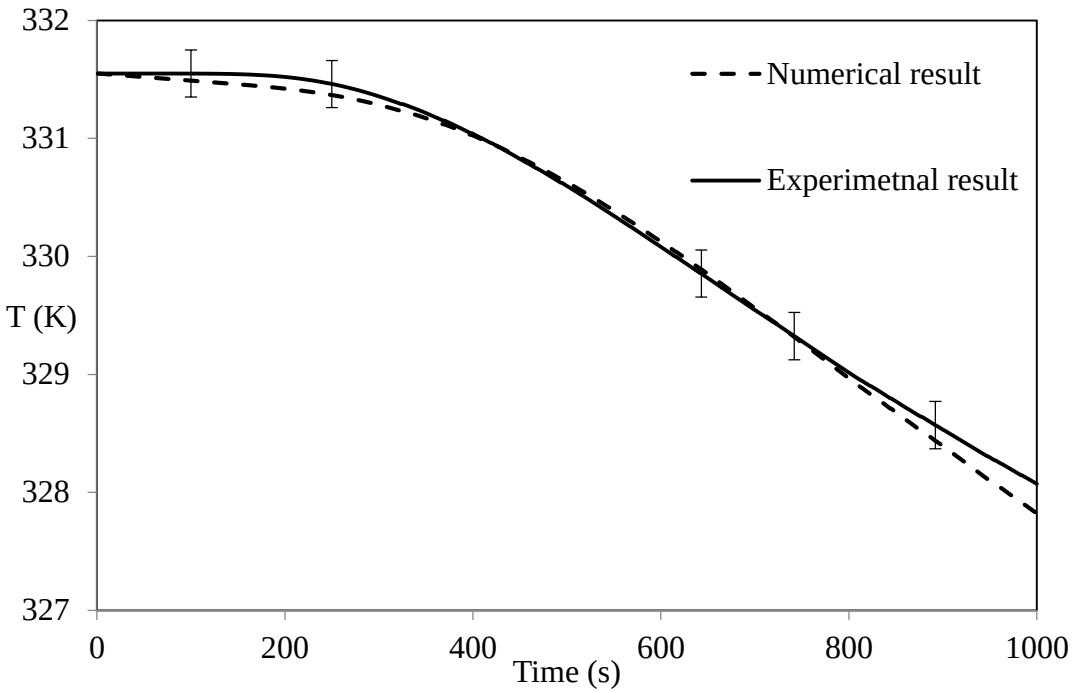

Figure 6-13 Experimental and IHTP numerical temperature profiles at x/L=0.29 for the mixture of silicagel particles (½[(2.36<d_p<2.80)+ (d_p= 1.6mm)]), Conduction test, dry heated packed bed, T_{bed}=61℃, T_{Al}=24℃.

6.2 Comparison with Theoretical Models

Tavman (1996) points out the minimum and maximum possible values of the effective thermal conductivity of a two-phase porous medium with known porosity. The minimum and maximum values are given by series and parallel phase distribution respectively. In the case of series distribution of the solid and gaseous phases the thermal conductivity can be expressed as:

$$k_{eff} = \frac{k_s k_f}{\varepsilon k_s + (1-\varepsilon) k_f} \qquad (6.1)$$

In the case of parallel distribution the thermal conductivity will have its maximum value, which is:

$$k_{eff} = \varepsilon k_g + (1-\varepsilon) k_s \qquad (6.2)$$

In the case of random distribution the effective thermal conductivity is given by weighted geometric mean, which is:

$$k_{eff} = k_s^{(1-\varepsilon)} k_g^{\varepsilon} \qquad (6.3)$$

Table 6-2 lists different values of the effective thermal conductivity estimated by different theoretical and semi-empirical models.

IHTP estimated effective thermal conductivities are between the maximum and minimum possible values for the effective thermal conductivity of the particle bed. Arrangement of the packed bed plays a role in other presented theoretical models. As in Zehner and Schlunder's model the particles are in point contact with each other in the direction of one-dimensional heat flux (Tavman, 1996), but silicagel particles are nearly spherical while the non-uniformities in shape can produce deviation from the point contact assumption.

Woodside and Messmer's model is based on the thermal resistance of the mixed parallel and series distribution of the solid and gaseous phase, and this model is for spherical particles in a cubic shape volume with the porosity is 0.47 (Tavman, 1996). The randomly packed feature of silicagel particle bed produces the difference between the IHTP estimated value and the expected value from Woodside and Messmer's model.

Listed models in Table 6-2 are for steady state conditions, but during the studied transient test temperature which is one of the influencing variables on effective thermal conductivity is changing continuously. Therefore, one can expect the differences between the reported thermal conductivities in the transient test versus the steady state test.

Gurgel and Klüppel (1996) reproted the thermal conductivity of the anhydrous packed bed of silicagel particles ($d_p = 3.5$ mm) as $0.196 \frac{W}{m.K}$. They found that any water content in the packed bed relsuted in increase of effective thermal conductivity. Also, increase in the pressure of the gasoeus phase had the same effect as well. As mentioned before, decrease in particle size increases effective thermal conductivity because of more possible contact points between the particles.

Table 6-2- Comparison of thermal conductivity for different models

Particle	Transparent silicagel $2.36<d_p<2.80$	Transparent silicagel $2.00<d_p<2.36$	Blue silicagel $d_p= 1.6mm$	Mixed sample ½[$(2.36<d_p<2.80)$+ $(d_p= 1.6mm)$]
Estimated effective thermal conductivity[2]	0.234	0.239	0.180	0.230
Minimum theoretical thermal conductivity	0.022	0.022	0.023	0.022
Maximum theoretical model	0.548	0.534	0.452	0.548
Geometric mean value	0.117	0.113	0.089	0.117
Zehner and Schlunder(1970)	0.091	0.088	0.072	0.091
Woodside and Messmer(1961)	0.132	0.127	0.100	0.132

6.3 Steady State Test of Effective Thermal Conductivity

The effective thermal conductivity of the packed bed of silicagel particles was measured during a steady state test by using a FOX314 heat flow meter instrument (Laser Comp). The FOX314 consists of a chamber that is used to measure the thermal conductivity

[2] All thermal conductivities are in $(\frac{W}{m.K})$

of solid materials. The chamber consists of a stationary cold plate at the top, movable hot plate at the bottom and insulating walls around the chamber. The sample is placed between these two plates and the thickness of the sample is determined by the sensors monitoring the position of the lower plate. An accurate heat flow meter (HFM) that is square shaped (101±1mm) and mounted at the center of each plate is able to measure the steady state heat flux in the sample. The guarded area in the chamber installed around the sample ensures one dimensional heat transfer between the plates through the sample (Figure 6-14). While there is a 25℃ temperature difference between the plates in the steady state condition the top plate is considered as the cold plate and the bottom plate is the hot plate. The theory of the instrument is based on the one-dimensional Fourier-Biot law (*FOX200 and FOX300 Series Instruments Manual*, 1999-2004):

$$q = k\frac{\Delta T}{\Delta X} \qquad (6.4)$$

where q is the heat flux (W/m^2), k is the thermal conductivity ($\frac{W}{m.K}$), and $\frac{\Delta T}{\Delta X}$ is the temperature gradient along the sample. Considering the sample is a solid material with flat surfaces at the top and bottom the instrument can make sure there is a uniform temperature field in the sample while it contacts the plates on each boundary. Thousands of thermocouples on each HFM measure the temperature across the HFM as well as the temperature of the upper and lower plates.

Each HFM is a homogenous solid material with known thermal properties. Knowing the temperature difference between the surfaces of the heat flow meter, one can find the heat flux through the HFM. Calibrating the output voltage (*V)* of thermocouples, which measure the temperature difference between the surfaces of the heat flow meter, the heat flux can be measured as

$$q = s_{cal}V \qquad (6.5)$$

where q is the heat flow through the upper/lower plate, s_{cal} is the calibration factor, and V is the output voltage of the thermocouples. Each plate has its own calibration factor consisting

of the thermal conductivity of the heat flow meter, length of the HFM, and a factor to convert voltage to the temperature. A view of the heat flow meter is shown in Figure 6-14.

The FOX 314 records the voltage of thermocouples for each HFM and finds the thermal conductivity based on the heat flux at each plate. The final thermal conductivity is the average of the obtained thermal conductivities of the lower and upper plates at steady state conditions.

The FOX314 is designed to measure the thermal conductivity of homogenous solid materials that are rigidly flat at the top and bottom. It is important that the contact area of the sample with each plate is larger than the HFM to ensure enough accuracy. The extra space between two plates in the chamber should be filled with the insulation guards (Figure 6-15).

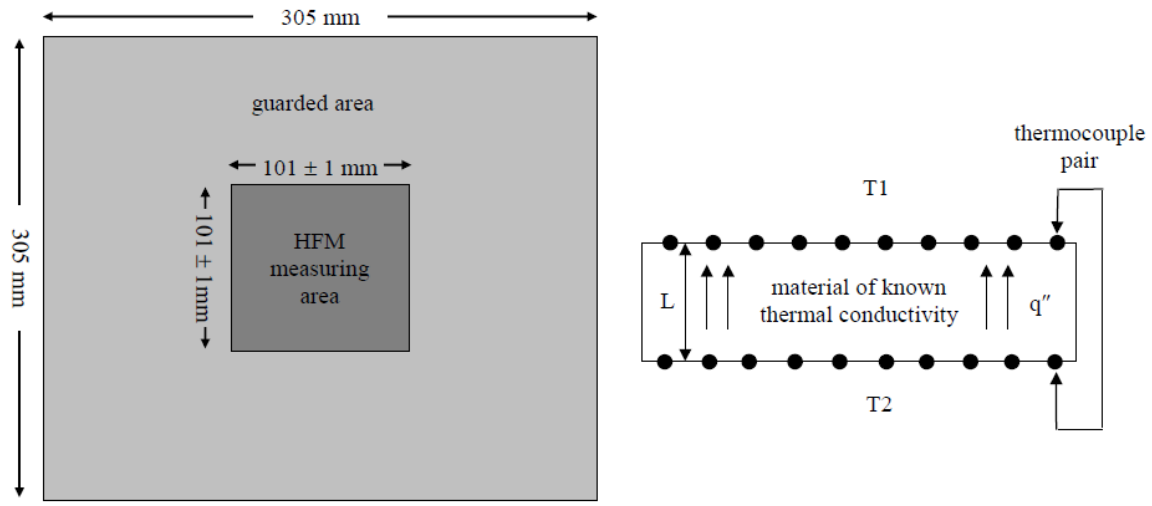

Figure 6-14- A schematic view of upper/lower plate and the heat flow meter in FOX314[3].

A plastic bag (a 25 *cm*×25 *cm* Ziploc bag with 1 *mm* layer thickness), filled with the dry silicagel particles was used as a randomly packed bed. By shaking and pressing the plastic bag an attempt was made to flatten the surfaces at the top and bottom of the packed bed and to remove the empty spaces inside the bag in order to have a compact packed bed. The dimensions of the plastic bag were larger than the HFM surface area and the extra space around the particle bed was insulated with Styrofoam to prevent any heat transfer other than the conductive heat transfer through the packed bed in the chamber. The temperature of the

[3] Department of Mechanical Engineering, University of Saskatchewan.2012. *Mechanical Engineering Laboratory (ME318.H3)*

upper plate was considered at 10℃ and the temperature of the lower plate was considered as 35℃. Knowing the output voltage and the calibration factor one can determine the heat flux by using equation (6.5). The effective thermal conductivity of the particle bed can be found by using equation (6.4) while the temperature difference and the height of the test bed are known. A schematic view of the experimental design can be seen in Figure 6-15. Also, a view of the FOX413 and the prepared sample of blue silicagel particles can be seen in Figure 6-16.

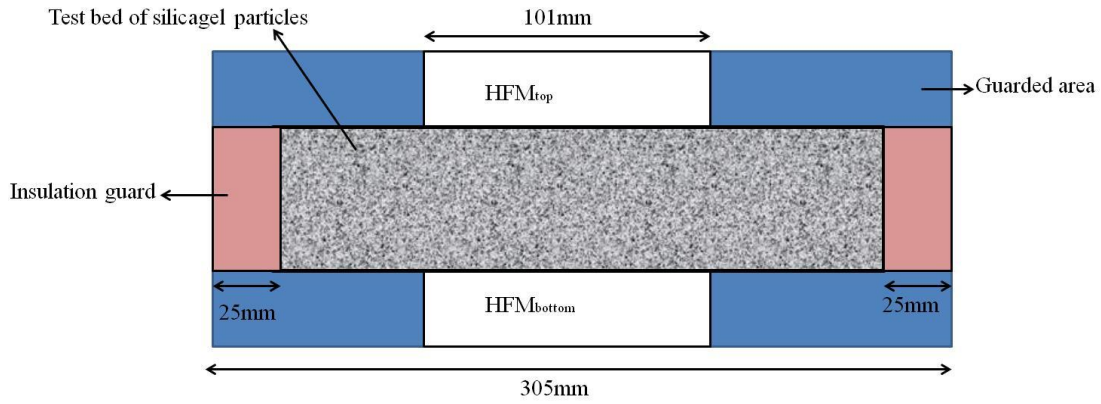

Figure 6-15 Schematic view of the experimental device used to measure the effective thermal conductivity of the randomly packed bed of silicagel particles in steady state conditions

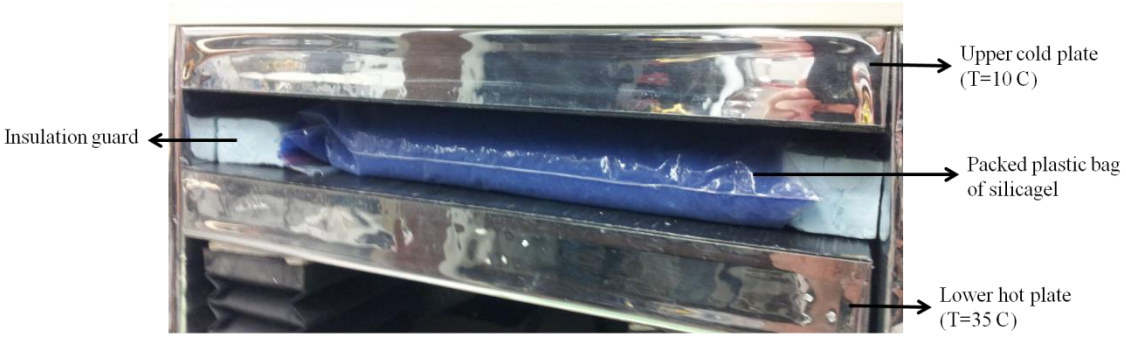

Figure 6-16 A view of the FOX314 with a bag of blue silicagel as the packed bed

Each type of particle bed was tested three times in the same conditions. Table 6-3 lists the final result of steady state test for each type of particles. The porosity of each particle bed was different due to differences in the particle size and the height of the particle beds. As can be seen the particle bed with the bigger size has the greater porosity because of fewer contact points and more available space between the particles.

Table 6-3 Effective thermal conductivity and its uncertainty obtained from the steady state tests

Particle[4]	Porosity	Effective thermal conductivity ($\frac{W}{m.K}$)	Relative uncertainty (%)	Estimated IHTP Effective thermal conductivity($\frac{W}{m.K}$)
Transparent silicagel $2.36<d_p<2.80$	0.68	0.128	2.10	0.234
Transparent silicagel $2.00<d_p<2.36$	0.59	0.133	2.10	0.239
Blue silicagel (d_p= 1.6mm)	0.57	0.141	2.10	0.180
Mixed sample ½[($2.36<d_p<2.80$) + (d_p= 1.6mm)]	0.57	0.134	2.10	0.230

It is clear that the outcomes of the steady state tests are different from the estimated thermal conductivities obtained from inverse solution. The differences in porosities for each type of particle bed in transient and steady state tests is one of the reasons for differences in thermal conductivity values in IHTP and steady state test.

The cross section of the packed bag is square while the cross section of the used particle bed in the transient test in a circle. The depth of the packed bag is 13 times smaller than the depth of the transient packed bed, so the geometry differences between the packed beds used in the steady state test and transient tests produces deviation between the results of these two tests.

[4] All the ranges of the particle size are in (mm)

As previously mentioned, the FOX314 is designed to measure the heat flux when the heat direction is completely from the bottom plate to the top plate. The polystyrene guards installed in the chamber around the packed bag were in touch with the cold and hot plates as well. Differences in the thermal resistances of the packed bed and the polystyrene guard caused heat flux between them which influenced the final calculated heat flux in the FOX314. The final measured thermal conductivity is influenced by the thermal conductivity of silicagel packed bag (solid phase and gaseous phase) and thermal conductivity of the polystyrene guard.

A steady state conduction test requires a uniform solid contact between the top and bottom surfaces of the sample and the cold and hot plates, respectively. The silicagel particles were packed in a zipped plastic bag. The surface of the plastic bag, which was in contact with the plates, was not uniformly rigid and flat, so it caused larger air gaps between the plates and the particle bed especially close to the edges of the bag. This non-uniformity on the outer layer of the plastic bag, curved shaped boundaries of the packed bag, deviates the packed bag from being a square uniform specimen. The thermal resistances of the air gaps influences the the final measured effective thermal conductivity of silicagel packed bed in steady state conditions.

As a result, non-satisfying boundaries of the packed bed, disturbances of the insulation guards and possible air gaps, differences in porosities, and different geometries in steady state sample and silicagel packed bed used in transient tests are the main factors in differences between the obtained effective thermal conductivity from steady state test versus results of the IHTP estimation.

Figure 6-17 to Figure 6-20 demonstrate comparison between the temperature profile obtained by applying the IHTP estimation of thermal conductivity, and the temperature profile obtained by using the thermal conductivity, which is the outcome of the steady state test. As shown, the numerical simulation, which uses the thermal conductivity obtained from the steady state test cannot predict the temperature profile of the packed bed. On the other side, the same numerical model yields a good agreement between the numerical and experimental temperature profiles when the IHTP estimation of effective thermal conductivity is applied.

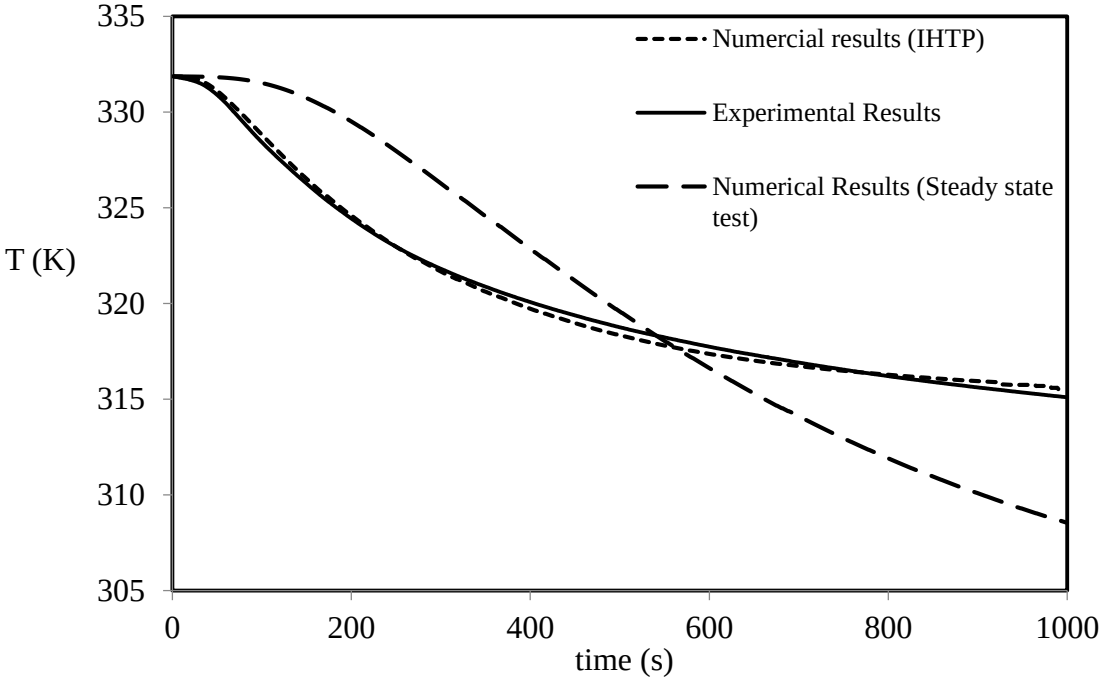

Figure 6-17 Comparison between experimental, and numerical temperature profiles using estimated k_{eff}, and numerical temperature profiles using steady state k_{eff} at x/L=0.02 for the transparent silicagel (2.36mm<d_p<2.80mm).

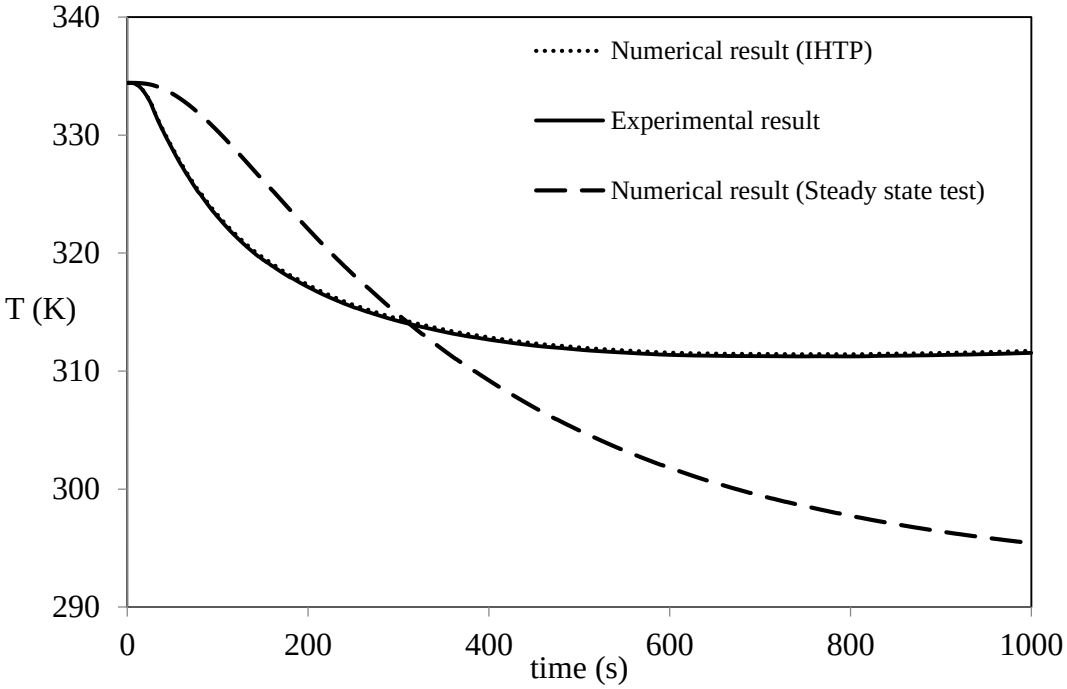

Figure 6-18 Comparison experimental, and numerical temperature profiles using estimated k_{eff}, and numerical temperature profile using steady state k_{eff} at x/L=0.02 for the transparent silicagel (2.00*mm*<dp<2.36*mm*).

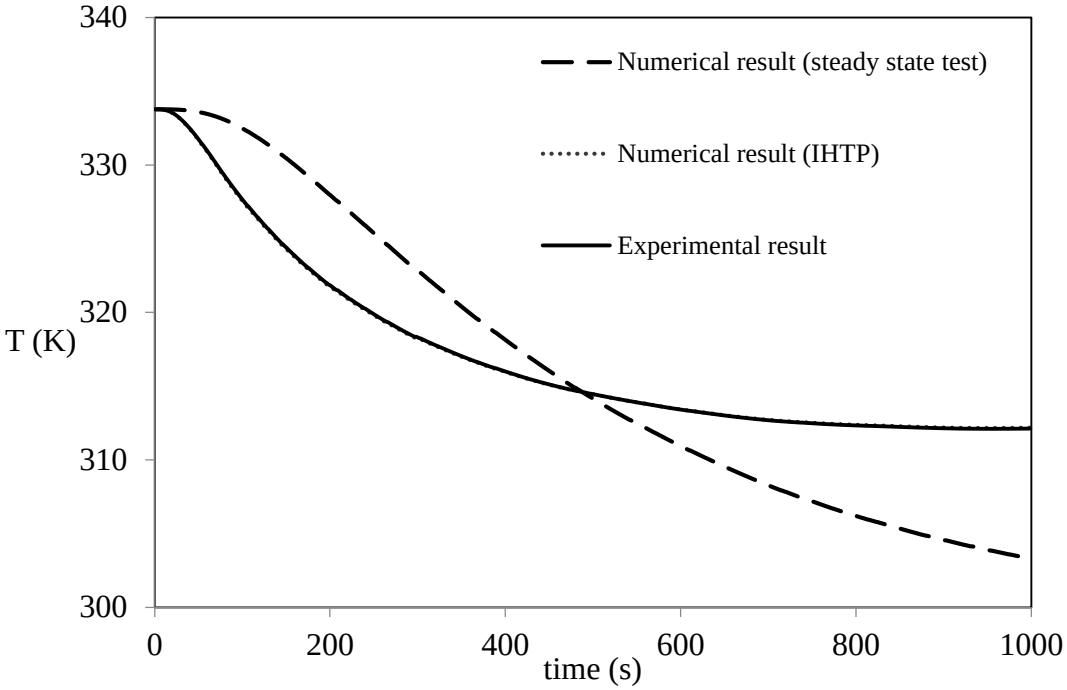

Figure 6-19 Comparison experimental, and numerical temperature profiles using estimated k_{eff}, and numerical temperature profile using steady state k_{eff} at x/L=0.02 for blue silicagel (d_p=1.6*mm*).

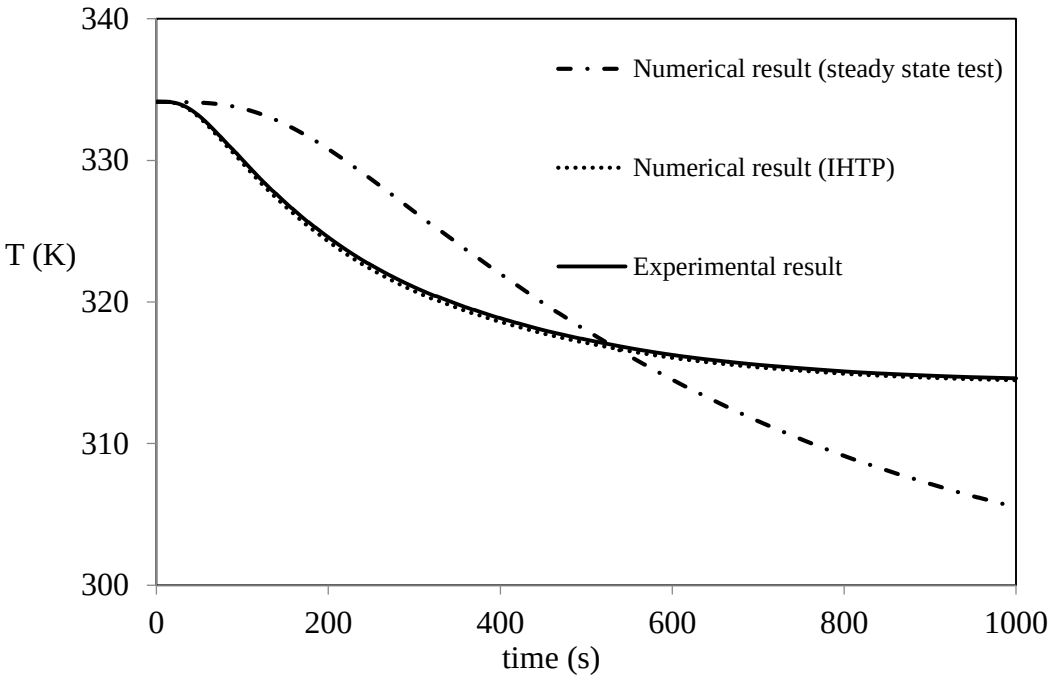

Figure 6-20 Comparison between experimental, and numerical temperature profiles estimated k_{eff}, and numerical temperature profile using steady state k_{eff} at x/L=0.02 for the mixed sample (½[(2.36*mm*<d_p<2.80*mm*)+ (d_p= 1.6*mm*)]).

6.4 Validating the IHTP Estimation by Modeling a Different Conduction Transient Test

The same transient conduction test used to provide measurements for the IHTP analysis was performed while the dry packed particle bed was at room temperature and the aluminum disk was heated. The transient experimental temperature profile of the particle bed at x/L=0.02 was measured. The conduction test was simulated numerically by using the direct solution in which the estimated effective thermal conductivity obtained from the IHTP analysis was applied. Experimental outcomes and numerical outcomes were compared to investigate the validity of the inverse solution.

Four different types of particle bed with the same properties as those used in the previous conduction test were used in these tests. The particles were heated in the oven for 24h to remove all possible moisture content. Dry airflow at room temperature passed through the particle bed to create a uniform temperature along the bed. The aluminum plate was heated to 60℃ and then mounted on the top of the particle bed in good contact with the inlet. The experimental process was the same and all the assumptions made for the previous conduction test were applied here as well.

A direct problem numerical model was applied to simulate the heat transfer between the dry packed bed at room temperature and the heated aluminum plate. The estimated effective thermal conductivity found in the IHTP analysis was applied for each type of particle bed.

The experimental and numerical temperature profiles of the packed bed at $\frac{x}{L} = 0.02$ were compared in order to validate the IHTP estimated effective thermal conductivity. As shown, in all the cases the objective function (sum of the residuals) was smaller than $100K^2$. It can be concluded that the estimated values of the effective thermal conductivity obtained from the IHTP analysis can be used for simulating other transient tests.

Table 6-4 lists the sum of the residuals, which is the difference between the measured and calculated temperature values for each type of particle bed.

As shown, in all the cases the objective function (sum of the residuals) was smaller than $100K^2$. It can be concluded that the estimated values of the effective thermal conductivity obtained from the IHTP analysis can be used for simulating other transient tests.

Table 6-4 sum of squared residuals for each type of particle bed at x/L=0.02, conduction test of dry randomly packed bed and heated aluminum plate.

Particle[5]	Objective function (K^2)
Transparent silicagel $2.36<d_p<2.80$	82.53
Transparent silicagel $2.00<d_p<2.36$	50.06
Blue silicagel $d_p= 1.6$	99.85
Mixed sample ½[$(2.36<d_p<2.80)$+ ($d_p= 1.6$mm)]	63.94

Figure 6-21 to Figure 6-24 show the experimental and numerical temperature profiles at x/L=0.02 for each type of particle bed were in good agreement during the transient test.

[5] All the ranges of the particle size are in (*mm*)

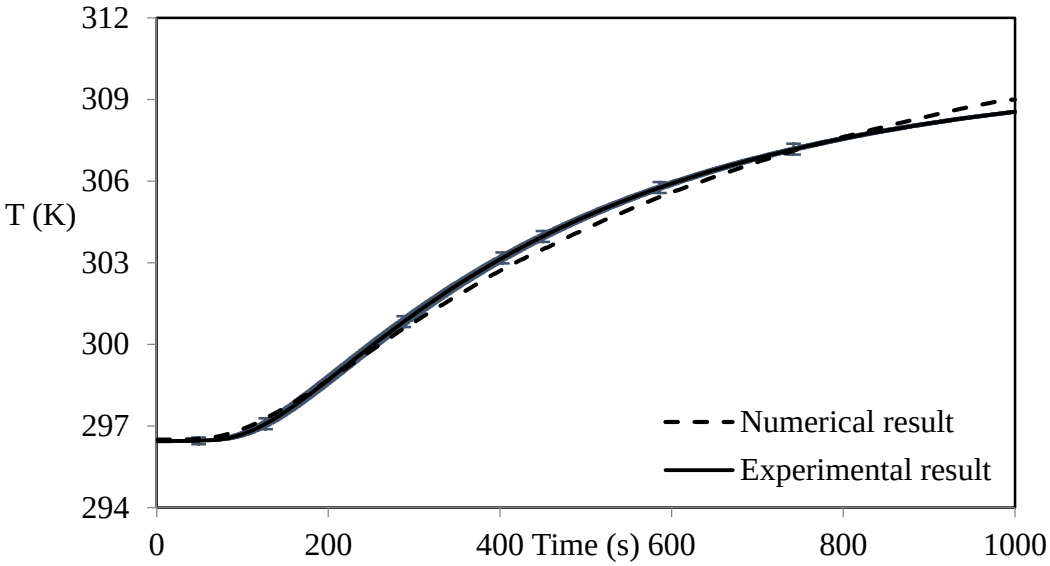

Figure 6-21- Experimental and numerical temperature profile at x/L=0.02, dry packed bed of transparent silicagel (2.36*mm*<d_p<2.80*mm*), T_{bed}=24℃, T_{Al}=62℃.

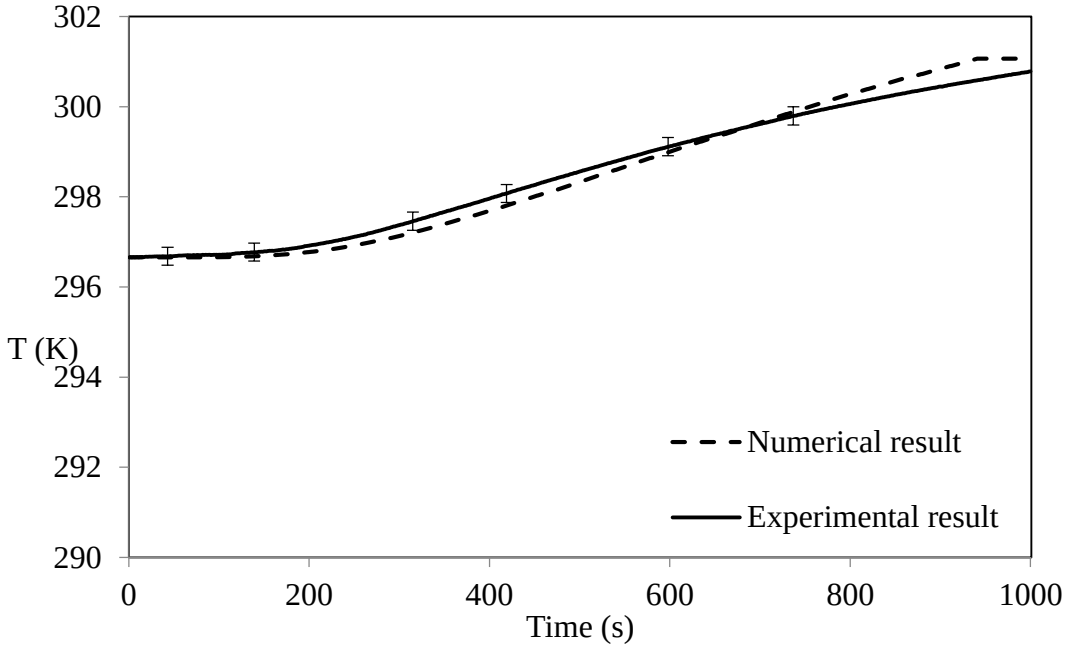

Figure 6-22- Experimental and numerical temperature profile at x/L=0.02, dry packed bed of transparent silicagel (2.00*mm*<d_p<2.36*mm*), T_{bed}=24℃, T_{Al}=60℃.

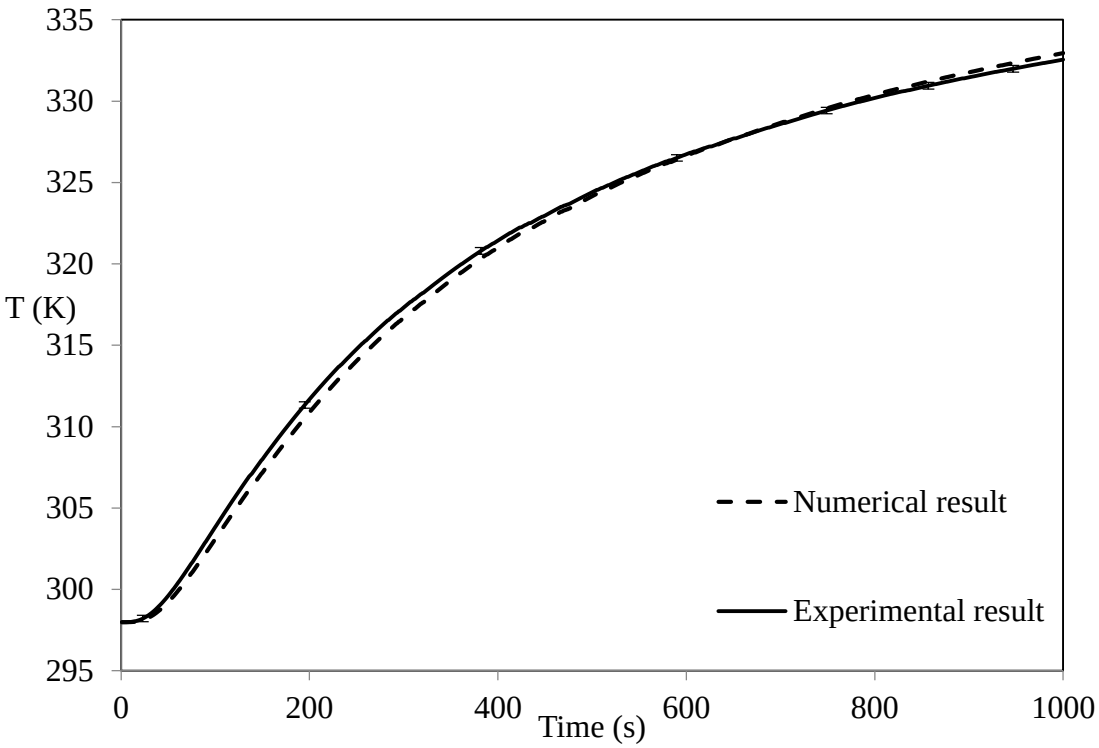

Figure 6-23 Experimental and numerical temperature profile at x/L=0.02, dry packed bed of blue silicagel (d_p=1.6*mm*), T_{bed}=24℃, T_{Al}=63℃.

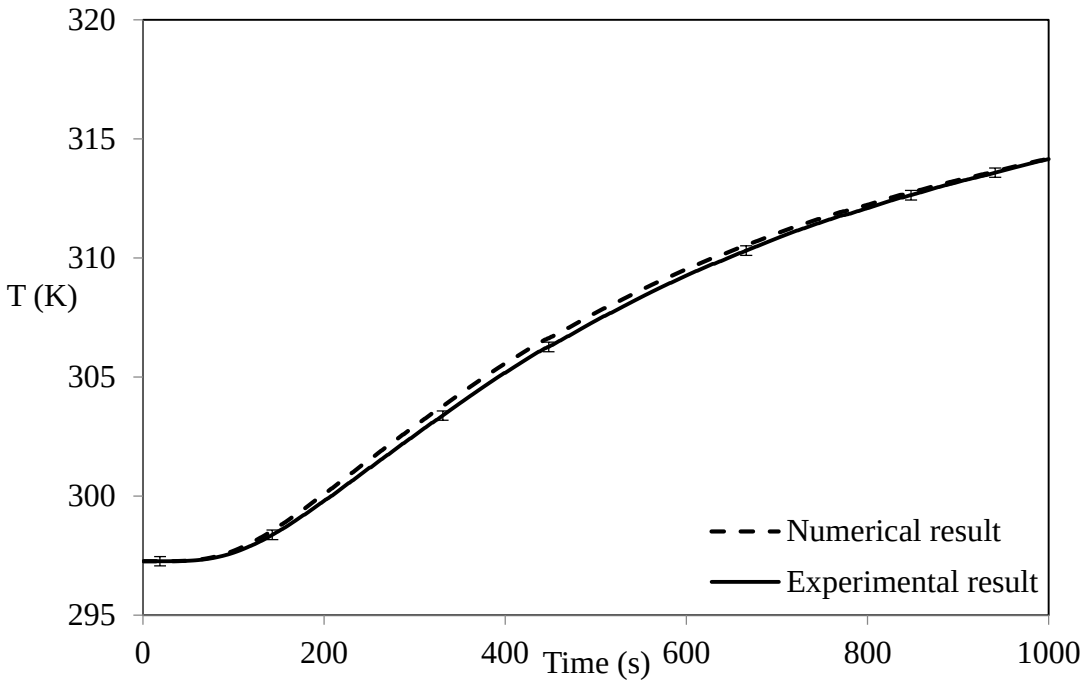

Figure 6-24 Experimental and numerical temperature profile at x/L=0.02, Mixed sample (½[(2.36mm<dp<2.80mm)+ (dp= 1.6mm)]), Tbed=24℃, TAl=63℃.

CHAPTER 7 SUMMARY, CONCLUSION AND FUTURE WORK

7.1 Summary

Study of heat and moisture transfer in the packed bed of particles is of interest during physical and chemical reactions for the processing or production, storage, and bulk transfer particles. A prediction of the values of the transport properties of the particle beds is necessary for numerical simulation of heat and mass transfer in them. In most cases, direct measurement of these properties, especially in transient step changes, is not possible.

This thesis introduces a methodology to estimate the energy transport properties of the particles by investigating the convective heat transfer coefficient, and effective conductivity of a packed bed of silicagel particles. Two different types of transient energy transfer tests, one for convection heat transfer and one for conduction heat transfer were performed on the packed beds. The transient temperature distribution in the packed bed for each test was used in IHTP analysis to estimate the unknown parameters. The estimation method in the IHTP solution was based on minimizing the experimental temperature profile measurements, and numerical temperature profiles, which was the outcome of direct numerical simulation of the transient test.

This research study can be summarized as follows:

1) Transparent silicagel particles (SigmaAldrich) and blue silicagel particles (Fisher Scientific) were used in the transient tests. Both of these particles had internal pores. The density of the solid phase (SiO_2) for the transparent silicagel particles, and the bulk density of the blue silicagel particles were available from the source companies. Two different methods were used to measure the total porosity, internal porosity, and external porosity of each type of particles. The mass and volume of the transparent silicagel particle bed were used to find the total porosity, while the mass and volume of the blue silicagel particle bed were used to find the external porosity of the packed bed. The result of a BET test provided the volume of the internal pores, which was used to find the internal porosity.

A sieving method was used to find the particle size of the transparent silicagel particles, and an optical method was used to find the particle size of the blue silicagel particles.

Specific volumetric surface area ($\frac{m^2}{m^3}$) was found using three different methods for each type of particles (Carmen correlation, BET, and particle diameter), and discussion was made about the confidence level of each method.

2) An experimental setup was designed to perform the convective heat transfer between the dry particle packed bed and dry airflow. This setup was able to apply a single temperature step change to start the convective transient test. Six different flow rates of dry air at room temperature passed through the heated packed bed (65℃), entering from the top. Convective heat transfer was the dominant heat transfer type between the dry bed and the airflow.

   Thermocouples recorded the transient temperature changes at three different positions in the packed bed. The best thermocouple was selected for use in the IHTP analysis based on the sensitivity study.

   A direct numerical simulation was used to simulate the convective transient tests. The experimental temperature profile at the chosen position and the numerical temperature profile at the same position were used in IHTP analysis. An inverse solution estimated the convective heat transfer coefficient at each flow rate by minimizing the difference between the experimental and numerical temperature profiles. The estimated value at each flow rate was used to simulate the temperature distribution in the whole bed and comparison between the experimental and numerical temperature distribution was made to examine the validity of the IHTP method. A new correlation was introduced for the changes of Nusselt number versus Reynolds number, and it was compared with one of the recent correlations.

3) A small change at the inlet section of the experimental setup used for the convection tests was applied in order to perform conduction transient tests between the heated silicagel packed bed and an aluminum plate mounted at the top of the packed bed in contact with the particles. The same IHTP procedure used

for estimation of the convective heat transfer coefficient was used for the effective conductivity of the packed bed. The estimated value of the thermal conductivity in each case was used to numerically simulate the transient tests, and comparison between the experimental and numerical temperature profiles was made in order to examine the validity of the inverse solution. Furthermore, the estimated effective thermal conductivity values were compared with the theoretical models and related discussions were made.

A direct steady state test was performed to find the effective thermal conductivity, and comparison was made between the results of the steady state tests and IHTP analysis. The causes of the differences between these two results and the validity of each method were discussed as well.

Temperature distribution of the packed beds during a new set of transient tests was compared with temperature distribution of the numerical simulation, which used the IHTP estimated thermal conductivity to model the tests, and good agreement was seen between the experimental and numerical results.

7.2 Conclusions

The following conclusions can be made about the thermal transport properties of silicagel particles in a test cell:

1- Both transparent silicagel particles and blue silicagel particles are nearly spherical. The diameter of the transparent silicagel particles is larger than the diameter of blue silicagel particles. Specific volumetric surface area has a direct relation with the square of diameter and has an inverse relation with the cube of diameter. As a result, as the diameter increases it is expected that the specific surface area decreases. This is in agreement with three different methods used to find the specific volumetric surface area.

   Carmen correlation, geometric method, and BET method, which were used to investigate the specific surface area, have significant differences. The geometric method is based on the assumption of point contact between the particles, which is not a strong assumption in an actual particle bed. BET analysis cannot distinguish

the external and internal surface areas because of lack of accurate boundaries and constraints that are necessary to recognize these two types of surfaces. Therefore, the Carmen correlation, which is based on the permeability measurement, can be used to estimate the external volumetric surface area. Errors are still expected because of the internal pores in the particles.

The internal porosity in the transparent silicagel particles is greater in comparison with the blue silicagel particles. Internal porosity is mostly related to the crystallization method used during the manufacture of the particles. The external porosity of the transparent silicagel particles is smaller than the blue silicagel particles due to the more compressed arrangement of transparent particles in the packed bed, which is the result of their larger density.

2- The convective heat transfer coefficient increases as the flow rate of the air increases during the transient tests. Higher flow rate results in a higher rate of convection between the heated packed bed and the airflow. The convective heat transfer coefficient for the transparent particles is greater than the one for blue silicagel particles at the same flow rate, while the external surface area is smaller in transparent particles in comparison with the blue particles. As a result, one can conclude that the same convection rate is seen in the packed bed of blue silicagel particles and transparent silicagel particles.

3- The experimental temperature distribution is in good agreement with the numerical temperature distribution obtained from the numerical model using the estimated convective heat transfer coefficient at each flowrate. The new correlation for the relation between the Nusselt number and Reynolds number is in agreement with the previous introduced correlation for spherical particles, which verifies the high confidence in the IHTP analysis.

4- The effective thermal conductivity of the packed bed decreases with an increase in the particle size. The contact points between the particles increases with a decrease in the particle size, so the thermal conductivity of the porous bed increases. Furthermore, the structure of the particles is another important parameter in effective thermal conductivity. Blue silicagel particles, which have

5% Cobalt Chloride inside their mass, have a smaller thermal conductivity in comparison with transparent silicagel particles.

5- Good agreement is seen between the experimental transient temperature distribution in the packed bed and the temperature distribution obtained numerically by using the estimated thermal conductivity in IHTP method. Furthermore, the estimated effective thermal conductivity is in the acceptable range for the packed bed. The theoretical values of effective thermal conductivity for each type of packed bed cannot yield a good agreement between the experimental and numerical temperature distribution.

6- The results of the steady state tests for each type of particle bed show more than 50% difference from the estimated thermal conductivity obtained from IHTP analysis. The instrument used to measure the effective thermal conductivity directly is not designed for porous materials. Furthermore, the temperature distribution obtained from the numerical simulation by using the experimentally measured thermal conductivity is not in agreement with the experimental tests. Using the estimated value of thermal conductivity in the numerical simulation of another type of transient test leads to good agreement between the numerical and experimental results. As a result, the IHTP analysis presents the most accurate estimation of the effective thermal conductivity.

7- The methodology used for the silicagel particles can be used to find the thermophysical properties of other particles and porous materials in order to create a modified simulation of heat and mass transfer in the porous beds.

7.3 Future Work

This work presents a new methodology to find the heat transport properties of particle beds by applying the methodology on a packed bed of silicagel particles. Further studies could be pursued on the following suggested ideas:

1- Transient tests of moisture transfer could be designed to estimate the convective mass transfer coefficient and mass diffusivity of porous beds by using inverse analysis. In the case of adsorption, the moisture uptake during the transient tests can be measured by using syringes to take samples and to isolate them (Nie, 2010).

2- More attention could be applied to the uncertainties of known properties of a porous bed, such as porosity, specific surface area, density, and heat capacity, to enable an IHTP analysis with a higher confidence level. Lower uncertainty in these properties will lead to smaller errors in the estimated values of unknown parameters. Inverse analysis could be used to find the properties mentioned above as well.

3- An IHTP solution could be applied to estimate the effective thermal conductivity at the interface of a particle bed and another medium (solid or fluid). Better understanding of the effective thermal conductivity at the interface with the packed bed, would provide a better estimation of the thermal conductivity.

4- Different algorithms could be used in the IHTP analysis of the thermophysical properties to investigate the best algorithm that could provide the fastest and most accurate estimation.

REFERENCES

Albouchi, F., Fetoui, M., Rigollet, F., Sassi, M., & Ben Nasrallah, S. (2005). Optimal design and measurement of the effective thermal conductivity of a powder using a crenel heating excitation. *International journal of thermal sciences, 44*(11), 1090-1097.

American Society of Heating, R., & Air-Conditioning, E. (1985). *ASHRAE handbook*. Atlanta, Ga.: American Society of Heating, Refrigerating, and Air-Conditioning Engineers.

Beck, J. V. (1979). Criteria for comparison of methods of solution of the inverse heat conduction problem. *Nuclear Engineering and Design, 53*(1), 11-22.

Beck, J. V., & Arnold, K. J. (1977). *Parameter estimation in engineering and science* (Vol. 8): Wiley New York.

Besant, R., & Simonson, C. (2003). Air-to-Air Exchangers. *ASHRAE JOURNAL, 45*, 42-52.

Blackwell, B., & Beck, J. V. (2010). A technique for uncertainty analysis for inverse heat conduction problems. *International Journal of Heat and Mass Transfer, 53*(4), 753-759.

Carman, P. C. (1938). Determination of the Specific Surface of Powders I. *Journal of the Society Chemical Industry, 57*, 225-234.

Chen, R. G., Chen, H., Besant, R. W., & Evitts, R. W. (2004). Properties required to determine moisture transport by capillarity, gravity, and diffusion in potash beds. *Industrial & engineering chemistry research, 43*(17), 5365-5371.

Coleman, W., & Steele, J. (1999). Experimentation and Uncertainty Analysis for Engineers: John Wiley & Sons, INC., USA.

Cui, M., Gao, X., & Zhang, J. (2012). A new approach for the estimation of temperature-dependent thermal properties by solving transient inverse heat conduction problems. *International journal of thermal sciences, 58*, 113-119.

de Matos Jorge, L. M., Jorge, R. M. M., & Giudici, R. (2010). Experimental and numerical investigation of dynamic heat transfer parameters in packed bed. *Heat and mass transfer, 46*(11-12), 1355-1365.

Dennis, J. J. E., & Schnabel, R. B. (1983). *Numerical methods for unconstrained optimization and nonlinear equations* (Vol. 16). Englewood Cliffs, N.J.: Prentice-Hall.

Evitts, R. W., Yungwirth, T., & Besant, R. W. (2006). Measuring moisture content of potash bulk fertilizers using a steel ball in a transient heat transfer process. *Industrial & engineering chemistry research, 45*(9), 3287-3292.

FOX200 and FOX300 Series Instruments Manual. (1999-2004). LaserComp Inc., Saugus, MA, USA.

Gurgel, J. M., & Klüppel, R. P. (1996). Thermal conductivity of hydrated silica-gel. *The Chemical Engineering Journal and the Biochemical Engineering Journal, 61*(2), 133-138.

Hadamard, J. (1952). Lectures on Cauchy's problem: In linear partial differential equations. New York: Dover.

Huang, C.-H., & Yeh, C.-Y. (2002). An inverse problem in simultaneous estimating the Biot numbers of heat and moisture transfer for a porous material. *International Journal of Heat and Mass Transfer, 45*(23), 4643-4653.

Incropera, F., & DeWitt, D. (2002). *Fundamentals of Heat and Mass Transfer*. New York: J.Wiley & Sons.

Jiang, P.-X., Xu, R.-N., & Gong, W. (2006). Particle-to-fluid heat transfer coefficients in miniporous media. *Chemical Engineering Science, 61*(22), 7213-7222.

Kar, K., & Dybbs, A. (1982). Internal heat transfer coefficients of porous metals. *NASA STI/Recon Technical Report A, 84*, 13239.

Kaviany, M. (1995). *Principles of Heat Transfer in Porous Media*. New York: Springer-Verlag.

Kuye, A., Oko, C., & Nnamchi, S. (2010). Determination of the thermal conductivity and specific heat capacity of neem seeds by inverse problem method. *Journal of Engineering Science and Technology Review, 3*(1), 1-6.

Lee, D.-Y., & Vafai, K. (1999). Analytical characterization and conceptual assessment of solid and fluid temperature differentials in porous media. *International Journal of Heat and Mass Transfer, 42*(3), 423-435.

Ng, K., Chua, H., Chung, C., Loke, C., Kashiwagi, T., Akisawa, A., & Saha, B. (2001). Experimental investigation of the silica gel–water adsorption isotherm characteristics. *Applied Thermal Engineering, 21*(16), 1631-1642.

Nie, X. (2010). Heat and moisture migration within a porous urea particle bed. Phd, University of Saskatchewan.

Nie, X., Evitts, R., Besant, R., & Bolster, J. (2011). A new technique to determine convection coefficients with flow through particle beds. *Journal of heat transfer, 133*(4).

Nie, X., Evitts, R. W., & Besant, R. W. (2008). Simulation of moisture uptake and transport in a bed of urea particles. *Industrial & engineering chemistry research, 47*(20), 7888-7896.

Nield, D. A., & Bejan, A. (2006). *Convection in porous media*. New York: springer.

Ofuchi, K., & Kunii, D. (1965). Heat-transfer characteristics of packed beds with stagnant fluids. *International Journal of Heat and Mass Transfer, 8*(5), 749-757.

Ozisik, M. N., & Orlande, H. R. (2000). *Inverse heat transfer: fundamentals and applications*. New York: Taylor & Francis.

Patankar, S. V. (1980). *Numerical heat transfer and fluid flow*. New York: McGraw-Hill.

Peng, S., Besant, R. W., & Strathdee, G. (2000). Heat and mass transfer in granular potash fertilizer with a surface dissolution reaction. *The Canadian Journal of Chemical Engineering, 78*(6), 1076-1086.

Pesaran, A. A., & Mills, A. F. (1987). Moisture transport in silica gel packed beds—I. Theoretical study. *International Journal of Heat and Mass Transfer, 30*(6), 1037-1049.

Prat, M. (1989). On the boundary conditions at the macroscopic level. *Transport in porous media, 4*(3), 259-280.

Prat, M. (1990). Modelling of heat transfer by conduction in a transition region between a porous medium and an external fluid. *Transport in porous media, 5*(1), 71-95.

Rawle, A. Particle Sizing - An Introduction. Retrieved 2013.9.13, from http://www.silver-colloids.com/Tutorials/psintro.html

Raynaud, M. (1999). Strategy for experimental design and the estimation of parameters. *High Temperatures-High Pressures, 31*(1), 1-15.

Shah, R., & London, A. (1978). Laminar Flow Forced Convection in Ducts: a Source Book for Compact Heat Exchanger Analytical Data, Supl. 1: Academic Press, New York.

Singh, R. (2004). Effective thermal conductivity of highly porous two-phase systems. *Applied Thermal Engineering, 24*(17), 2727-2735.

Solmuş, İ., Rees, A. S., Yamalı, C., & Baker, D. (2012). A two-energy equation model for dynamic heat and mass transfer in an adsorbent bed using silica gel/water pair. *International Journal of Heat and Mass Transfer, 55*(19), 5275-5288.

Sun, J. (2003). An investigation of temperature and humidity variations during silica gel-moisture interactions. MSc, University of Saskatchewan.

Sun, J., & Besant, R. W. (2005). Heat and mass transfer during silica gel–moisture interactions. *International Journal of Heat and Mass Transfer, 48*(23), 4953-4962.

Tavman, I. (1996). Effective thermal conductivity of granular porous materials. *International Communications in Heat and Mass Transfer, 23*(2), 169-176.

Telejko, T., & Malinowski, Z. (2004). Application of an inverse solution to the thermal conductivity identification using the finite element method. *Journal of Materials Processing Technology, 146*(2), 145-155.

Vadasz, P. (2005). Explicit conditions for local thermal equilibrium in porous media heat conduction. *Transport in porous media*, *59*(3), 341-355.

Wen, D., & Ding, Y. (2006). Heat transfer of gas flow through a packed bed. *Chemical Engineering Science*, *61*(11), 3532-3542.

Whitaker, S. (1972). Forced convection heat transfer correlations for flow in pipes, past flat plates, single cylinders, single spheres, and for flow in packed beds and tube bundles. *AIChE Journal*, *18*(2), 361-371.

Yang, J., Wang, J., Bu, S., Zeng, M., Wang, Q., & Nakayama, A. (2012). Experimental analysis of forced convective heat transfer in novel structured packed beds of particles. *Chemical Engineering Science*, *71*, 126-137.

Znaidia, S., Albouchi, F., Mzali, F., Jemnia, A., & Nasrallah, S. B. (2009). Optimal Experiment Design and Measurement of the Effective Thermal Conductivity of a Porous Medium in the Presence of Free Convection. *Journal of Porous Media*, *12*(6).

Zueco, J., Alhama, F., & González-Fernández, C. (2006). Inverse determination of temperature dependent thermal conductivity using network simulation method. *Journal of Materials Processing Technology*, *174*(1), 137-144.

APPENDIX A CALIBRATION OF THE TEMPERATURE AND RELATIVE HUMIDITY SENSORS

All the thermocouples and relative humidity sensors were calibrated in the ranges used for the experiments. The range of temperature used in the experiments was between 20℃ and 65℃, and the relative humidity range was between 10% up to 100%.

A.1 Thermocouple Calibration

A Fluke Hart Scientific 9107 Ultracold Dry-Well Calibrator (uncertainty ±0.1 K) was used to calibrate 15 thermocouples used in the transient experiments. The temperature of the calibrator is considered as the reference temperature during the calibration. A view of the calibrator can be seen in Figure A-1.

Figure A-1 Fluke Hart Scientific 9107 Ultracold Dry-Well Calibrator

All the thermocouples were connected to a board with 24 channels, and the board was connected to the DAS system (SXI-1000, NATIONAL INSTRUMENTS). Thermocouples were T-type model with a thickness of less than 1 *mm*. Figures A-2 and Figure A-3 show the channel board and DAS, respectively.

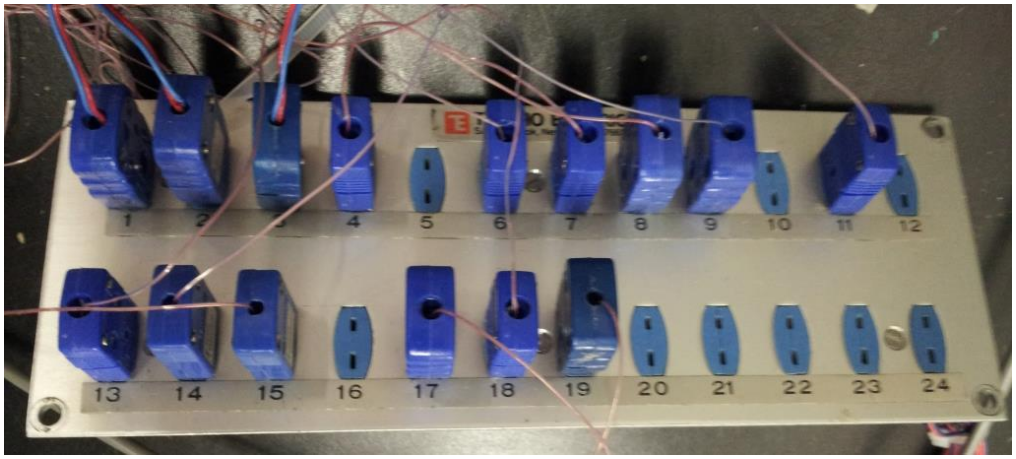

Figure A-2 Channel board is used to connect the thermocouples to DAS

Figure A-3 National Instrument data acquisition system

The temperature of the calibrator was considered as a reference temperature and readings from each thermocouple were corrected by a calibration curve which can be presented as

$$T_{reference} = a.T_{reading} + b \qquad \text{(A.1)}$$

a and b can be determined for each thermocouple and R^2 values of each calibration curve are 1.

A.1.1 Calibration process

1- Setting the temperature of the calibrator at 15 ℃ and putting four thermocouples in its chamber; then waiting until each thermocouple shows a stable reading of the temperature.

2- Record the readings of each thermocouple 60 times (1 Hz).

3- Repeating step 1 and 2 while the temperature of the calibrator is set to 20℃, 25℃, 30℃, 35℃, 40℃, 45℃, 50℃, 55℃, 60℃, 65℃, 70℃, 75℃, 80℃, and 85℃.

4- Repeating steps 1 and 2 while decreasing the temperature of the chamber of the dry-well calibrator with a step of 10℃ from 85℃ to15℃.

5- Repeating steps 1 and 2 for the increase in temperature of the calibrator with a step of 15 ℃ from 15℃ to 75℃.

A.1.2 Calibration and uncertainty analysis:

15 channels were calibrated using a Dry-Well Calibrator and data acquisition system (DAS). 60 readings were documented for each channel in 28 different reference temperatures. The arithmetic mean of the readings at each reference temperature is considered as the measured temperature. Therefore, standard deviation for each set of readings in a reference temperature can be found by using the following formulation (Coleman & Steele, 1999)

$$S = \left[\frac{\sum_{n=1}^{N}(T_n - T_{ave})^2}{N-1}\right] \qquad \text{(A.2)}$$

where N is the number of readings, T_n is the nth reading of the temperature and T_{ave} is the average of temperature readings.

Also, precision of temperature reading can be calculated as

$$P = t\frac{S}{\sqrt{N}} \tag{A.3}$$

where t is the two-tailed value of the student t distribution for the 95% confidence level and is equal to 2.0 for more than 30 readings in the same situation of the experiment (Coleman & Steele, 1999).

Average value and reference are compared with each other to find the calibration curve for each thermocouple. A linear curve fitting estimation ($T_{ref} = aT_{ave} + b$) is used to convert actual data to the calibrated data. The values of a, b, and R^2 are listed in Table A-1.

Systematic uncertainty that is a fixed error can be determined by calculating the data reduction error and data acquisition errors. The uncertainty of the calibrator is 0.1K.

Data reduction error happens because of replacing the actual data with values obtained from a curve fitting equation. First, it is required to find the standard error of estimate (SEE) that is

$$SEE = \left[\frac{\sum_{k=1}^{N}(T_{fit} - T_{reference})^2}{N - C}\right] \tag{A.4}$$

where C is the number of constants in the curve fitting equation (C=2), T_{fit} is the temperature obtained from the equation of curve at each reference temperature, and N is the number of data points used in the curve fitting (N=15). The bias error of the curve fit can be estimated as

$$B_{fit} = t(SEE) \tag{A.5}$$

where t is the two-tailed value of the student t distribution for N-C (2.16).

The total bias uncertainty in each reference temperature can be calculated using the following equation

$$B_{total} = \sqrt{{B_{fit}}^2 + {B_{instrument}}^2} \quad \text{(A.6)}$$

where $B_{instrument}$ is the bias error presented by the company which is 0.1 for the Ultracold Dry-Well Calibrator.

The uncertainty of calibration for each channel, can be calculated by adding precision and bias errors

$$U = \sqrt{{B_{total}}^2 + P^2} \quad \text{(A.7)}$$

Table A-2 shows the calibration uncertainty for each channel at each reference temperature.

Table A-1 Constants of curve fitting for each thermocouple

Channel number	A	B	R^2
#1	1.0053	-0.0534	1
#2	1.0419	-0.7744	1
#3	1.0089	-0.2334	1
#4	1.0166	-0.8264	1
#5	1.0225	-1.5032	1
#6	1.0290	-1.8202	1
#7	1.0268	-1.1567	1
#8	1.0133	-1.2758	1
#9	1.0256	-2.3077	1
#10	1.0194	-1.2447	1

Channel number	A	B	R^2
#11	1.0235	-1.6970	1
#12	1.0114	-1.1130	1
#13	1.0149	-1.0121	1
#14	1.0146	-1.0113	1
#15	1.0192	-0.6919	1

Table A-2 Uncertainty values for each thermocouple at different reference temperatures

Temperature (℃)	15	20	25	30	35	40	45	50	55	60	65	70	75	80	85
Channel	Uncertainty (℃)														
Channel #1	0.1413	0.1455	0.1413	0.1414	0.1414	0.1417	0.1413	0.1413	0.1413	0.1415	0.1416	0.1413	0.1420	0.1413	0.1413
Channel #2	0.1326	0.1332	0.1327	0.1327	0.1330	0.1332	0.1328	0.1326	0.1329	0.1339	0.1333	0.1326	0.1330	0.1332	0.1337
Channel #3	0.1084	0.1083	0.1081	0.1081	0.1081	0.1081	0.1081	0.1081	0.1081	0.1081	0.1081	0.1082	0.1081	0.1081	0.1081
Channel #4	0.1254	0.1316	0.1254	0.1254	0.1254	0.1257	0.1253	0.1254	0.1254	0.1254	0.1258	0.1254	0.1257	0.1254	0.1253
Channel #5	0.1082	0.1084	0.1082	0.1083	0.1082	0.1082	0.1082	0.1084	0.1082	0.1082	0.1083	0.1083	0.1087	0.1083	0.1082
Channel #6	0.1923	0.1951	0.1923	0.1923	0.1923	0.1924	0.1926	0.1923	0.2025	0.1928	0.1927	0.2417	0.1928	0.1942	0.1923

Temperature (℃)	15	20	25	30	35	40	45	50	55	60	65	70	75	80	85
Channel	Uncertainty (℃)														
Channel #7	0.1220	0.1258	0.1219	0.1219	0.1220	0.1220	0.1219	0.1219	0.1220	0.1223	0.1220	0.1219	0.1221	0.1221	0.1222
Channel #8	0.1268	0.1331	0.1268	0.1268	0.1268	0.1273	0.1268	0.1268	0.1268	0.1269	0.1268	0.1268	0.1274	0.1268	0.1268
Channel #9	0.1058	0.1060	0.1059	0.1059	0.1058	0.1058	0.1058	0.1058	0.1058	0.1058	0.1059	0.1058	0.1067	0.1059	0.1058
Channel #10	0.1136	0.1136	0.1136	0.1136	0.1136	0.1136	0.1136	0.1136	0.1136	0.1136	0.1136	0.1136	0.1136	0.1136	0.1136
Channel #11	0.1176	0.1176	0.1176	0.1177	0.1177	0.1177	0.1176	0.1176	0.1176	0.1179	0.1185	0.1176	0.1178	0.1177	0.1176
Channel #12	0.1075	0.1076	0.1075	0.1076	0.1074	0.1074	0.1075	0.1074	0.1074	0.1075	0.1075	0.1075	0.1079	0.1076	0.1074
Channel #13	0.1678	0.1680	0.1676	0.1690	0.1677	0.1683	0.1676	0.1676	0.1676	0.1676	0.1676	0.1680	0.1677	0.1676	0.1676
Channel #14	0.1333	0.1332	0.1328	0.1328	0.1329	0.1329	0.1328	0.1328	0.1328	0.1328	0.1328	0.1332	0.1329	0.1328	0.1328
Channel #15	0.1697	0.1698	0.1696	0.1697	0.1698	0.1697	0.1698	0.1698	0.1699	0.1699	0.1721	0.1744	0.1696	0.1696	0.1696

A.2 Calibration of Relative Humidity Sensors

A "1200 Humidity Generator[6]" (uncertainty 1%) was used to calibrate 3 relative humidity sensors in the range of 10% to 90%. A humidity generator generates humid air at the needed relative humidity in a test chamber while the temperature is kept constant. A view of the humidity generator is shown in Figure A-4. The relative humidity of the generator is considered as the reference relative humidity. Relative humidity sensors are fixed in the chamber in contact with the humid air and are connected to the DAS (SXCI-1000, NATIONAL INSTRUMENTS) which reads the voltage recorded by the sensors during the calibration. Three different temperatures (30℃, 45℃, and 60℃) are considered as the constant temperature at which the desired relative humidity is generated.

Figure A-4 A view of the "1200 Humidity Generator"

The recorded voltages of each relative humidity sensor are compared to the reference relative humidity from the generator and corrected by using the curve fitting equation as

$$RH_{reference} = a.(Voltage) + b \qquad \text{(A.8)}$$

a and b must be found for each relative humidity sensor at each constant temperature. Also, R^2 of the curve fitting analysis ranges from 0.9903 to 0.9985.

[6] THUNDER SCIENTIFIC CORPORATION. Albuquerque, NM, USA.

A.2.1 Calibration process

1- Setting the temperature of the test chamber (30℃).

2- Placing the relative humidity sensors in the chamber, and adjust the relative humidity of the chamber at 10%.

3- Waiting for the sensors to show a stable voltage reading, and then recording the readings 40 times (1 Hz).

4- Repeating the previous step at 20%, 30%, 40%, 50%, 60%, 70%, 80%, and 90% relative humidity, respectively.

5- Repeating step 3 for a decrease in relative humidity of the test chamber from 90% to 10% with a step of 20%.

6- Seting the temperature of the chamber at 45℃ and repeating steps 3, 4, and 5.

7- Seting the temperature of the chamber at 60℃ and repeating steps 3, 4, and 5.

A.2.2 Calibration and uncertainty calculation:

40 readings were recorded at 14 different relative humidity values while the temperature was kept constant. The relative humidity of the generator was considered as the reference value.

The arithmetic means of the voltage readings (range from 0 to 5) are compared with the reference relative humidity and the calibration curve (Equation (A.8)) is used to convert voltage readings to the relative humidity. a and b in equation (A.8) for each sensor can be found in Table A-3. The calibration curve for one of the sensors at 30℃ is shown in Figure A-5.

Standard deviation and precision error can be calculated by using equations (A.2) and (A.3) for each specific relative humidity. The bias error of the curve fitting can be found by using equation (A.5) considering the bias error of the “1200 Humidity Generator” as 1%. The total bias error can be calculated using equation (A.6). Finally the total uncertainty of each sensor at each temperature is obtained using equation (A.7). Table A-4 shows the concluded uncertainty values for each relative humidity sensor.

Table A-3 Constants in equation (A.8) for each relative humidity sensor

Sensor	a	b	R^2
T=30℃			
1	34.2051	- 25.5861	0.9985
2	34.3390	- 25.6411	0.9983
3	34.1935	- 25.3355	0.9981
T=45℃			
1	35.8440	- 25.9614	0.9984
2	36.1464	- 26.3774	0.9983
3	35.9444	- 25.7890	0.9984
T=60℃			
1	37.3391	-32.3192	0.9881
2	37.4714	- 32.3303	0.9818
3	36.9794	- 30.1162	0.9903

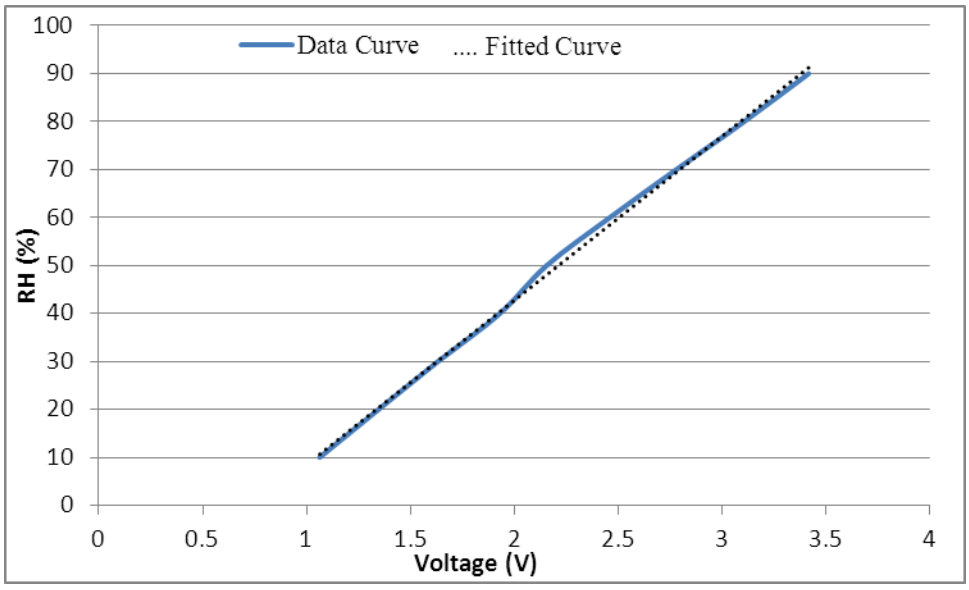

Figure A-5 Fitted curve for sensor #, T=30℃

Table A-4 Uncertainty values of RH sensors

RH (%)	10	20	30	40	50	60	70	80	90
Sensor	Uncertainty (%)								
	T=30℃								
#1	2.5101	2.5105	2.5105	2.5105	2.5101	2.5101	2.5101	2.5101	2.5101
#2	2.6691	2.6691	2.6691	2.6691	2.6691	2.6691	2.6691	2.6691	2.6691
#3	2.5980	2.5980	2.5980	2.5980	2.5980	2.5980	2.5980	2.5980	2.5980
	T=45℃								
#1	2.5811	2.5811	2.5811	2.5811	2.5811	2.5811	2.5811	2.5811	2.5811
#2	2.6348	2.6348	2.6348	2.6348	2.6348	2.6348	2.6348	2.6348	2.6348
#3	2.5650	2.5650	2.5650	2.5650	2.5650	2.5650	2.5650	2.5650	2.5650
	T=60℃								
#1	5.9868	5.986	5.9868	5.9868	5.9868	5.9868	5.9868	5.9868	5.9868
#2	7.3820	7.3820	7.3820	7.3820	7.3820	7.3820	7.3820	7.3820	7.3820
#3	5.4170	5.4170	5.4170	5.4170	5.4170	5.4170	5.4170	5.4170	5.4170

APPENDIX B Physical Properties of Silicagel Particles

B.1 Porosity

Porosity of a particle bed is the ratio of the total void space between the solid particles to the total volume of the particle bed. Silicagel particles are porous, which means that an internal porosity can be defined based on the fraction of space in each particle that is available for the gaseous phase. Also, the external porosity can be defined based on the fraction of void space between the particles by assuming particles as solid non-porous material in the packed bed.

Two types of silicagel particles are used in the particle bed: transparent silicagel particles (manufactured by Sigma Aldrich) and blue silicagel particles (manufactured by Fisher Scientific). There is no available information about the bulk density of transparent white silicagel. As a result, the nominal value of density for pure silicagel (SiO_2) is used to analyze the porosity. The bulk density of blue silicagel particles is based on the manufacturer's information. As a result, two different methodologies are used to find the porosity of blue silicagel and transparent silicagel.

In both methods, the weight and total volume of the particle bed are measured for use in the equations. The volume of the particle bed, which is considered as a cylinder, can be found by measuring its dimensions, which are 26cm in height and 10.1cm in diameter. The experimental procedure used to measure the mass of the particle bed is as follows:

1- Measure the weight of the empty bed.

2- Measure the weight of the filled particle bed.

3- Find the net weight of the particle bed ($M_{particle\ bed}$)

Figure B-1 shows a view of the mass measurement device used to determine the needed weights.

In the first method, which is used for the transparent particles, the total porosity of the particle can be calculated based on the density of the porous bed and the density of the pure solid phase; then external porosity and internal porosity can be determined by using related equations.

In the second method, which is used for the blue silicagel particles, first the external porosity can be found by knowing the volume occupied by the particles and the total volume of the particle bed. After that the internal porosity and total porosity can be calculated by using related equations.

Table B-1 Mass and volume of the particle bed for each type of the silicagel particles

Silicagel Particle	$M_{particle\ bed}(gr)$	$V_{particle\ bed}$ (cm^3)
2.36mm<d_p<2.80mm	1639.25	2106
2.00mm<d_p<2.36mm	1650.18	2106
Blue silicagel $d_{p(average)}$ =1.6mm	1742.46	2106
Equal Mix: $\frac{1}{2}[(2.36\text{mm} < d_p < 2.80\text{mm}) + (d_{p(average)} = 1.6mm)]$	1725.86	2106

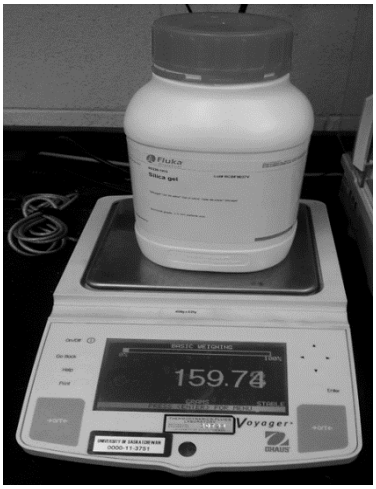

Figure B-1 measuring the mass of the particles

B.1.1 Blue Silicagel

a) External porosity of the particle bed

The external porosity of the particle bed is the ratio of the volume of the void space between the particles to the total volume of the particle bed. The external void space in the particle bed is the difference between the total volume of the particle bed and the volume occupied by the particles which is

$$V_s = \frac{M_{particle\ bed}}{\rho_{silicagel}} \tag{B.1}$$

where V_s is the total volume of the spherical particles, $M_{particle\ bed}$ is the mass of the particles that can occupy $V_{particle\ bed}$, and $\rho_{silicagel}$ is the density of the porous silicagel particles ($2.2\frac{gr}{ml}$). The mass of the air trapped in the internal pores of the particles can be ignored. As a result, the mass of the particle bed is the same as the mass of the solid phase, which is pure silicagel.

Also, external porosity of the particle bed can be calculated as

$$\varepsilon_e = 1 - \frac{V_s}{V_{particle\ bed}} \tag{B.2}$$

where $V_{particle\ bed}$ is the volume of the particle bed and ε_e is the external porosity.

b) Internal porosity of the particle bed

Internal porosity is the ratio of the available void space inside the particles to the total volume occupied with the silicagel particles. The internal available volume per gram of the particles can be found using BET analysis (B.3.3). The product of the density of silica gel particles ($^{gr}/_{cm^3}$) and pore volume per gram of sample ($^{cm^3}/_{gr}$) gives the internal porosity of the particle bed.

$$\varepsilon_i = \rho_{silicagel} \times (pore\ volume\ per\ gram\ of\ sample) \quad \text{(B.3)}$$

c) porosity of the particle bed

The porosity of the particle bed is the ratio of the total available space for the gaseous phase in the particle bed to the net volume of the particle bed

$$\varepsilon = \frac{V_g}{V_{particle\ bed}} \quad \text{(B.4)}$$

Porosity of the particle can be found by using the relation between the total porosity of the particle bed, internal porosity, and external porosity (Nie, 2010)

$$\varepsilon = \varepsilon_e + (1 - \varepsilon_e)\varepsilon_i \quad \text{(B.5)}$$

External porosity, internal porosity, and the total porosity of blue silicagel particles are listed in Table B-2.

Table B-2 Porosity properties of blue silicagel particles

External porosity	Internal porosity	Total porosity
0.61	0.24	0.70

B.1.2 Uncertainty determination of the porosity

a) External porosity

The uncertainty of the external porosity can be found by using the uncertainty propagation for equations (B.1) and (B.2), (Coleman & Steele, 1999).

$$\left[\frac{U(\varepsilon_e)}{(1-\varepsilon_e)}\right]^2 = \left[\frac{U\left(M_{particle\ bed}\right)}{M_{particle\ bed}}\right]^2 + \left[\frac{U(\rho_{silica})}{\rho_{silica}}\right]^2 + \left[\frac{U\left(V_{particle\ bed}\right)}{V_{particle\ bed}}\right]^2 \quad \text{(B.6)}$$

It is assumed that the uncertainty of the bulk density of blue silicagel is a maximum of 10% (Nie, 2010). The uncertainty of volume of the particle bed is

$$\left[\frac{U\left(V_{particle\ bed}\right)}{V_{particle\ bed}}\right]^2 = \left[\frac{U(L)}{L}\right]^2 + \left[\frac{2U(D)}{D}\right]^2 \quad \text{(B.7)}$$

where L and D are height and diameter of the cylindrical particle bed, respectively. The uncertainty of the length measurement is considered as 0.1mm based on the accuracy of the digital caliper that was used.

b) Internal porosity

The uncertainty of the internal porosity can be calculated by applying the uncertainty propagation equation (B.3)

$$\left[\frac{U(\varepsilon_i)}{\varepsilon_i}\right]^2 = \left[\frac{U(\rho_{silica})}{\rho_{silica}}\right]^2 + \left[\frac{U(Pore\ volume)}{Pore\ volume}\right]^2 \quad \text{(B.8)}$$

The uncertainty of the pore volume, measured by the BET experiment, is considered as a maximum of 10% of the measured value.

c) Porosity of the particle bed:

The uncertainty of the total porosity of the packed blue silicagel particles can be formulated as

$$U^2(\varepsilon) = [(1-\varepsilon_e)\,U(\varepsilon_i)]^2 + [(1-\varepsilon_i)\,U(\varepsilon_e)]^2 \quad \text{(B.9)}$$

Table B-3 shows the uncertainty values of the porosity of the packed bed of blue silicagel particles.

Table B-3 Uncertainty values of the porosity properties for the packed bed of blue silicagel

$U(M_{particle\ bed})$=0.01(gr)		$\frac{U(V_{particle\ bed})}{V_{particle\ bed}}$=0.2%
Uncertainty	External porosity	0.04
	Internal porosity	0.03
	Total porosity	0.03

B.1.3 Transparent silicagel particles:

a) Porosity of the particle bed

The density of the particle bed can be found by using the density of the gaseous phase (air), density of the solid phase, and the porosity of the particle bed:

$$\rho_{particle\ bed} = (1-\varepsilon)\rho_s + \varepsilon\rho_g \quad \text{(B.10)}$$

where ρ_s is the density of pure silicagel, ρ_g is the density of the air, and ε is the porosity of the particle bed. The density of the particle bed can be found by measuring the mass and the volume of the particle bed

$$\rho_{particle\ bed} = \frac{M_{particle\ bed}}{V_{particle\ bed}} \quad \text{(B.11)}$$

By calculating the density of the particle bed, finding the nominal density of pure silicagel (ρ_s=2.19$\frac{gr}{ml}$) (Sun, 2003), and the density of the air in atmospheric condition (ρ_g=0.00118$\frac{gr}{ml}$), the porosity of the particle bed can be obtained.

b) External porosity of the particle bed

Available external void space is the difference between total void space in the particle bed and the total internal void space available in the particles. The total available void space can be found using the porosity formula

$$V_g = \varepsilon \times V_{particle\ bed} \tag{B.12}$$

Also, the total internal available space in the particles can be found by using the BET results

$$V_{g,internal} = M_{particle\ bed} \times (pore\ volume\ per\ gram\ of\ sample) \tag{B.13}$$

Finally, the external porosity of the particle bed is

$$\varepsilon_e = \frac{V_g - V_{g,internal}}{V_{particle\ bed}} \tag{B.14}$$

c) Internal porosity of the particle bed:

Internal porosity of the particle bed can be calculated using the relation between the internal porosity, external porosity and the total porosity of the particle bed, equation (B.5).

Table B-4 lists external porosity, internal porosity, and the porosity of the transparent silicagel particle bed.

Table B-4 Porosity properties of transparent silicagel particles

Silicagel Particle	Total Porosity(ε)	Internal porosity(ε_i)	External porosity(ε_e)
2.36mm<d_p<2.80mm	0.62	0.43	0.33
2.00mm<d_p<2.36mm	0.63	0.43	0.35

B.1.4 Uncertainty determination of the porosity properties of the transparent silicagel particles:

a) Porosity of the particle bed:

The porosity of the particle bed can be calculated using equation (B.10), and the uncertainty can be deduced from the uncertainty propagation

$$\left[\frac{U(\varepsilon)}{\varepsilon}\right]^2 = \left[\frac{U\left(\rho_{particle\ bed} - \rho_s\right)}{\left(\rho_{particle\ bed} - \rho_s\right)}\right]^2 + \left[\frac{U\left(\rho_g - \rho_s\right)}{\left(\rho_g - \rho_s\right)}\right]^2 \quad \text{(B.15)}$$

Uncertainty of $\left(\rho_{particle\ bed} - \rho_s\right)$ and $\left(\rho_g - \rho_s\right)$ can be calculated as

$$[U\left(\rho_{particle\ bed} - \rho_s\right)]^2 = U^2\left(\rho_{particle\ bed}\right) + U^2(\rho_s) \quad \text{(B.16)}$$

$$[U\left(\rho_g - \rho_s\right)]^2 = U^2\left(\rho_g\right) + U^2(\rho_s) \quad \text{(B.17)}$$

where the uncertainty of the density of the air and density of the pure silicagel are considered as 10%. Also, the uncertainty of the density of the particle bed is

$$\left[\frac{U\left(\rho_{particle\ bed}\right)}{\rho_{particle\ bed}}\right]^2 = [\frac{U\left(M_{particle\ bed}\right)}{M_{particle\ bed}}]^2 + [\frac{U\left(V_{particle\ bed}\right)}{V_{particle\ bed}}]^2 \quad \text{(B.18)}$$

where uncertainties of $M_{particle\ bed}$ and $V_{particle\ bed}$ are the same values that were used for the uncertainty analysis of the blue silicagel particles.

b) External porosity

The uncertainty of the external porosity can be calculated by using uncertainty formulation equation (B.14).

$$\left[\frac{U(\varepsilon_e)}{\varepsilon_e}\right]^2 = \left[\frac{U(V_g - V_{g,internal})}{(V_g - V_{g,internal})}\right]^2 + [\frac{U\left(V_{particle\ bed}\right)}{V_{particle\ bed}}]^2 \qquad \text{(B.19)}$$

while the uncertainty of $(V_g - V_{g,internal})$ is

$$[U(V_g - V_{g,internal})]^2 = U^2\left(V_g\right) + U^2\left(V_{g,internal}\right) \qquad \text{(B.20)}$$

Equation (B.12) is used to find the total void space available in the particle bed. Uncertainty of this parameter can be deduced as

$$U^2\left(V_g\right) = [U(\varepsilon)V_{particle\ bed}]^2 + [\,\varepsilon U\left(V_{particle\ bed}\right)]^2 \qquad \text{(B.21)}$$

Also, the uncertainty of the internal void volume of this parameter is deduced by using the following formula

$$[\frac{U\left(V_{g,internal}\right)}{V_{g,internal}}]^2 = [\frac{U\left(M_{particle\ bed}\right)}{M_{particle\ bed}}]^2 + [\frac{U(Pore\ volume)}{Pore\ volume}]^2 \qquad \text{(B.22)}$$

Again, uncertainty of the pore volume (cm^3/gr) is considered as a maximum of 10% of the outcome value from the BET measurement.

c) Internal porosity:

Internal porosity of the particle bed can be found using equation (B.5). The uncertainty propagation of this equation is

$$U^2(\varepsilon_i) = \left[\left(\frac{1}{1-\varepsilon_e}\right) U(\varepsilon)\right]^2 + \left[\frac{(\varepsilon-1)}{(1-\varepsilon_e)^2} U(\varepsilon_e)\right]^2 \quad \text{(B.23)}$$

Table B-5 has listed the uncertainty of the porosity properties of the packed bed of transparent silicagel particles.

Table B-5 Uncertainty of the porosity properties of the packed bed of transparent silicagel particles

Silicagel Particle	U(ε)	U(ε_i)	U(ε_e)
2.36mm<d_p<2.80mm	0.12	0.21	0.12
2.00mm<d_p<2.36mm	0.12	0.21	0.12

B.2 Particle Size

Two different types of silicagel particles were used for the transient experiments. The first one used the white transparent silicagel particles (amorphous silica) and the second type used the blue silicagel particles. The transparent silicagel consisted of spherical particles manufactured by Sigma Aldrich Corporation with a size ranging from 1mm to 3mm. Blue Silicagel particles (amorphous silica) are spheres with 0-10% weight of Cobaltous chloride and are manufactured by Fisher Scientific in sizes ranging from 1*mm* to 2*mm* in diameter.

B.2.1 Transparent silicagel particles:

These spherical particles are in the range of 1*mm* to 3*mm* in diameter, a wide range to be studied. Available electronic instruments are not able to measure the average diameter of these particles for two reasons. First is the wide range of particle size and the second is that the available instruments are not able to analyze large particles (bigger than 2*mm* in diameter). Therefore, a sieving method was used to find the proper size range and average diameter of the particles. Figure B-2 shows a sample of transparent silicagel particles.

Figure B-2 A view of transparent white spherical silicagel particles

Based on the US sieving range and by considering the nominal size range (1*mm* to 3*mm*), sieves used to analyze and separate the particles in the narrow ranges were #6, #7, #8, #10, #12, #14, and #16. Each 200 grams of particles were sieved for 10 minutes in an electric shaker. A picture of the electronic shaker can be seen in figure B-3. Table B-6 shows the mass fraction of spherical particles for the consecutive range of sieving. As can be seen most of the particles are in the range of sieves #7 and #8 and after that sieves #8 to #10. As a result, only these two groups of particles are considered as the objective particles to be used as the packed bed in the transient tests.

Table B-6 Size analysis of transparent spherical silicagel particles

Sieving range	Diameter range (mm)	Mass fraction (%)
#6 to #7	$2.80<d_p<3.36$	5.29
#7 to #8	$2.36<d_p<2.80$	78.56
#8 to #10	$2.00<d_p<2.36$	15.35
#10 to #12	$1.68<d_p<2.00$	0.15
#12 to #14	$1.41<d_p<1.68$	0.46
#14 to #16	$1.19<d_p<1.41$	0.12

Figure B-3 A view of the electronic shaker used to sieve the transparent silicagel particles

Transparent silicagel particles with a range of $2.36mm<d_p<2.80mm$ were considered for the dry convection test. The average diameter considered was 2.53mm, being the arithmetic mean of the upper and lower bound of the size range. Also, silicagel particles with the range of $2.00mm<d_p<2.36mm$ were considered for the conduction test and the average diameter considered for use was $2.18mm$.

B.2.2 Blue silicagel particles:

Blue silicagel particles are amorphous spherical particles with less than 10% mass fraction of Cobaltous chloride, which is the reason for their blue color. These particles lose their color in contact with moisture and become light pink in the saturation condition. These spherical particles were in the range of 1mm to 2mm in diameter. A view of the blue silicagel particles is shown in Figure B-4.

Figure B-4 A view of blue silicagel spherical particles

An electron microscope yields a mean diameter based on a two-dimensional measurement and is not reliable when the mass or volume fraction is needed. Laser diffraction devices (LALS) [7] can analyze the particles based on the volume distribution where the density is constant and is more reliable in engineering.

An "Optical Master Sizer" (Mastersizer 2000E particle size analyzer, Malvern Instruments Ltd, UK) was used to analyze the size range to find the average diameter of these spheres. Master Sizer, a laser diffraction device, analyzes a small portion of the particles by using an optical laser to find the range of diameters and their average diameter based on different theories. If the mean diameters calculated using different methods are changing in a narrow range, it means that the particles are likely spherical.

A random portion of 3 grams of these particles was analyzed. Table B-7 shows the information obtained from the Master Sizer. The surface area moment mean D[3,2] is often used in the industries, especially when the surface area is important. The average diameter of the particles was deduced to be 1.5mm based on the area moment mean method. Figure B-5 shows the volume fraction distribution of the sample.

[7] Low Angle Light Scattering

Table B-7 Size distribution of blue spherical silicagel particles

Particle size (μm)	Volume Fraction (%)
647.41<d_p<754.23	0.66
754.23<d_p<878.67	1.63
878.67<d_p<1023.66	3.62
1023.66<d_p<1192.56	7.43
1192.56<d_p<1389.33	13.89
1389.33<d_p<1618.57	21.25
1618.57<d_p<1885.64	24.26
1885.64<d_p<2196.77	16.12
2196.77<d_p<2559.23	8.63
2559.23<d_p<2981.51	2.18
2981.51<d_p<3473.45	0.00

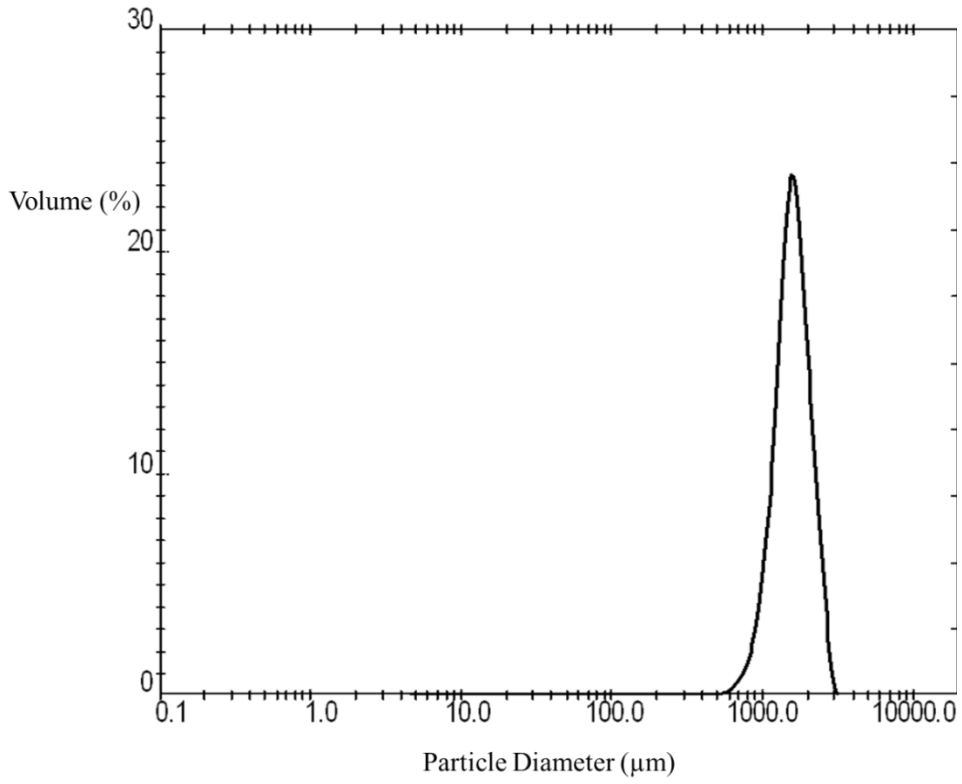

Figure B-5 Volumetric distribution of the blue silicagel particles based on the diameter

B.3 Specific External Volumetric Surface Area

The external surface area of silicagel particles is important in studying the convective heat transfer coefficient because it determines the contact surface of the solid-fluid in the particle bed. When the surface area exposed to the fluid is larger, the convective heat transfer will happen in a higher rate. It is assumed that silicagel particles are spherical, so an average diameter can be defined for them. On the other hand, the silicagel particles have internal pores, and fluids can be adsorbed and trapped inside the particles. Therefore, the internal surface area, which is the available surface area inside the particles, can be defined as well. Accurate distinction between the internal surface area and external surface area especially in the regions near the outer surface is not physically possible, because the internal structure of the silicagel particles makes it hard to measure the external surface area with a low uncertainty.

The arrangement of the particles in the packed bed is another effective factor on the specific surface area. As the particle bed is tighter the contact points between the particles increases which results in a smaller specific surface area. Therefore, there are more contact points between the particles in a structured particle bed in comparison with a randomly packed bed (Yang et al., 2012). Also, a randomly shaken packed bed has smaller specific surface area in comparison with an unshaken randomly packed bed because the particles in the shaken bed occupy the voids made available for them during the shaking process. In general, a higher external porosity of the particle bed results in a higher external surface area because of the bigger available void space between the particles.

Particle size is another effective variable in determining the specific surface area per unit volume ($\frac{m^2}{m^3}$). A decrease in the size of the particles results in more contact points between the particles. On the other hand, considering the particles as spheres, the bigger the diameter the smaller the specific surface area, because the surface area is proportional to the square of the diameter, while the volume is proportional to the cube of the particle's diameter.

Three different methods were used to determine the external porosity of the particle bed and the results were compared together. In all the cases it is assumed that the silicagel particles were spherical and had a smooth external surface area to simplify the analysis (Nie, 2010).

B.3.1 Calculating specific external surface area using Carmen correlation

Carman (1938, 1939) found an equation for the specific surface area per volume of the solid phase for a porous bed of spherical particles with smooth surface. The Carman equation can be written as

$$A_{sf} = \left[\frac{1}{k_k}.\frac{{\varepsilon_e}^3}{(1-\varepsilon_e)^2}.\frac{1}{K}\right]^{1/2} \qquad \text{(B.24)}$$

where A_{sf} is the specific surface area per volume of the solid particles ($\frac{m^3}{m^3}$), assuming that the particles are non-porous, which means there is no airflow inside the particles, ε_e is the external porosity of the packed bed, and K is the permeability of the particle bed (m^2). In equation (B.24), k_k is called Kozeny constant and is estimated to be 5 for spherical particles. External porosity was discussed for each type of porous bed in section B.1 .

The permeability of the particle bed can be found using the Darcy momentum equation

$$U_D = \frac{K}{\mu}.\frac{\Delta P}{L} \qquad \text{(B.25)}$$

where U_D is the flow rate of air ($\frac{m}{s}$), μ is the dynamic viscosity of the air ($Pa.s$) ΔP is the pressure drop of the air flow along the particle bed (Pa), and L is the length of the particle bed.

The Darcy equation is valid at low Reynolds numbers based on the particle diameter ($Re_{d_p} = \frac{U_D.d_p}{\nu}$), because when Re_{d_p} <10, only viscous forces are involved in the balancing pressure driving forces.

B.3.1.1 Permeability measurement

The pressure drop for each type of particle bed was measured in the range of the Darcy velocity. A micromanometer (8704-DP-CALC) was used to measure the pressure difference at the inlet and outlet of the packed bed while the dry airflow passed through the

dry packed bed of silicagel particles. The airflow was measured and controlled with a mass flow controller (MKS, Maximum: 50 *lpm*) before entering the particle bed. Both the packed bed and airflow were at room temperature, which means there was no heat transfer between them. The length of the particle bed was constant (260*mm*) for all the tests. The temperature of the particle bed was monitored using two thermocouples at the inlet of the particle bed. A pressure drop along the particle bed was measured at different flow rates that were in the range of Darcy regime (Re_{d_p} <10). Both the diameter and the length of the particle bed were large enough compared to the particle size to minimize the wall effect and the entrance effect. The uncertainty of the permeability can be calculated using the propagation equation. The permeability equation can be written as

$$K = \frac{L\mu}{\Delta P}.\frac{4Q}{\pi D^2} \tag{B.26}$$

where $Q$is the volumetric flow rate ($\frac{m^3}{s}$). Therefore the uncertainty of the permeability can be formulated as

$$(\frac{U(K)}{K}) = \sqrt{(\frac{U(L)}{L})^2 + (\frac{U(\Delta P)}{\Delta P})^2 + (\frac{U(Q)}{Q})^2 + (2\frac{U(D)}{D})^2} \tag{B.27}$$

$U(\Delta P)$ is the uncertainty of the micromanometer, estimated as 1(Pa) by the company, and $U(Q)$ is the uncertainty of the mass flow controller, which is 1% of the maximum mass flow rate allowed through the controller (50 *lpm*).

It is expected that the permeability of the particle bed at low Reynolds numbers (Re_{d_p} <10) was independent of the flow rate. Table B-8 and Table B-9 list the permeability at different flow rates for two types of silicagel particles, which require their specific surface areas to be determined. It shows that the uncertainty is decreasing as the flow rate is increasing. It also shows that for the range of Reynolds number of 1 to 10, the permeability is more consistent far from the range bounds.

Table B-8 Permeability test of the transparent silicagel particles (2.36mm<d_p<2.80mm)

$Q\ (\frac{m^3}{s})$	Re_{d_p}	$K\ (m^2)$	$\frac{U(K)}{K}$
4.31667×10^{-5}	0.87	4.57×10^{-9}	0.167
12.5833×10^{-5}	2.55	4.21×10^{-9}	0.056
20.9167×10^{-5}	4.24	4.29×10^{-9}	0.037
33.4667×10^{-5}	6.79	4.17×10^{-9}	0.028
41.8167×10^{-5}	8.49	4.09×10^{-9}	0.025

Table B-9 Permeability test of the blue silicagel particles ($d_{p(average)}$ =1.6mm)

$Q\ (\frac{m^3}{s})$	Re_{d_p}	$K\ (m^2)$	$\frac{U(K)}{K}$
4.3333×10^{-5}	0.54	1.72×10^{-9}	0.065658
9.4166×10^{-5}	1.18	1.61×10^{-9}	0.033664
16.9167×10^{-5}	2.13	1.60×10^{-9}	0.025004
28.5167×10^{-5}	3.59	1.60×10^{-9}	0.021924
42.1833×10^{-5}	5.31	1.56×10^{-9}	0.020893
0.0005955	7.49	1.53×10^{-9}	0.020462
0.000708333	8.91	1.50×10^{-9}	0.020334

Figures B-6 and Figure B-7 show the permeability data and the average permeability based on the arithmetic mean for the transparent silicagel and blue silicagel particles, respectively. Clearly the average permeability is in the uncertainty bounds of the permeability values which means the average permeability can be used as the independent permeability value when Re_{d_p} <10. Table B-10 lists the average permeability and its uncertainty for each type of particle bed. Bigger particle size results in higher permeability because of the reduced number of contact points between the particles, which leads to more interactions between the particles and airflow and more pressure drop within the packed bed. The uncertainty values

are in agreement with Nie (2010) who investigated the uncertainty of the permeability of a urea packed bed at 5%.

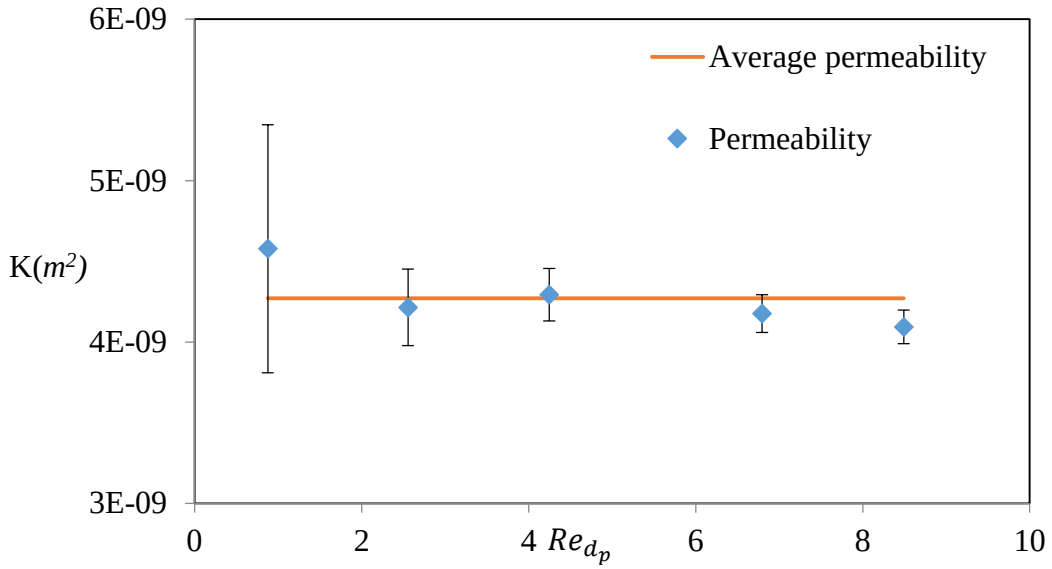

Figure B-6 Permeability of the randomly packed particle bed for different Reynolds numbers, transparent silicagel particles (2.36mm<d_p<2.80mm)

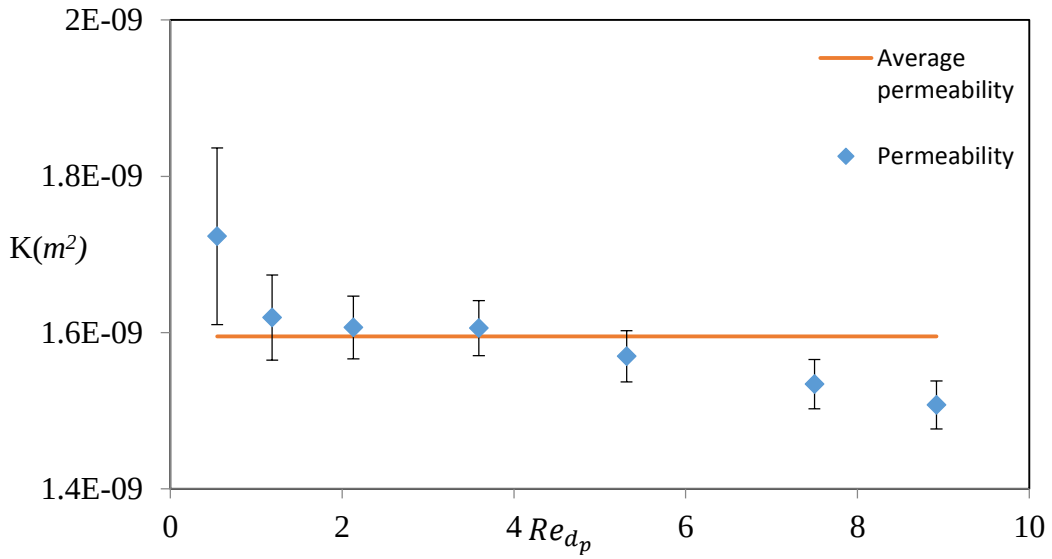

Figure B-7 Permeability of the randomly packed particle bed for different Reynolds numbers, blue silicagel particles ($d_{p(average)}$ =1.6mm)

Table B-10 Average permeability and its uncertainty for each type of the packed particle bed

Particle	$K\ (m^2)$	$U(K)$	$\frac{U(K)}{K}$
silicagel particles 2.36mm<d_p<2.80mm	4.27×10^{-9}	0.23×10^{-9}	0.05
blue silicagel particles $d_{p(average)}$ =1.6mm	1.59×10^{-9}	0.07×10^{-9}	0.04

B.3.1.2 Specific external surface area and its uncertainty (Carman correlation)

Table B-11 lists the external specific surface area per unit volume of the silicagel particles ($\frac{m^3}{m^3}$) for each type of particle bed. Uncertainty values are calculated using the uncertainty propagation for equation (B.24).

$$\frac{U(A_{sf})}{A_{sf}} = [\frac{1}{2}\frac{U(K)}{K}]^2 + [\frac{3}{2}\frac{U(b)}{b}]^2 + [\frac{U(c)}{c}]^2 \qquad \text{(B.28)}$$

where $b = \varepsilon_e$ and $c = 1 - \varepsilon_e$ and $\frac{U(K)}{K}$ is the relative uncertainty of the permeability, which was found in the previous section. Also, uncertainty of the external porosity was investigated in section B.1. Higher external porosity and smaller permeability of the blue silicagel particles in comparison with the transparent silicagel particles (2.36mm<d_p<2.80mm) are the reasons for the big difference in external specific surface area between these two types of particles.

For the transparent silicagel particles the relative uncertainty of external porosity ($\frac{U(\varepsilon_e)}{\varepsilon_e}$), is estimated at 36%, which is the dominant parameter in determining the uncertainty of the external specific surface area. Therefore, the relative uncertainty of the specific external surface area ($\frac{U(A_{sf})}{A_{sf}}$) is 57%, which is different from the relative uncertainty of the specific external surface area of the blue silicagel particles (14%). The smaller particle size and different structure of blue silicagel particles, which results in a different density from the transparent particles, are the reasons for differences in the specific surface area and its uncertainty between these two particles.

Table B-11 External specific surface area and its uncertainty for each type of particle bed

Particle	A_{sf} $(\frac{m^3}{m^3})$	$U(A_{sf})$	$\frac{U(A_{sf})}{A_{sf}}$
silicagel particles 2.36mm<d_p<2.80mm	1936.27	1112.86	0.57
blue silicagel particles $d_{p(average)}$ =1.6mm	13678.95	1963.54	0.14

B.3.2 Calculating external surface area using geometrical properties

Specific external surface area can be found by using the physical properties of the silicagel particles. Assuming the particles are spherical, randomly arranged in a cylindrical insulation and are in point contact with each other, one can consider that the whole surface area of each sphere is available for exposure to the airflow. As a result, the specific external surface area is the ratio of the surface area of the sphere to its volume.

$$A_{sf} = \frac{6}{d_p} \tag{B.29}$$

where d_p is the average diameter of the particles (section B.2). Table B-12 shows the specific external surface area of the particle bed. The uncertainty can be analyzed based on the uncertainty of the particle diameter.

$$\frac{U(A_{sf})}{A_{sf}} = \frac{U(d_p)}{d_p} \tag{B.30}$$

This method to find the specific external surface area is not an accurate estimation. First of all, the particles are not completely spherical which increases the uncertainty of the assumption. Second, there is not any certain structure that can be applied to the randomly packed bed. As a result, it is not expected that the particles are in point contact with each other.

Table B-12 Specific external surface area based on the particle size

Particle	A_{sf} $(\frac{m^3}{m^3})$	$\frac{U(A_{sf})}{A_{sf}}$
silicagel particles 2.36mm<d_p<2.80mm	2325.58	0.01
blue silicagel particles $d_{p(average)}$ =1.6mm	3750	0.01

B.3.3 Determination of the particle properties using BET

The Brunauer, Emmett and Teller (BET) theory of gas sorption which models adsorption and desorption in the particles can be used to determine the micro- scale properties of porous materials such as silicagel particles. The BET method investigates the surface area and pore structure of the particles by determining the sorption or desorption isotherm. Sorption or desorption is stated as a mass or molar quantity of gas at standard temperature or pressure (STP) trapped or released by the initially clean and dry surface of the particles, at a constant temperature, *T* (Nie, 2010). The adsorption isotherm is the adsorbed volume or mass plotted as a function of the partial pressure of the adsorbate gas (Figure B-8). In the BET method, liquid Nitrogen at 1*atm* and 77*K* is commonly used as the test gas to investigate the adsorption isotherm of the solid porous material. The form of the adsorption isotherm depends on the composition of the adsorbate gas as well as the pore size and physical properties of the porous material.

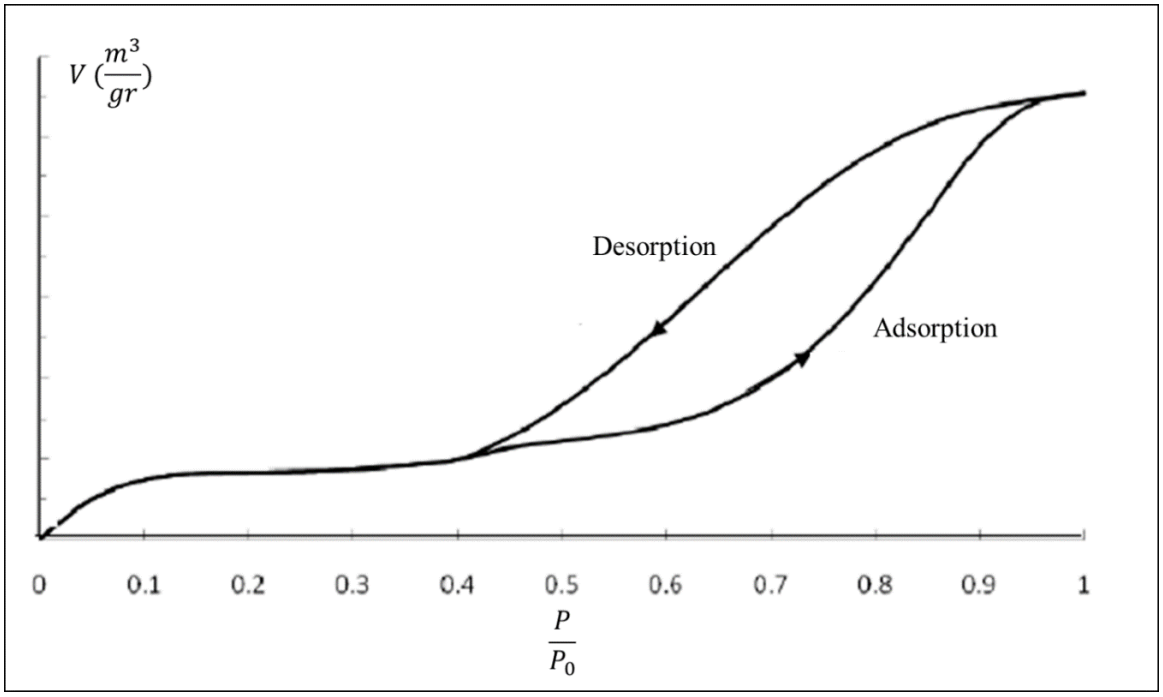

Figure B-8 Typical adsorption and desorption isotherms for a porous material (Nie, 2010)

A "Micromeritics ASAP 2000" was used to analyze the surface area and pore size of the silicagel particles.

In the BET method, nitrogen is used when the available specific surface area is more than 10($\frac{m^2}{gr}$), and Krypton can be used when the total specific surface area is less than 10($\frac{m^2}{gr}$). During the test an initially clean and completely dry solid sample (e.g silicagel) is suddenly exposed to the nitrogen in a test chamber. A degassing process removes the previously adsorbed water and impurities in the particles and provides dried and clean specimens to be analyzed in the BET device. The pressure of the chamber is monitored during the test while the volume of the chamber is kept constant. Contained by the closed constant volume of the chamber, the nitrogen pressure decreases as the particles adsorb the gas molecules. After a certain period of time, which depends on the test sample, the gas pressure reaches a new steady state condition. Monitoring the transient changes of pressure and temperature one can find the amount of adsorbed gas on the available surface of the particles. Interested readers can refer to Nie (2010) for more detailed information about the BET method.

Transparent silicagel particles ($2.36mm<d_p<2.80mm$) and blue silicagel particles ($d_{p(average)} = 1.6mm$) were used in the BET analysis. Each sample was heated in the oven

for 24 hours to be completely dry for the BET test. Also, a degassing process makes sure that the samples are completely clean and dry and the available surfaces can be exposed to the nitrogen thoroughly. Table B-13 lists the BET results of each sample.

Table B-13 Pore size and specific surface area for each type of silicagel particles using the BET method.

Particle	BET surface area ($\frac{m^2}{gr}$)	External surface area ($\frac{m^2}{gr}$)	Total pore volume of pores less than 1259.800 Å ($\frac{cm^3}{gr}$)	Average pore width (Å)
silicagel particles 2.36mm<d_p<2.80mm	677.86	532.34	0.359	21.21
blue silicagel particles $d_{p(average)}$ =1.6mm	556.96	512.42	0.292	20.95

As illustrated the BET test is not a reliable method to find the specific external surface area. The obtained specific external surface area for both samples is very large and far from the calculated values of the Carmen correlation and the geometrical method.

As mentioned before, nitrogen, which has different properties from air, is used as the adsorbate gas in the BET analysis. Moreover, considering the internal pores of the particles, it is hard to distinguish between the internal available surface area and external available surface. As a result, the deduced values for external and internal specific surface areas can not represent the real definition of these variables.

APPENDIX C Discretization of Governing Equations and Boundary Conditions

One- dimensional finite volume method (Patankar, 1980) is used to discretize the governing equations and boundary conditions for both of the transient convection test and transient conduction test.

In this method, each control volume consists of one grid point and two faces at the upstream and downstream of the control volume. Thermal and physical properties for the grid point in each control volume are defined by using the properties of the grid points at the upstream and downstream control volumes. Also, the properties of the faces are determined by using the properties of the gird points in their adjacent control volumes. Figure C-1 shows a view of the different components of the control volume in the domain. *I-1* is the grid point in the upstream control volume, *I+1* is the grid point in the downstream control volume and I is the grid point of the control volume which is being studied. The control volumes in the Figure C-1 have the same geometrical properties which means $\Delta X_a = \Delta X_{b=} \Delta X_I$.

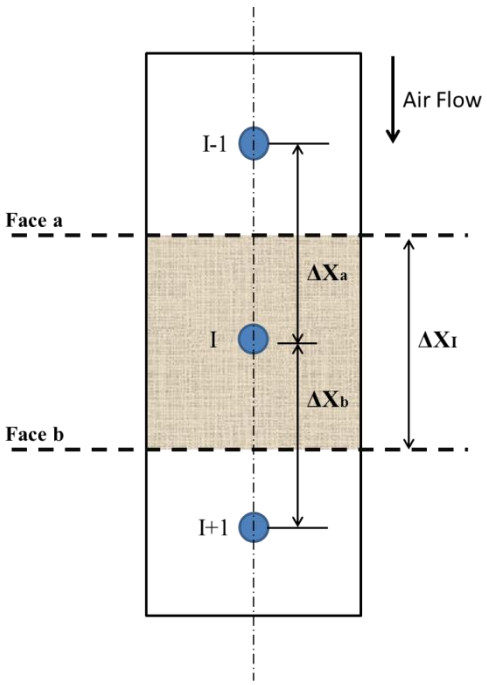

Figure C-1 Control volumes and their components used for heat transfer analysis at node I

Figure C-2shows the particle bed as a solution domain that was used to analyze the transient convection heat transfer and transient conduction heat transfer in the IHTP solution. As it can be seen, particle is divided to N control volumes while each control volume includes two faces and one grid point.

The control volumes have the same length along the particle bed except the ones which are adjacent to the boundaries which are half of the size of the other control volumes. Figure C-3 shows a view of the boundary control volumes.

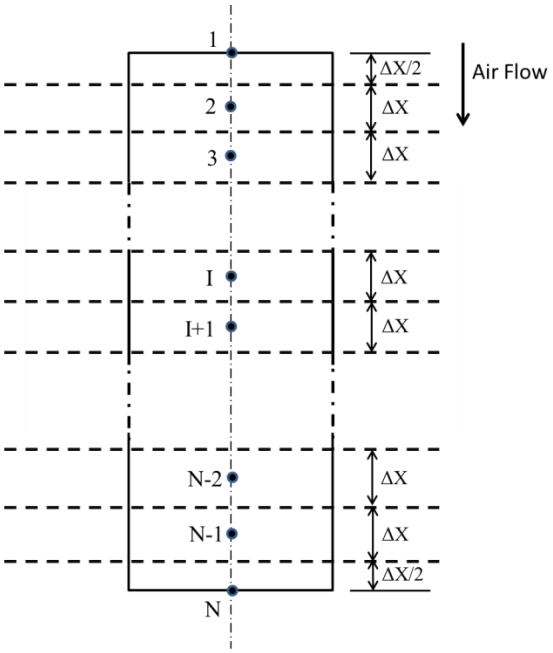

Figure C-2 Schematic view of the nodes in the packed particle bed as the solution domain

Governing equations and boundary condition equations can be discretized over each control volume from one face to another and over the time period from t to $t + \Delta t$. In the equations, properties which belong to the time *t* have the superscript "0" while the properties which belong to the time $t + \Delta t$ have the superscript "1".

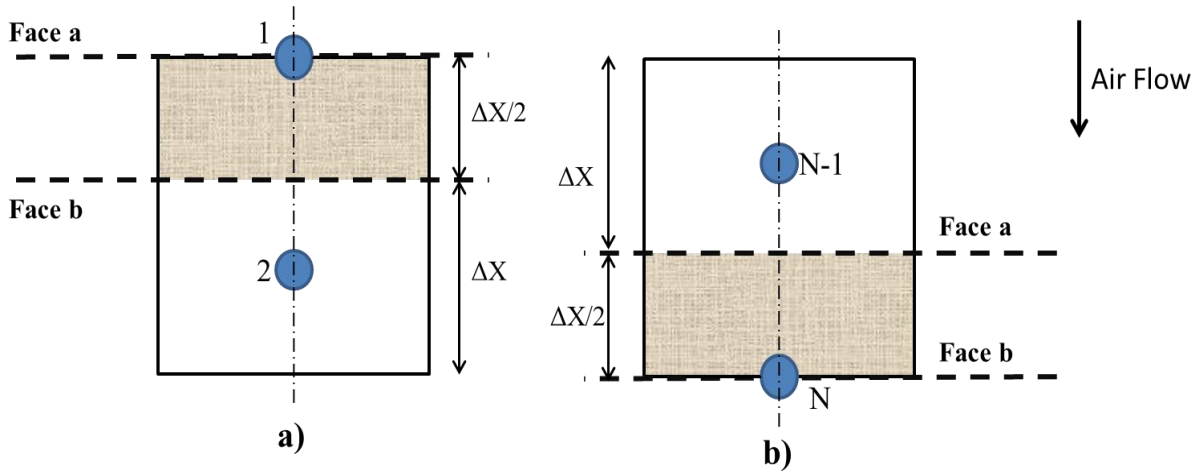

Figure C-3 Schematic view of the control volume at the boundary condition: a) boundary condition at the top of the particle bed (entrance). B) Boundary condition at the bottom of the particle bed (exit).

C.1 Convection Heat Transfer

C.1.1 Governing equations: energy transport of silicagel particles

The partial equation for the energy balance for the silicagel particles along the bed is

$$\frac{\partial}{\partial t}\left(\rho_s C_{p_s}(1-\varepsilon_e)T_s\right) = \frac{\partial}{\partial x}\left(k_{eff,s}\frac{\partial T_s}{\partial x}\right) + A_{sf,v}h_t\left(T_{g,i}-T_s\right) \qquad \text{(C.1)}$$

In an arbitrary control volume *I*, the equation is integrated from face *a* to face *b* and over the time t to $t+\Delta t$

$$\int_a^b \int_t^{t+\Delta t} \frac{\partial}{\partial t}\left(\rho_s C_{p_s}(1-\varepsilon_e)T_s\right) dt\, dx =$$

$$\int_a^b \int_t^{t+\Delta t} \frac{\partial}{\partial x}\left(k_{eff,s}\frac{\partial T_s}{\partial x}\right) dt\, dx + \int_a^b \int_t^{t+\Delta t} [A_{sf,v}h_t\left(T_{g,i}-T_s\right) \qquad \text{(C.2)}$$

After integrating of each term, one gets

$$\int_a^b \int_t^{t+\Delta t} \frac{\partial}{\partial t}\left(\rho_s C_{p_s}(1-\varepsilon_e)T_s\right) dt\, dx = (1-\varepsilon_e)\left[C_{p_s}\rho_s T_s - C_{p_s}^{\,0}\rho_s^0 T_s^0\right]_I \Delta x \tag{C.3}$$

$$\int_a^b \int_t^{t+\Delta t} \frac{\partial}{\partial x}\left(k_{eff,s}\frac{\partial T_s}{\partial x}\right) dt\, dx = k_{eff,s}\left[\frac{\partial T_s}{\partial x}|_b - \frac{\partial T_s}{\partial x}|_a\right]\Delta t \tag{C.4}$$

$$\int_a^b \int_t^{t+\Delta t} [A_{sf,v}h_t\left(T_{g,i}-T_s\right)_I + B(T_{surr}-T_s)_I]dt\, dx = [A_{sf,v}h_t\left(T_{g,i}-T_s\right)_I]\,\Delta t\,\Delta x \tag{C.5}$$

While

$$\frac{\partial T_s}{\partial x}|_b = \frac{T_s|_{I+1} - T_s|_I}{\Delta x} \tag{C.6}$$

$$\frac{\partial T_s}{\partial x}|_a = \frac{T_s|_I - T_s|_{I-1}}{\Delta x} \tag{C.7}$$

Arranging the equations in the form of $a_I T_s|_I + a_{I-1} T_s|_{I-1} + a_{I+1} T_s|_{I+1} = b$, one gets

$$\begin{aligned}\left[(1-\varepsilon_e)(C_{p_s}\rho_s)_I \Delta x + \frac{2k_{eff,s}\Delta t}{\Delta x} + A_{sf,v} h_t \Delta t\, \Delta x\right] T_s|_I \\ + \left[-\frac{k_{eff,s}\Delta t}{\Delta x}\right] T_s|_{I-1} + \left[-\frac{k_{eff,s}\Delta t}{\Delta x}\right] T_s|_{I+1} \\ = (1-\varepsilon_e)(C_{p_s}{}^0 \rho_s^0 T_s^0)_I \Delta x + A_{sf,v} h_t (T_{g,i})_I \Delta t\, \Delta x\end{aligned} \qquad \text{(C.8)}$$

The bulk density of the silicagel particles is

$$\rho_s|_I = (1-\varepsilon_i)\rho_{silica} + \varepsilon_i \rho_{g,i} \qquad \text{(C.9)}$$

$$\rho_s^0|_I = (1-\varepsilon_i)\rho_{silica} + \varepsilon_i \rho_{g,i}^0 \qquad \text{(C.10)}$$

While the density of the internal gaseous phase is

$$\rho_{g,i} = \frac{P}{R\, T_s|_I} \qquad \text{(C.11)}$$

$$\rho_{g,i}^0 = \frac{P}{R T_s^0|_I} \qquad \text{(C.12)}$$

Also, the heat capacity of the silicagel particle is

$$C_{p_s}|_I = \left[(1-\varepsilon_i) C_{p_{silica}} \rho_{silica} + \varepsilon_i \rho_{g,i} C_{p_g}\right] / \rho_s|_I \qquad \text{(C.13)}$$

$$C_{p_s}{}^0|_I = \left[(1-\varepsilon_i)C_{p_{silica}}\rho_{silica} + \varepsilon_i \rho_{g,i}^0 C_{p_g}\right]/\rho_s^0|_I \qquad \text{(C.14)}$$

C.1.2 Governing equations: energy transport of external gaseous phase

The partial differential equation for the external gaseous phase which consists of the void spaces between the particles is

$$\frac{\partial}{\partial t}\left(\rho_{g,e}C_{p_{g,e}}\varepsilon_e T_{g,e}\right) + \frac{\partial}{\partial x}\left(\rho_{g,e}C_{p_{g,e}}U_d \partial T_{g,e}\right) = A_{sf,v}h_t\left(T_s - T_{g,e}\right) \qquad \text{(C.15)}$$

Integrating in the control volume *I* from face *a* to face *b* and over the time t to $t+\Delta t$ yields

$$\int_a^b \int_t^{t+\Delta t} \frac{\partial}{\partial t}\left(\rho_{g,e}C_{p_{g,e}}\varepsilon_e T_{g,e}\right) dtdx = C_{p_{g,e}}\varepsilon_e\left[\rho_{g,e}T_{g,e} - \rho_{g,e}^0 T_{g,e}^0\right]_I \Delta x \qquad \text{(C.16)}$$

$$\int_a^b \int_t^{t+\Delta t} \frac{\partial}{\partial x}\left(\rho_{g,e}C_{p_{g,e}}U_d \partial T_{g,e}\right) dtdx = U_d C_{p_{g,e}}[(\rho_{g,e}T_{g,e})|_b - (\rho_{g,e}T_{g,e})|_a]\Delta t \qquad \text{(C.17)}$$

$$\int_a^b \int_t^{t+\Delta t} [A_{sf,v}h_t\left(T_s - T_{g,e}\right)]\, dtdx = [A_{sf,v}h_t\left(T_s - T_{g,e}\right)|_I]\Delta x \Delta t \qquad \text{(C.18)}$$

$\rho_{g,e}$ at the interfaces of two control volumes (face *a* and face *b*) is determined by using the spatial averaging

$$\rho_{g,e|_b} = \frac{2\rho_{g,e|_{I+1}}\rho_{g,e|_I}}{\rho_{g,e|_{I+1}} + \rho_{g,e|_I}} \tag{C.19}$$

$$\rho_{g,e|_a} = \frac{2\rho_{g,e|_{I-1}}\rho_{g,e|_I}}{\rho_{g,e|_{I-1}} + \rho_{g,e|_I}} \tag{C.20}$$

Also, the temperature at the interfaces can be determined using the arithmetic mean value

$$T_{g,e}|_b = \frac{T_{g,e}|_{I+1} + T_{g,e}|_I}{2} \tag{C.21}$$

$$T_{g,e}|_a = \frac{T_{g,e}|_{I-1} + T_{g,e}|_I}{2} \tag{C.22}$$

Arranging the energy equation of the external gaseous phase in the packed bed of the particle bed yields $a_I T_{g,e}|_I + a_{I-1} T_{g,e}|_{I-1} + a_{I+1} T_{g,e}|_{I+1} = b$ which a_I, a_{I-1}, a_{I+1}, and b are

$$a_I = \varepsilon_e C_{p_{g,e}} (\rho_{g,e})_I \Delta x + U_d C_{p_{g,e}} \Delta t \left(\frac{\rho_{g,e|_b} - \rho_{g,e|_a}}{2}\right) + A_{sf,v} h_t \Delta x \Delta t \tag{C.23}$$

$$a_{I-1} = \frac{U_d C_{p_{g,e}} \rho_{g,e|_a} \Delta t}{2} \tag{C.24}$$

$$a_{I+1} = -\frac{U_d C_{p_{g,e}} \rho_{g,e|_b} \Delta t}{2} \quad \text{(C.25)}$$

$$b = A_{sf,v} h_t \Delta x \Delta t (T_s)_I + \varepsilon_e C_{p_{g,e}} (\rho_{g,e} T_{g,e})_I^0 \Delta x \quad \text{(C.26)}$$

Density of the gaseous phase can be discretized as

$$(\rho_{g,e})_I = \frac{P}{R\, T_{g,e}|_I} \quad \text{(C.27)}$$

$$(\rho_{g,e})_{I-1} = \frac{P}{R\, T_{g,e}|_{I-1}} \quad \text{(C.28)}$$

$$(\rho_{g,e})_{I+1} = \frac{P}{R\, T_{g,e}|_{I+1}} \quad \text{(C.29)}$$

$$(\rho_{g,e})_I^0 = \frac{P}{R\, T_{g,e}|_I^0} \quad \text{(C.30)}$$

C.1.3 Boundary condition equations: energy transport of silicagel particles at x/L=0

It is considered that there is no heat flux in the silicagel particles at the top of the particle bed (x=0) which means

$$\frac{\partial T_s}{\partial x} = 0 \quad \text{(C.31)}$$

The energy equation at the boundary is the same as equation (C.1). The discretization process of that equation is the same as equation (C.2) while face *a* and face *b* are shown in Figure C-3a. The discretized form of the energy equation of the silicagel particles at x=0 is as below

$$\int_a^b \int_t^{t+\Delta t} \frac{\partial}{\partial t}\left(\rho_s C_{p_s}(1-\varepsilon_e)T_s\right) dt\, dx = (1-\varepsilon_e)\left[C_{p_s}\rho_s T_s - C_{p_s}{}^0\rho_s^0 T_s^0\right]_1 \frac{\Delta x}{2} \tag{C.32}$$

$$\int_a^b \int_t^{t+\Delta t} \frac{\partial}{\partial x}\left(k_{eff,s}\frac{\partial T_s}{\partial x}\right) dt\, dx = k_{eff,s}[\frac{\partial T_s}{\partial x}|_b - \frac{\partial T_s}{\partial x}|_a]\Delta t \tag{C.33}$$

$$\int_a^b \int_t^{t+\Delta t} A_{sf,v}h_t\left(T_{g,i}-T_s\right)_1 dt\, dx = A_{sf,v}h_t\left(T_{g,i}-T_s\right)_1 \Delta t\ \frac{\Delta x}{2} \tag{C.34}$$

While

$$\frac{\partial T_s}{\partial x}|_b = \frac{T_s|_2 - T_s|_1}{\Delta x} \tag{C.35}$$

$$\frac{\partial T_s}{\partial x}|_a = 0 \tag{C.36}$$

Arranging this equation in the form of $a_I T_s|_I + a_{I-1} T_s|_{I-1} + a_{I+1} T_s|_{I+1} = b$, one gets

$$\left[(1-\varepsilon_e)(C_{p_s}\rho_s)_1 \frac{\Delta x}{2} + \frac{k_{eff,s}\Delta t}{\Delta x} + (A_{sf,v}h_t + B)\Delta t\ \frac{\Delta x}{2}\right] T_s|_1 + \left[-\frac{k_{eff,s}\Delta t}{\Delta x}\right] T_s|_2 = (1-\varepsilon_e)(C_{p_s}{}^0\rho_s^0 T_s^0)_1 \frac{\Delta x}{2} + A_{sf,v}h_t(T_{g,i})_1 \Delta t\ \frac{\Delta x}{2} \quad \text{(C.37)}$$

The bulk densities and specific heat capacities can be calculated by using equations (C.9)and (C.13) and considering I=1.

C.1.4 Boundary condition equations: energy transport of external gaseous phase at x/L=0

It is considered that the temperature of the external gaseous phase at the entrance of the particle bed (x=0) is constant and equal to the inlet temperature.

$$T_{g,e}|_0 = T_{inlet} \quad \text{(C.38)}$$

C.1.5 Boundary condition equations: energy transport of silicagel particles at x/L=1

The boundary condition of energy transport in silicagel particles at x=L is the same as boundary condition at x=0 which means there is no heat flux at the bottom of the particle bed.

The energy equation at x=L is the same as equation (C.1). The discretization process of that equation is the same as equation (C.2) while face *a* and face *b* are shown in Figure C-3b. The discretized form of the energy equation of the silicagel particles at x=L is

$$\int_a^b \int_t^{t+\Delta t} \frac{\partial}{\partial t}\left(\rho_s C_{p_s}(1-\varepsilon_e)T_s\right) dt\, dx = (1-\varepsilon_e)\left[C_{p_s}\rho_s T_s - C_{p_s}{}^0\rho_s^0 T_s^0\right]_N \frac{\Delta x}{2} \quad \text{(C.39)}$$

$$\int_a^b \int_t^{t+\Delta t} \frac{\partial}{\partial x}\left(k_{eff,s}\frac{\partial T_s}{\partial x}\right) dt\, dx = k_{eff,s}[\frac{\partial T_s}{\partial x}|_b - \frac{\partial T_s}{\partial x}|_a]\Delta t \tag{C.40}$$

$$\int_a^b \int_t^{t+\Delta t} A_{sf,v}h_t\left(T_{g,i} - T_s\right)_N dt\, dx = A_{sf,v}h_t\left(T_{g,i} - T_s\right)_N \Delta t\, \frac{\Delta x}{2} \tag{C.41}$$

Where

$$\frac{\partial T_s}{\partial x}|_a = \frac{T_s|_N - T_s|_{N-1}}{\Delta x} \tag{C.42}$$

$$\frac{\partial T_s}{\partial x}|_b = 0 \tag{C.43}$$

Arranging this equation in the form of $a_I T_s|_I + a_{I-1}T_s|_{I-1} + a_{I+1}T_s|_{I+1} = b$ yields

$$\left[(1-\varepsilon_e)(C_{p_s}\rho_s)_N \frac{\Delta x}{2} + \frac{k_{eff,s}\Delta t}{\Delta x} + A_{sf,v}h_t\Delta t\, \frac{\Delta x}{2}\right] T_s|_N + \left[-\frac{k_{eff,s}\Delta t}{\Delta x}\right] T_s|_{N-1} = (1-\varepsilon_e)(C_{p_s}^{\,0}\rho_s^0 T_s^0)_N \frac{\Delta x}{2} + A_{sf,v}h_t(T_{g,i})_N \Delta t\, \frac{\Delta x}{2} \tag{C.44}$$

The bulk densities and specific heat capacities can be calculated by using equations (C.9) and (C.13) and by considering I=N.

C.1.6 Boundary condition equations: energy transport of external gaseous phase at x/L=1

It is considered that there is no heat flux through the external gaseous phase at the exit of the particle bed (x=L) which means:

$$\frac{\partial T_{g,e}}{\partial x}|_{x=L} = 0 \tag{C.45}$$

The energy equation at x=L is the same as equation (C.15). The discretization process of that equation is the same as equation (C.16) while face *a* and face *b* are shown in Figure C-3b. The discretized form of the energy equation of the external gaseous phase at the bottom of the particle bed (x=L)

$$\int_a^b \int_t^{t+\Delta t} \frac{\partial}{\partial t}\left(\rho_{g,e} C_{p_{g,e}} \varepsilon_e T_{g,e}\right) dt dx = C_{p_{g,e}} \varepsilon_e \left[\rho_{g,e} T_{g,e} - \rho^0_{g,e} T^0_{g,e}\right]_N \frac{\Delta x}{2} \tag{C.46}$$

$$\int_a^b \int_t^{t+\Delta t} \frac{\partial}{\partial x}\left(\rho_{g,e} C_{p_{g,e}} U_d \partial T_{g,e}\right) dt dx = U_d C_{p_{g,e}} [(\rho_{g,e} T_{g,e})|_b - (\rho_{g,e} T_{g,e})|_a] \Delta t \tag{C.47}$$

$$\int_a^b \int_t^{t+\Delta t} [A_{sf,v} h_t (T_s - T_{g,e})]\, dt dx = [A_{sf,v} h_t (T_s - T_{g,e})|_N] \frac{\Delta x}{2} \Delta t \tag{C.48}$$

while

$$\rho_{g,e|_b} = \rho_{g,e|_N} = \frac{P}{R\, T_{g,e}|_N} \tag{C.49}$$

$$\rho_{g,e|_a} = \frac{2\rho_{g,e|_{N-1}}\rho_{g,e|_N}}{\rho_{g,e|_{N-1}} + \rho_{g,e|_N}} \quad \text{(C.50)}$$

Also,

$$T_{g,e}|_b = T_{g,e}|_N \quad \text{(C.51)}$$

$$T_{g,e}|_a = \frac{T_{g,e}|_{N-1} + T_{g,e}|_N}{2} \quad \text{(C.52)}$$

Arranging the discretized form of the energy equation of the external gaseous phase at the of the particle bed yields $a_I T_{g,e}|_N + a_{I-1} T_{g,e}|_{N-1} = b$ whicha_N, anda_{n-1} , and b are

$$a_N = \varepsilon_e C_{p_{g,e}} (\rho_{g,e})_N \frac{\Delta x}{2} + U_d C_{p_{g,e}} \Delta t \left(\frac{\rho_{g,e|_b} - \rho_{g,e|_a}}{2}\right) + A_{sf,v} h_t \frac{\Delta x}{2} \Delta t \quad \text{(C.53)}$$

$$a_{N-1} = \frac{U_d C_{p_{g,e}} \rho_{g,e|_a} \Delta t}{2} \quad \text{(C.54)}$$

$$b = A_{sf,v} h_t \frac{\Delta x}{2} \Delta t (T_s)_N + \varepsilon_e C_{p_{g,e}} (\rho_{g,e} T_{g,e})_N^0 \frac{\Delta x}{2} \quad \text{(C.55)}$$

The density of the gaseous phase can be discretized as below:

$$(\rho_{g,e})_{N-1} = \frac{P}{R\, T_{g,e}|_{I-1}} \quad \text{(C.56)}$$

$$(\rho_{g,e})_N^0 = \frac{P}{R\, T_{g,e}|_N^0} \tag{C.57}$$

C.2 Conductive Heat Transfer

One dimensional finite volume method is used to discretize the governing equation in the packed bed of the silicagel particle bed and boundary condition equations which are being used to simulate conduction heat transfer from the particle bed to the aluminum plate at the top of the packed bed.

The governing equations are determined using the LVA (Local Volume Averaging) method. It is considered that all the possible phases in the particle bed are in thermal equilibrium with each other.

C.2.1 Governing equation: energy transport in the particle bed

The partial differential equation of the heat transfer in the packed bed is

$$\frac{\partial}{\partial t}\left(\rho_{eff} C_{p_{eff}} T\right) = \frac{\partial}{\partial x}\left(k_{eff} \frac{\partial T}{\partial x}\right) \tag{C.58}$$

Integrating the governing equations in an arbitrary control volume and over the time period t to $t + \Delta t$ yields is shown

$$\int_a^b \int_t^{t+\Delta t} \frac{\partial}{\partial t}\left(\rho_{eff} C_{p_{eff}} T\right) dt dx = \left(\rho_{eff} C_{p_{eff}} T - C_{p}{}^{0}_{eff} \rho^0_{eff} T^0\right)|_I \Delta x \tag{C.59}$$

$$\int_a^b \int_t^{t+\Delta t} \frac{\partial}{\partial t}\left(k_{eff} \frac{\partial T}{\partial x}\right) dt dx = k_{eff} \Delta t \left(\frac{T_{I+1} - T_I}{\Delta x} - \frac{T_I - T_{I-1}}{\Delta x}\right) \tag{C.60}$$

Arranging the discretized equations in the form as $a_I T|_I + a_{I-1} T|_{I-1} + a_{I+1} T|_{I+1} = b$, one can determine a_I, a_{I-1}, and a_{I+1} as

$$a_I = \rho_{eff} C_{p_{eff}} \Delta x + 2k_{eff} \frac{\Delta t}{\Delta x} \tag{C.61}$$

$$a_{I-1} = -k_{eff} \frac{\Delta t}{\Delta x} \tag{C.62}$$

$$a_{I+1} = -k_{eff} \frac{\Delta t}{\Delta x} \tag{C.63}$$

$$b = \rho_{eff} C_{p_{eff}} \Delta x T^0 \tag{C.64}$$

The effective density (ρ_{eff}) and effective heat capacity ($C_{p_{eff}}$) are obtained by using following formulation

$$\rho_{eff} = (1 - \varepsilon)\rho_{silica} + \varepsilon \rho_g \tag{C.65}$$

$$C_{p_{eff}} = \left[(1 - \varepsilon) C_{p_{silica}} \rho_{silica} + \varepsilon \rho_g C_{p_g}\right] / \rho_{eff} \tag{C.66}$$

The density of the gaseous phase in the particle bed can be determined as

$$\rho_g = \frac{P}{R T_I} \tag{C.67}$$

C.2.2 Boundary condition equation: energy transport in the particle bed at x/L=0

It is assumed that the aluminum plate at the top of the particle bed (x=0) is the only source for the heat transfer. As a result, the boundary condition equation at the top of the bed is the conduction heat transfer equation between the aluminum plate and its adjacent control volume in the particle bed (as it shown in Figure C-1a). The partial differential equation at the x=0 is

$$C_{p_{Al}} m_{Al} \frac{\partial T_{Al}}{\partial t} = A_c k_{eff_c} \frac{\partial T}{\partial x}|_{x=0} \qquad \text{(C.68)}$$

Integrating above equation from face *a* to face *b* and over the time t to $t + \Delta t$ gives

$$\int_a^b \int_t^{t+\Delta t} C_{p_{Al}} m_{Al} \frac{\partial T_{Al}}{\partial t} dt dx = \int_a^b \int_t^{t+\Delta t} (A_c k_{eff_c} \frac{\partial T}{\partial x}|_{x=0})\, dt dx \qquad \text{(C.69)}$$

$$\frac{C_{p_{Al}} m_{Al} \Delta x}{2 A_c k_{eff_c}} (T_{Al} - T_{Al}^0) = \frac{T - T^0}{2} \Delta t \qquad \text{(C.70)}$$

Discretized equations can be written in the form of$a_1 T|_1 + a_2 T|_2 = b$, while

$$a_1 = -\frac{\Delta t}{2} \qquad \text{(C.71)}$$

$$a_2 = \frac{\Delta t}{2} \qquad \text{(C.72)}$$

$$b = \frac{C_{p_{Al}} m_{Al} \Delta x}{2 A_c k_{eff_c}} (T_{Al} - T_{Al}^0) \tag{C.73}$$

C.2.3 Boundary condition equation: Energy transport in the particle bed at x/L=1

It is assumed that the heat flux at the bottom of the bed (x=L) is zero because of the insulation at that position. Integrating the equation in the control volume which is shown in Figure 3-Cb and over the time t to the $t + \Delta t$ gives

$$\int_a^b \int_t^{t+\Delta t} \frac{\partial}{\partial t}\left(\rho_{eff} C_{p_{eff}} T\right) dt dx = (\rho_{eff} C_{p_{eff}} T - C_{p_{eff}}^{\ 0} \rho_{eff}^0 T^0)|_N \frac{\Delta x}{2} \tag{C.74}$$

$$\int_a^b \int_t^{t+\Delta t} \frac{\partial}{\partial t}\left(k_{eff} \frac{\partial T}{\partial x}\right) dt dx = k_{eff} \Delta t (-\frac{T_N - T_{N-1}}{\Delta x}) \tag{C.75}$$

Arranging the above equation in the form of $a_N T|_N + a_{N-1} T|_{N-1} = b$ yields

$$a_N = \rho_{eff} C_{p_{eff}} \frac{\Delta x}{2} + k_{eff} \frac{\Delta t}{\Delta x} \tag{C.76}$$

$$a_{N-1} = -k_{eff} \frac{\Delta t}{\Delta x} \tag{C.77}$$

$$b = \frac{\Delta x}{2} C_{p_{eff}}^{\ 0} \rho_{eff}^0 T_N^0 \tag{C.78}$$

APPENDIX D SENSITIVITY STUDY OF GRID SIZE, TIME STEP, CONVERGENCE ERROR, AND RELAXATION FACTOR

The sensitivity of the used grid size and the time step in the direct simulation of the convective and conductive transient tests were studied, respectively. Different time steps and grid sizes were chosen and compared with the used ones in the numerical simulation to check the effect of the time step and grid size on the simulation.

Furthermore, sensitivity of the direct simulation to the applied relaxation factor and convergence error, which are introduced in equation (3-17) and equation (3-18), respectively, were investigated.

D.1 Convective Heat Transfer

Considering the silicagel particle bed as a homogeneous and isotropic porous medium, the heat transfer between the heated bed and dry airflow can be simulated in the axial direction. An axial grid size sensitivity study was performed on the packed bed. Figure D-1 illustrates the numerical temperature profile of the particle bed at the chosen position for the IHTP analysis for different grid sizes and compares it with the experimental data. As can be seen, for the grid sizes smaller than 2% of the total length of the bed (L), the numerical temperature result is independent of the grid size. Therefore, it can be concluded that dx=0.01L, which is the selected grid size for the numerical simulation, is an acceptable value.

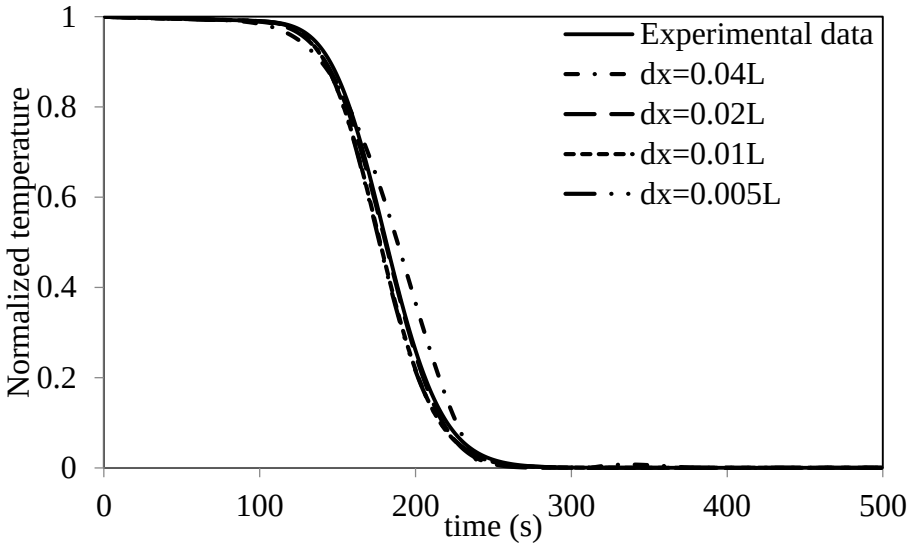

Figure D-1 Experimental normalized temperature profile of the packed bed at $\frac{x}{L}$=0.48, and corresponding numerical normalized temperature for different grid sizes (dx), transparent silicagel particles (2.38mm<d_p<2.80mm), $T_{0|bed}$=65℃, $T_{airflow|inlet}$=26℃, Re_{d_h} =82.

Figure D-2 shows the sensitivity of the numerical analysis of the time step for the packed bed of transparent silicagel particles in a specific Reynolds number. As shown, when the time step was less than 4 seconds, the numerical temperature profile was independent of the value of the time step. On the other side, the temperature was recorded every one second during the transient test. Therefore, 1s was chosen as the time step in the numerical simulation.

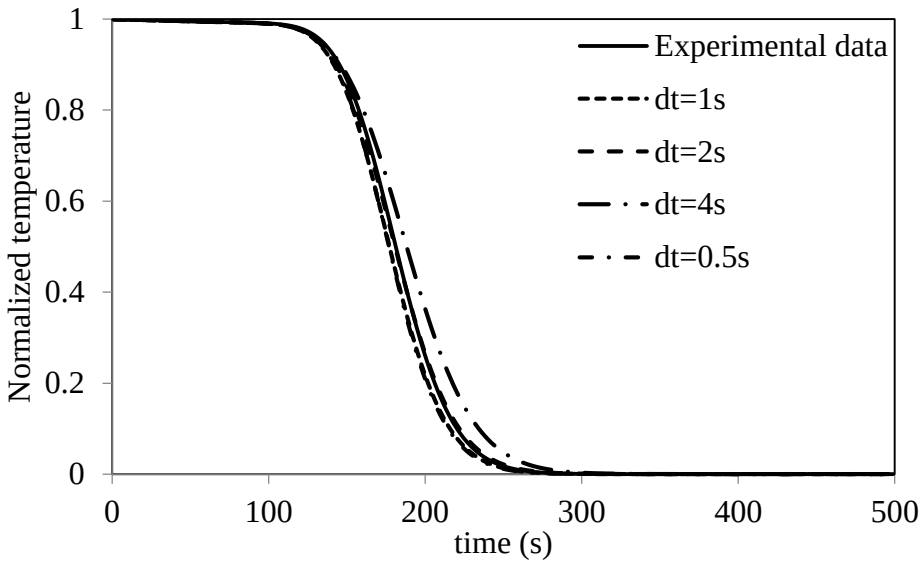

Figure D-2 Experimental normalized temperature profile of the packed bed at $\frac{x}{L}$=0.48, and corresponding numerical normalized temperature for different time steps (dt), transparent silicagel particles (2.38mm<d_p<2.80mm), $T_{0|bed}$=65℃, $T_{airflow|inlet}$=26℃, Re_{d_h} =82.

D.2 Conductive Heat Transfer

Conductive heat transfer between a heated packed bed of silicagel particles and a cold aluminum plate (at room temperature) was studied in the conduction test. It was assumed that the heat transfer between the cold plate and the packed bed was in an axial direction. Therefore, an axial grid size was considered to simulate the heat transfer in the packed bed.

Figure D-3 shows the sensitivity of the numerical model to the grid size. The plots show that for a grid size equal to 1% of the total length (L) or less, the numerical temperature profile is independent of the grid size. It also shows that when the grid size is further decreased (less than 1%), the numerical results are no longer in very good agreement with the experimental results. Therefore, dx=0.01L is the acceptable grid size to be used in the simulation.

Figure D-4 illustrates the sensitivity of the numerical model to the time step. It can be seen that the numerical temperature profile is independent of the time step, so a time step of 1second can be applied in the numerical model. This is the same time step that was used in the temperature recording of the packed bed during the transient test.

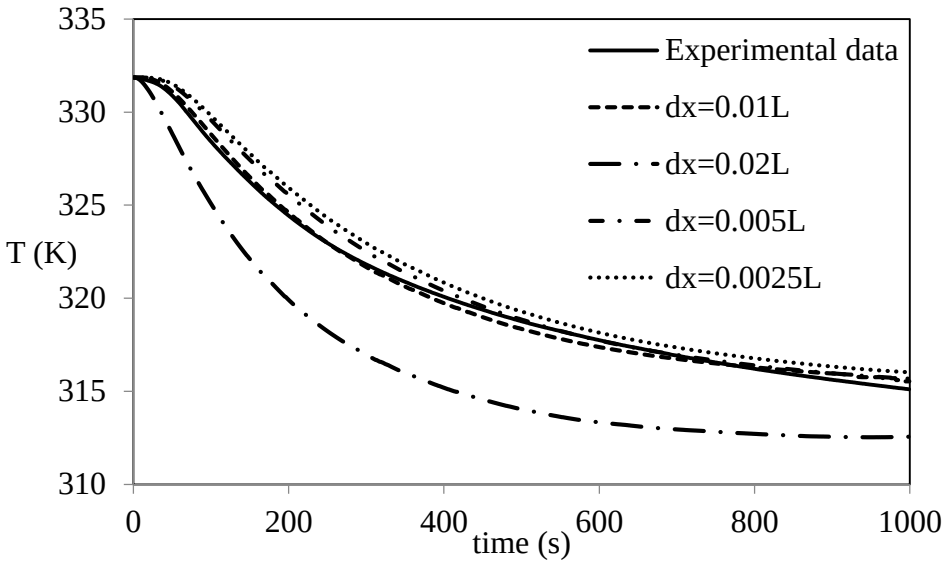

Figure D-3 Experimental temperature profile of the packed bed at $\frac{x}{L} = 0.02$, and corresponding numerical temperature profiles for different grid sizes (dx), transparent silicagel (2.36*mm*<dp<2.80*mm*), Conduction test, dry heated packed bed, T_{bed}=59℃, T_{Al}=24℃.

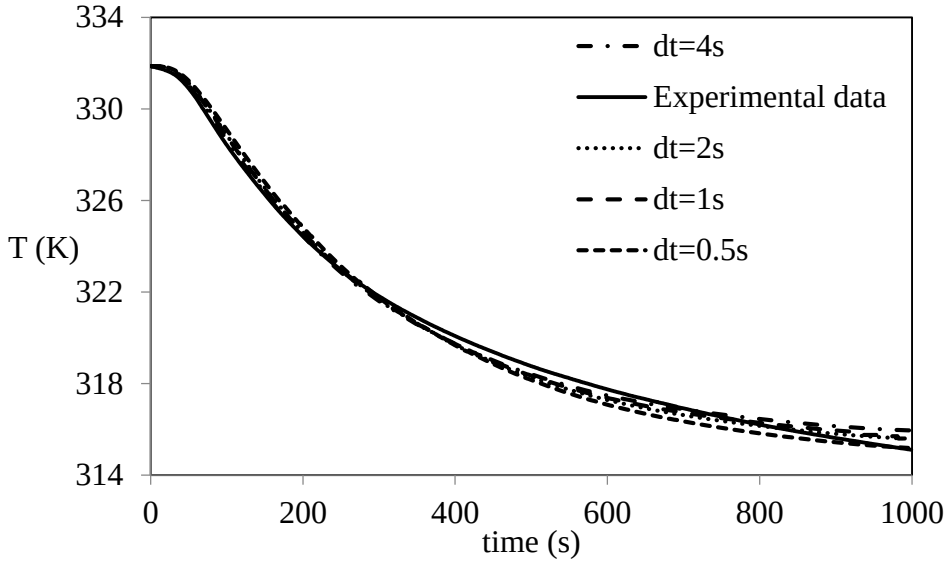

Figure D-4 Experimental temperature profile of the packed bed at $\frac{x}{L} = 0.02$, and corresponding numerical temperature profiles for different time steps (dt), transparent silicagel (2.36*mm*<dp<2.80*mm*), Conduction test, dry heated packed bed, T_{bed}=59℃, T_{Al}=24℃.

D.3 Sensitivity Study of Relaxation Factor

Figure D-5 shows the sensitivity of the direct numerical simulation to the relaxation factor. As it can be seen, the output of the numerical simulation, temperature profile, is not sensitive to the relaxation factor. The main effect of relaxation factor is in the needed running time of the code to achieve the outputs. The independency of the numerical temperature profile to the relaxation factor demonstrates stability of the Matlab code.

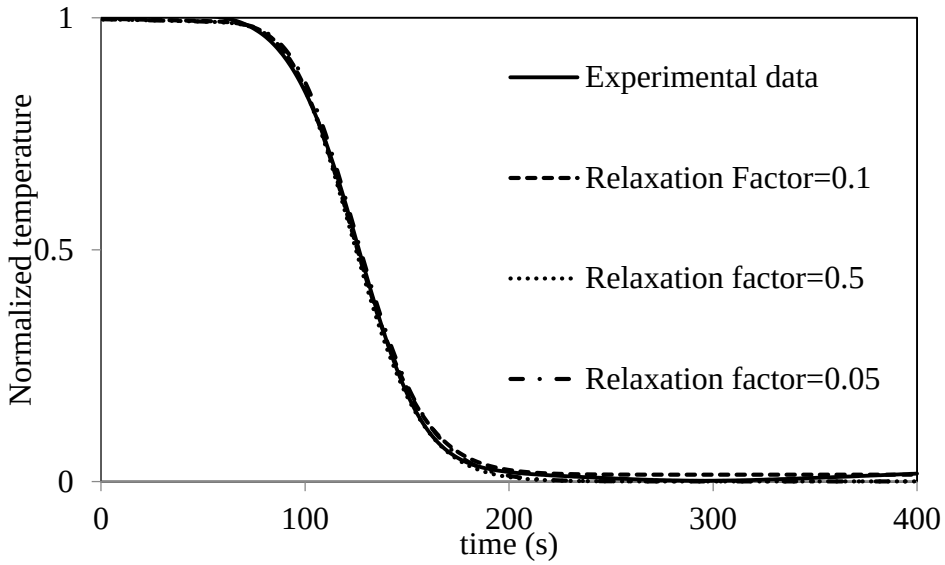

Figure D-5 Experimental normalized temperature profile of the packed bed at $\frac{x}{L}$=0.48, and corresponding numerical normalized temperature for different relaxation factors, blue silicagel particles (1.00mm<d_p<2.00mm), $T_{0|bed}$=65℃, $T_{airflow|inlet}$=26℃, Re_{d_h} =102.

D.4 Sensitivity Study of Convergence Error

The convergence error is used to control and recognize the convergence of the iteration, so the Matlab code will move forward to find the temperature profile in the next time step only when the difference between two consecutive guesses of temperature profile is less than the convergence error.

A big convergence error leads to inaccurate guess of the outputs, and very small convergence error may not accept the convergence because of unnecessary level of accuracy. As a result, it is important to find the biggest convergence error which can show the convergence of the simulation without decreasing the accuracy.

Figure D-6 demonstrates the sensitivity of the direct numerical modeling to the convergence error. As it shows, convergence error equal to 10^{-5} is the usable value as for the smaller values no difference can be seen in the output results, but for values bigger than that the accuracy is decreasing.

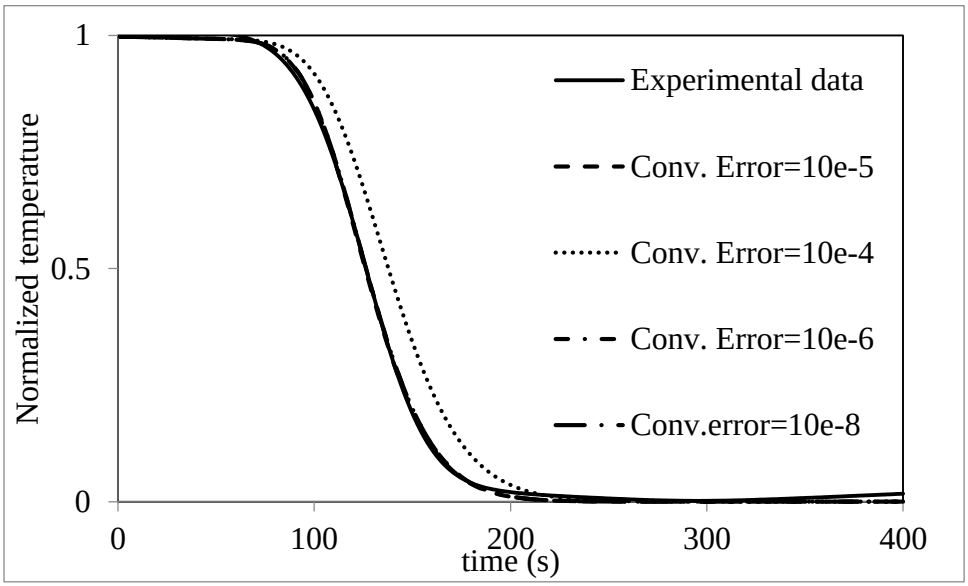

Figure D-6 Experimental normalized temperature profile of the packed bed at $\frac{x}{L}$=0.48, and corresponding numerical normalized temperature for different convergence errors, blue silicagel particles (1.00mm<d_p<2.00mm), $T_{0|bed}$=65℃, $T_{airflow|inlet}$=26℃, Re_{d_h} =102.